ECONOMIC GEOLOGY AND GEOCHEMISTRY OF SELECTED PERLITE OCCURRENCES IN SOUTHWEST NEW MEXICO

By

Ernest F. Scharkan Jr.

New Mexico Bureau
of
Geology and Mineral Resources

Submitted in Partial Fulfillment of the
Requirement for the Degree of Master of Science
in Geology

New Mexico Institute of Mining and Technology
Socorro, New Mexico
May 1992

TABLE OF CONTENTS

LIST OF TABLES

LIST OF FIGURES

LIST OF FIGURES (continued)

LIST OF PLATES

All plates are in the envelope on the back cover.

ACKNOWLEDGMENTS

Many people have been invaluable in providing assistance and support throughout this study.

Dr. William Chavez, my committee chairman, contributed academic guidance, insight, ideas, and laboratory equipment which were important to this study. Bill's enthusiasm and sense of humor were appreciated during this project.

James Barker of the New Mexico Bureau of Mines and Mineral Resources provided this project and project funding through a Bureau-sponsored research assistantship. Jim provided access to many of the New Mexico Bureau of Mines and Mineral Resources research and information facilities. The staff at the New Mexico Bureau of Mines and Mineral Resources contributed to the project by conducting sample analyses, providing literature and preparing maps. Dr. George Austin of the Bureau provided helpful suggestions and was instrumental in my award of an Industrial Minerals scholarship sponsored by the Society for Mining, Metallurgy, and Exploration.

Dr. Andrew Campbell of the New Mexico Tech Geoscience department provided academic guidance, geochemical expertise, and assistance in the mass spectrometry laboratory. The project has benefited from reviews of the text and suggestions from Dr. Peter Mozely of the New Mexico Tech Geoscience department.

I would like to thank Bob King and Bob Bolton for

conducting analyses on some of the perlite samples and assisting me in the New Mexico Bureau of Mines and Mineral Resources perlite laboratory. Terry Pollock critically reviewed the thesis defense and did an exceptional job making 40 thin sections that were used in this study.

This work benefited from discussions with Dr. Richard Chamberlin, Dr. J. Renault, Chris McKee, Randy Ruff, and Scott Douglass.

Last, but certainly not least, I owe much to my parents, family, and God who have always given their support, encouragement, and unconditional love.

ABSTRACT

The United States produced about 550,000 t of perlite in 1989, with 85 % mined from deposits in central and north-central New Mexico. In addition to the commercial operations, perlite occurs in southwest New Mexico but it is not currently being mined. The geologic and geochemical characteristics of three inactive perlite occurrences in southwest New Mexico are discussed in this study. These prospects are referred to as the McDonald Ranch, Swartz, and Wallace Ranch perlite occurrences.

Field maps and petrography indicate McDonald Ranch perlite consists of glass flows related to local, rhyolitic extrusive centers and a glass chill margin of an overlying rhyolite flow. The Swartz occurrence consists of two glass zones that are not genetically related. The perlite horizon is a chill margin of the overlying Mimbres Peak rhyolite flow. A hydrated, welded tuff horizon occurs in an older lithic tuff unit. The Wallace Ranch perlite prospect is composed of a basal, granular perlite breccia and an overlying, classical perlite zone. The two units are either genetically related to the same endogenous extrusive event or the products of separate rhyolite extrusions.

Physical testing of expanded perlite from each field area indicates commercial grade perlite is present at the south margin of the McDonald Ranch, southeast margin of the Swartz area, and within granular perlite breccia and classical perlite units at Wallace Ranch. The expanded physical properties are not as favorable and consistent as the GREFCO standard. These factors will limit the end-use market of expanded perlite from the three occurrences.

Scanning electron microscope photomicrographs of perlite and expanded perlite from the three field areas indicate that the perlite has an interconnecting network of fractures (classical) or vesicles (pumiceous and granular). These features appear to aid expansion. Lack of these features in Swartz welded tuff may cause its poor expansion characteristics.

X-ray fluorescence spectrometry of perlite and rhyolite samples show similar concentrations of Al_2O_3, Fe_2O_3, and a similar Ti+V+Cr/Nb ratio in the McDonald Ranch perlite and overlying rhyolite. This data suggest the two units are genetically related. Sr versus Nb data and a common, narrow range of Ba concentrations suggest Swartz perlite and overlying rhyolite are genetically related. Oxide analyses (Al_2O_3 and TiO_2 vs SiO_2) of Wallace Ranch granular perlite breccia, classical perlite and overlying rhyolite indicate the three units are genetically related.

δO^{18} and D/H isotope analyses of Swartz perlite and welded tuff plagioclase phenocrysts indicate the welded tuff

has experienced a greater degree of secondary alteration than the perlite. Perlite and welded tuff δO^{18} and D/H values agree with previously published data.

The three perlite prospects have adequate reserves for mining. Inconsistent physical properties of the expanded product, remote location of each prospect, poor access and the large amount of high-quality perlite reserves at the GREFCO Socorro pit make these prospects uneconomical at the present time. Future perlite production in the United States will continue to be dominated by world-class perlite deposits at Socorro and No Agua Peaks.

INTRODUCTION

Perlite is a hydrated, siliceous glass produced by volcano-magmatic processes associated with rhyolitic volcanism. Pearly luster and abundant concentric fractures are characteristic macroscopic features of classical (onionskin) perlite; the industrial term "perlite" includes any volcanic glass that will expand appreciably by steam-driven vesiculation under appropriate heat treatment. Commercial grade perlite contains 2-6% H_2O as molecular water and hydroxyl ions. Vaporization of this water during rapid heating to temperatures in the softening range (900-1500^{o}F) results in vesiculation and consequent expansion, producing "expanded perlite", a frothy, glass product. Some obsidian (0-2 wt % H_2O) and pitchstone (+6 wt % H_2O) may also expand. Current uses for expanded perlite include plaster and concrete aggregate, horticulture, filler/extenders, filter aids, and cryogenic insulation. End use is determined primarily by the density, size distribution, and nonexpansible content of the expanded perlite.

The United States produced about 550,000 t of perlite in 1982, with 85% mined from deposits in central and north-central New Mexico. No Agua Peaks, the world's largest commercial-grade perlite deposit, is part of the Taos Plateau of northern New Mexico. Two other major

New Mexican perlite mines are at Socorro and East Grants Ridge. In addition to the commercial operations, perlite occurs in southwest New Mexico but these currently are not being mined. This research project discusses the geologic and geochemical characteristics of perlite occurrences near Silver City, New Mexico. These perlite prospects will be referred to as the Swartz, McDonald Ranch and Wallace Ranch perlite occurrences.

The above introductory information describing perlite and its uses is based on Weber and Austin (1982).

PURPOSE

The primary goal of this project is to conduct a systematic geologic and geochemical study of the Swartz, McDonald Ranch and Wallace Ranch perlite occurrences in southwest New Mexico. Previous work with commercial-grade deposits is used to compare and contrast the No Agua Peaks (Whitson, 1982) and Socorro (Weber and Austin, 1982) deposits with these perlite occurrences. Deposit characteristics such as structure, post depositional changes, and perlite texture, are used to interpret deposit genesis (emplacement), and hydration source. A genetic model for perlite formation used in conjunction with expanded perlite test results, is used to evaluate the Swartz, McDonald Ranch, and Wallace

Ranch perlite occurrences to establish deposit-type parameters and economic significance.

METHODS OF STUDY

An intial literature search for information pertaining to the geology and geochemistry of rhyolites, perlites and economic perlite deposits was conducted to obtain background information, with emphasis placed on information and previous work on New Mexican perlite, especially emphasizing perlite occurrences addressed in this study.

FIELD METHODS

Outcrop maps of three perlite occurrences in southwestern New Mexico were constructed at a scale of 1"=1000' by using enlarged portions of USGS 7.5' topographic maps as base maps. Outcrops of each area were mapped to define the perlite zones, adjacent lithologies, and structures. Samples of perlite and adjacent lithologies were collected for comparative petrography, physical testing and geochemical analysis. Samples were taken from each significant lithologic unit, giving representative sampling of each perlite occurrence. Samples were taken at 50 ft intervals perpendicular to strike, if sufficient perlite was exposed, permitting stratigraphic sampling of perlite

variations.

PERLITE PHYSICAL TEST PROCEDURES

The specialized applications for, and unique characteristics of, expanded perlite require physical testing of suitability. These tests determine if the perlite is of commercial-grade, and if it is capable of forming an expanded product of consistent physical specifications. A detailed description of each physical test is given by Barker and Hingtgen (1985). A brief description of each test used in this study follows.

Expanded Density. Density of expanded perlite is measured in lb/ft^3. The end use of expanded perlite is determined by its expanded density. An expanded density of 2.5 lb/ft^3 is suitable for filter aid and cryogenic insulation. Densities between 4 and 11 lb/ft^3 are suitable for horticulture, and plaster aggregate. Expanded density is determined with the following formula: sample wt. (g)/sample vol. (ml)) x 62.4 = lb/ft^3.

Furnace Yield. The perlite sample is crushed and sieved to -50+100 mesh and 100 g is expanded in an LVP Laboratory Furnace. Furnace yield is the percent of the original 100 g recovered.

Brightness. Brightness of expanded perlite is a measure of percent reflected when compared to reflection from a magnesia standard. Many end uses of expanded perlite are affected by the percent brightness. Filler/extenders require maximum brightness so they do not discolor the final product and filteraids for the food industry must be bright.

Nonexpansibles. A fraction of the expanded perlite is agitated in water. Unexpanded and partially expanded perlite or non-perlite will sink while fully expanded perlite will float. This determines the extent of full expansion and marketable percent of the furnace output.

Sieve Analysis. A 10 g fraction of expanded perlite is passed over 8 in. screens on a Tyler RO-TAP shaker. The percent retained on each screen is calculated. This test determines the expansion of perlite in various size fractions. Glass bubble shattering during expansion will increase the fine fractions. Each expanded size fraction has a possible end use.

Compacted Density. The expanded perlite is poured into a graduated cylinder and dropped 1000 times

forcing the perlite to compact under its own weight. The final volume in the graduated cylinder is then measured and recorded. Compacted density effects the thermal conductivity of expanded perlite insulation.

CHEMICAL ANALYSES OF SAMPLES

Several analytical techniques were used to obtain geochemical data to determine the H_2O content of perlite samples, whole-rock major element and trace element compositions, and whole rock and phenocryst isotope data. These data were necessary to assess possible genetic conditions of the perlite, and its genetic relationship to adjacent lithologies.

The Pennfield Test

The Pennfield test was used to determine the water content of 31 perlite samples. This procedure fuses a mixture of finely ground sodium tungstate flux and finely ground perlite sample at 900°C. This high temperature fusion releases all molecular and hydroxyl water contained in the perlite sample, with water vapor condensed in a cooled tube which is weighed. Jenkins (1972) discusses this procedure in detail.

X-Ray Fluorescence Spectrometry (XRF)

Whole-rock analysis by XRF determines the major and trace element chemical composition of perlite and rhyolite samples. Each sample was pulverized and pressed into a briquette for XRF analysis using a Rigaku/USA model 3064 sequential X-ray fluorescence spectrometer.

Hydrogen Isotope D/H Analysis

Importantly, an idea regarding the origin of the water of hydration in perlite can be ascertained by determining the deuterium-hydrogen ratio of water extracted from perlite samples. Measured in per mil, D/H values must be used in conjunction with δO^{18} values to determine the source of the water of hydration. The extraction of water from perlite was accomplished by placing 0.02 g of a -20+50 mesh sample in a quartz tube oven. The sample was maintained at 100°C for 8 hrs under high vacuum to drive off adsorbed water. The sample was then heated to 1100°C and the water vapor cryogenically frozen into a storage vessel. A manometer monitored vacuum line vapor pressure and indicated when all water had been extracted from the sample. All noncondensible gasses were evacuated from the vacuum line and the frozen water vapor cryogenically transferred to a capillary tube. The capillary tube was sealed with a flame. The extracted water was converted to hydrogen with a zinc conversion (Kendall and Coplen, 1985).

The hydrogen was analyzed with a Finnigan Mat delta E mass spectrometer to determine the D/H ratio. Hydrogen isotope values were corrected with respect to SMOW (δD=0 o/oo), GISP (δD=-196.55 vs SMOW), and SLAP (δD=-412 o/oo).

Oxygen Isotope Analysis (O^{18}/O^{16})

The origin of the water of hydration in perlite can be ascertained by comparing the O^{18}/O^{16} value of perlite to the value of cogenetic phenocrysts. The oxygen isotope ratio of perlite will have a value much different from its primary magmatic value due to exchange with meteoric waters during hydration (Taylor, 1968). Taylor (1968) states unaltered feldspar phenocrysts yield values representative of the melt from which the rock was formed. Isotope values were determined by extracting oxygen from the perlite (glass only) and feldspars (phenocrysts only) in a standard silica extraction line. Crushed perlite was sieved and the -20+50 mesh fraction was passed through a magnetic separator to segregate the magnetite-rich glass from feldspar phenocrysts. Feldspar phenocrysts and glass particles were hand-picked under a binocular microscope to ensure completely homogeneous samples were obtained. The perlite and feldspars were pulverized, weighed into 0.012 g samples, and loaded into silica extraction line reaction vessels. A ClF_3 compound extracted the oxygen from the

samples, the oxygen was converted to CO_2, and the oxygen isotope ratio of the recovered CO_2 was analyzed on a Finnigan Mat delta E mass spectrometer.

OPTICAL ANALYTICAL TECHNIQUES

Microscopic textures of field samples, expanded perlite and nonexpansibles can be distinguished using a variety of optical analytical techniques.

Thin Section Microscopy

Thirty-two thin sections of outcrop samples were made to aid identification of lithology, glass impurities, and rock textures.

Binocular Microscopy

The degree of expansion and vesicle size of expanded perlite can be determined, and nonexpansible particles can be identified, using a low-power binocular microscope.

Scanning Electron Microscopy

Textural comparisons of expansible versus nonexpansible perlite can be conducted using SEM techniques. Samples are glued to mounts and a freshly, broken surface is coated with an Au-Pd alloy. The coated surface is scanned by the SEM and photomicrographs of surface textures are taken. This

information will determine if micro-textures are related to expansibility and physical properties of expanded perlite.

LOCATION, ACCESS AND PHYSIOGRAPHY

The Swartz, McDonald Ranch, and Wallace Ranch perlite occurrences are in Grant County, southwestern New Mexico (Fig. 1).

The Swartz Perlite Occurrence

The Swartz Perlite occurrence is east of the town of Swartz, New Mexico and 15 mi northeast of City of Rocks State Park (Fig. 1). Perlite outcrops are on hills southwest of Tom Brown Canyon, in sec. 34, T. 18 S., R. 10 W. and sec. 3, T. 19 S., R. 10 W. The outcrops extend northwest along a strike length of about 1 mi, are parallel to Tom Brown Canyon, and are 1.1 mi west of NM Highway 61. A trail follows the arroyo northward along Tom Brown Canyon into the study area. Most perlite exposures occur on hillsides; adjacent lithologies are exposed along ridge tops and in stream cuts.

Elevations in the Swartz area range from 5376 ft above sea level in the east to 6084 ft in the west. The entire area is sparsely vegetated with various grasses, cat claw, short juniper, and cacti. All hillsides are steep and bare or

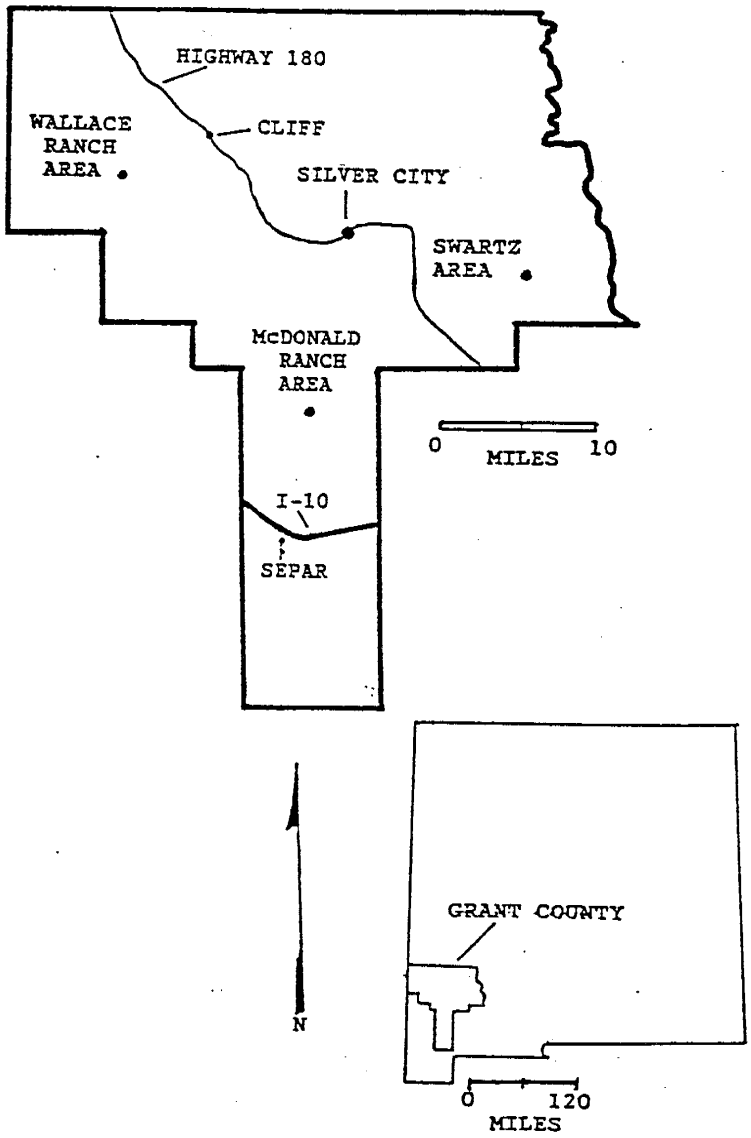

FIG. 1. Location map of the McDonald Ranch, Swartz, and Wallace Ranch perlite occurrences in Grant County, New Mexico.

covered with colluvium.

The area is cut by numerous ravines that trend north to Tom Brown Canyon or south to an unnamed wash. Landslide scars are numerous along the steeper slopes.

The McDonald Ranch Perlite Occurrence

The McDonald Ranch area is 16 mi north of Separ, New Mexico, along the Burro Cienaga (Fig. 1). The study area is in secs. 1, 11, 12, and 13, T. 22 S., R. 15 W. and sec. 18, T. 22 S., R. 14 W. Perlite crops out along a 2.5 mi trend on the northeast margin of Burro Cienaga. Access to the area is by I-10 to Separ, New Mexico, then north for 16 mi on NM Highway 189. NM Highway 189 is a graded dirt road for two-wheel drive vehicles when dry.

Exposures of perlite and adjacent lithologies occur on steep hillsides, ridge tops, ravines, and stream cuts. Elevations range from 5150 ft above sea level in the southeast section of the study area to 5542 ft in the northwest. Slopes are sparsely vegetated with various grasses, short juniper, and a cacti. Level areas adjacent to the Burro Cienaga stream bed are densely vegetated with tall grass, trees and bushes.

The McDonald Ranch area is cut by numerous drainages which trend southwest to the intermittent Burro Cienaga. Water flows in these drainages primarily during the spring and summer rainy seasons.

The Wallace Ranch Perlite Occurrence

The Wallace Ranch area is 15 mi southwest of Riverside, New Mexico (Fig. 1). Perlite underlies hills surrounding Pine Canyon in section 19, T. 16 S., R. 18 W. Additional perlite outcrops occur beyond the study area. Access to the Wallace Ranch area is via NM Highway 180 to 1.25 mi north of Riverside and west on Iron Bridge road. A graded dirt road continues west from Iron Bridge Road for 16 mi to the Wallace Ranch area. Most of the perlite is exposed on the hillsides of Pine Canyon.

Elevations in the study area range from 5600 ft above sea level in Pine Canyon to 6020 ft at hilltops to the southwest. Stands of juniper, and sage cover the bottom of Pine Canyon. Cat claw, juniper, and cacti are common on the steep slopes.

Pine Canyon and Rock House Canyon host intermittent streams which are the primary drainage routes for the study area. Small arroyos and washes drain to these canyons from surrounding hills.

PREVIOUS STUDIES

Elston and others (1976) describe the regional geology of southwest New Mexico as being dominated by Tertiary volcanic rocks. The volcanic landscape was modified and enhanced by subsequent Basin and Range faulting. Elston (1957) mapped and conducted a structural and stratigraphic study of the Cenozoic rocks of the Dwyer quadrangle. He identified two chemically distinct Tertiary volcanic series. Elston (1960) mapped the Virden quadrangle and described a rhyolite flow that contains perlitic zones of substantial size. Hedlund (1978) mapped the Werney Hill and Soldiers Farewell quadrangles. Hedlund identified a rhyolite dome in the Burro Cienaga and northwest-trending, high-angle, normal faults to the east. Finnell (1987) published a geologic map of the Cliff quadrangle. He expanded on Elston's work in the Virden quadrangle (1960). Finnell (1987) divided Elston's (1960) Tertiary volcanic formations into members based on lithology and composition.

Various authors described perlite occurrences in New Mexico. Weber and Austin (1982) described perlite deposits and occurrences in New Mexico, including the McDonald Ranch occurrence. The geology and genetic origin of the No Agua Peaks perlite deposit are described in detail by Whitson (1982). Whitson defined the genetic model for economic

perlite dome deposits and documented the mechanism for their formation. Whitson's model will be used in this study to evaluate selected perlite occurrences. Breese and Piper (1985) discuss possible mechanisms for hydration of the No Agua Peaks perlite. A detailed study of the geology and commercial potential of the Wallace Ranch perlite occurrence was conducted by Hahman (1989). Hahman divided Finnell's (1987) Sycamore Camp Rhyolite into members based on lithology and mapped them accordingly. Geologic mapping and drill hole data allowed Hahman to conclude a substantial perlite resource exists in the Wallace Ranch area. Barker and Hingtgen (1985) published a detailed description of standard physical tests conducted on perlite samples to determine if the perlite is of commercial grade.

Friedman and Smith (1958) studied the deuterium content of water in some volcanic glasses to determine the possible source of hydration for perlite. They concluded the water of hydration is "secondary" and is related to meteoric water. Friedman, Smith, and Long (1966) determined a relationship between the depth of hydration of rhyolitic glass and time. They determined that the rate of hydration is temperature dependent. The study of oxygen isotopes in hydrated rhyolitic glass by Taylor (1968) led him to conclude the hydration of perlite is a secondary process that involves local meteoric water. He states the process

of hydration involves the exchange of oxygen in the silicate glass with large amounts of water.

REGIONAL GEOLOGY

Elston et al. (1976) state Tertiary, volcanic intrusive and extrusive rocks associated with cauldrons of the Mogollon Plateau volcanic field are important, regional, geologic features of southwest New Mexico. Mid-Tertiary emplacement of plutons and cauldron formation was followed by a change in regional tectonic stress orientation and subsequent Basin and Range faulting (Elston et al., 1976). Cauldron formation was enhanced by regional Basin and Range fault development. A unique characteristic of the Mogollon Plateau is the development of a number of large-scale, discontinuous, arcuate, crudely concentric intrusions of flow-banded rhyolite ring dikes (Elston et al., 1976). These features reached the surface and now form entire mountain ranges (Sierra Diablo); Elston et al. (1976) refer to these structures as "framework rhyolites".

The several thousand meters of Tertiary volcanic rocks of this region can be divided into three overlapping suites: 1) calc-alkalic andesite to rhyolite (29-43 Ma), 2) high-silica alkali rhyolite (21-32 Ma), 3) basalt and basaltic andesite (0-37 Ma) (Elston et al., 1976). Basalt, andesite,

and latite flows of the calc-alkalic suite grade upward into quartz latite and rhyolite, mainly ash-flow tuff, air-fall tuff, and epiclastic rocks (Elston et al., 1976). High-silica alkali rhyolite rocks are confined to the Mogollon Plateau. This suite of rocks form large ash-flow tuff, ring-fracture and moat deposits of large central volcanoes, and large masses of flow-banded rhyolite (Elston et al., 1976). The basaltic suite erupted contemporaneously with mid-Tertiary felsic rocks, but only outside active felsic centers (Elston et al., 1976).

Rocks of Cretaceous to Precambrian age occur below the Tertiary volcanic rocks.

The structural geology of southwest New Mexico is complex and involves a transition zone that separates Colorado Plateau structures to the north from Basin and Range structures to the south (Trauger, 1972). The transition zone is a 50 to 75 mi wide, northwest-trending structural belt that includes most of northern Grant County (Fig. 2; Trauger, 1972). North-northwest striking, late-Tertiary Basin and Range faults of the Black Range and Rio Grande rift are predated by the northwest-striking Texas Lineament and northeast-striking Santa Rita Lineament. These deeply penetrating shear zones dominate the structural grain of Precambrian rocks in the southern Rocky Mountains and

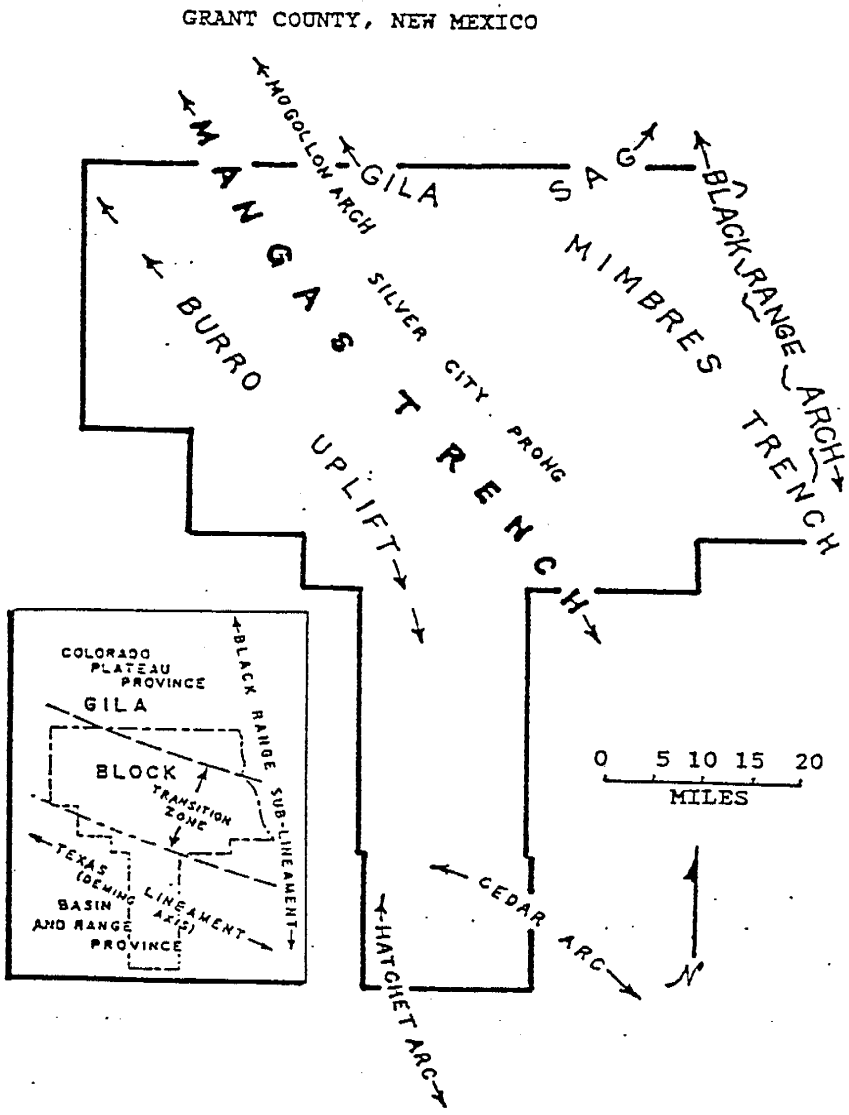

FIG. 2. Geologic structural elements of Grant County, New Mexico. Map modified from Trauger (1972).

allowed magmas to intrude the upper lithosphere (Chapin et al., 1976). Laramide plutons have been emplaced along the Santa Rita Lineament near Silver City.

Structural control of major mid-Tertiary volcanic activity and associated pluton emplacement is difficult to recognize. Elston and others (1976) propose crustal extension and associated normal-faulting provided room necessary for near-surface emplacement of mid-Tertiary plutons. Mid-Tertiary primary volcanic-structures were enhanced by Basin and Range faulting. Dips of postcauldron volcanic rocks were increased by doming as in the formation of the Black Range Anticlinorium (Elston et al., 1976). Eruption of basaltic andesite, formation of stratovolcanoes on the rim of the Mogollon Plateau and topographic modification of the entire Mogollon Plateau are attributed to the onset of the Basin and Range stress field and associated faulting (Elston et al., 1976).

LOCAL GEOLOGY

The McDonald Ranch Area. The local geology of the McDonald Ranch area is described by Ballman (1960). A Precambrian granite basement lies beneath the McDonald Ranch area, but no granite outcrops are visible locally. Ballmann (1960) describes a massive, coarse-grained granite horst exposed

10 mi to the north near NM Highway 180, along Silver City Draw.

In the Knight Peak area, Upper Ordovician to Lower Cretaceous rocks are missing due to erosion during the Big Burro uplift (Ballmann, 1960).

Tertiary volcanic rocks dominate the local area surrounding McDonald Ranch. These volcanic rocks are of primary interest and importance to this study. Ballmann (1960) divides the Tertiary volcanics in the Knight Peak area into five groups. These groups, starting with the oldest are: 1. Early rhyolite tuffs, perlite, and agglomerate; 2. Early andesitic flow and tuff; 3. Vitric rhyolite breccia; 4. Middle rhyolitic breccia; and 5. Intrusive andesite. Volcanism started in the Miocene with the early rhyolites; successive episodes produced the early andesites, middle rhyolites, and intrusive andesites (Ballman, 1960). The lowest of the early rhyolites is a massive, pink, lithic tuff with a welded matrix and a maximum thickness of 300 ft (Ballmann, 1960). The lithic tuff lies unconformably on Lobo Arkose or Precambrian granite. Locally, a perlite horizon overlies the lithic tuff. It originated from a perlite dome located at the Morrow Ranch, 3.5 mi northwest of the McDonald Ranch (Ballman, 1960). The upper portion of the perlite is brecciated and overlain by vitric tuffs and

agglomerates of the lower rhyolitic series (Ballmann, 1960). Hedlund (1978) mapped and constructed a cross-section of this area and concludes the Morrow Ranch is the location of a large rhyolite dome that has since been eroded. Designated the rhyolite dome of Burro Cienaga, Hedlund (1978) represents the perlite zones as horizons occurring between rhyolites. The perlite horizon near McDonald Ranch is described by Ballmann (1960) as being larger than the Morrow Ranch dome deposit. He states that it has the shape of a "malformed lens".

Ballmann's early andesitic flows, vitric rhyolite breccia, and middle rhyolite breccia overlie the early rhyolites in the northwest part of the Knight Peak area. These later series may correlate to Tertiary rhyolites, lithic ash flows, and ash flows Hedlund (1978) mapped as overlying the perlite in the McDonald Ranch area. Quaternary Gila Conglomerate (Qtg) and Pleistocene fan deposits (Qfo) derived from weathered Gila Conglomerate unconformably overlie Tertiary volcanics in the McDonald Ranch area (Hedlund, 1978).

The northern half of the Knight Peak range is bounded by the Malone normal fault on the west and the Taylor high-angle, normal fault to the east. Major movement along the Taylor fault transformed the Knight Peak range into a tilted

fault block typical of the Basin and Range province (Ballmann, 1960). High-angle, northwest striking, normal faults are inferred by Hedlund (1978) on his map of the Werney Hill Quadrangle. These two parallel normal faults are east of the McDonald Ranch area and are referred to as the Flat Canyon and White Rock Canyon faults (Hedlund, 1978). Vertical movement along these faults and numerous, smaller, sub-parallel faults in the McDonald Ranch area exposed the perlite horizons and cause the local strata to dip northeast.

The Swartz Area. The local geology of the Swartz area was described by Elston (1957).Locally, rocks of Precambrian to Late Cretaceous age are not exposed in the immediate Swartz area. These sequences lie beneath the Tertiary volcanic pile at Swartz.

Elston divides local Tertiary rocks into two sequences, the lower and upper volcanic sequences. The lower series is a typical calc-alkaline eruptive suite, grading upward from andesites, to latites, and finally rhyolites (Elston, 1957). The upper volcanic sequence begins with a formation composed of a lower andesitic member and an upper trachytic rhyolite member. An overlying basalt composed of flows, breccias, agglomerates, conglomerates and sandy tuffs occurs below the youngest rocks of the upper volcanic sequence; a

rhyolite composed of porphyritic flows and tuffs. Tertiary Santa Fe fanglomerates and conglomerates overlie the upper volcanic sequence. A marked chemical difference exists between the two volcanic sequences and each has a distinct magma source (Elston, 1957). The most mafic rocks of the lower volcanic sequence are pyroxene andesites, and the most felsic rocks are calc-alkaline rhyolites (Elston, 1957). The most mafic rocks of the calcic upper volcanic sequence are olivine basalts and the most felsic rocks are rhyolites considerably richer in CaO than those of the lower volcanic sequence (Elston, 1957).

The oldest member of the lower volcanic sequence is the Rubio Peak Formation. Locally, the Rubio Peak Formation crops out in a broad belt west of the Mimbres fault and reaches its maximum thickness in the Mimbres Peak area (Elston, 1957). Pyroclastic rocks are as common as flows and andesites tend to grade upward into latites (Elston, 1957). Elston (1957) states the Rubio Peak Formation lies unconformably on Silurian to Cretaceous rocks near the northern boundary of Dwyer quadrangle.

Elston (1957) considers the Sugarlump Tuff a transitional unit between intermediate rocks that form the lower horizon of the lower volcanic sequence and rhyolites that form its upper part. The Sugarlump consists of massive and bedded

green, white or pink tuffs with occasional massive beds of vitric, crystal tuffs. The formation reaches its maximum thickness near Mimbres Peak (Elston, 1957). Elston (1957) mapped angular, unconformable contacts with older Rubio Peak Andesite on upthrown blocks of the Blue Mountain and Mimbres faults, and conformable contacts on downthrown blocks, or at a considerable distance from the faults. Elston (1957) attributes this to a period of faulting at the end of the latite volcanic phase.

The Kneeling Nun Rhyolite is conformable with the well-bedded horizons of underlying Sugarlump Tuff and could be considered their uppermost member (Elston, 1957). This grayish-purple ignimbrite has phenocryst minerals similar to other local rhyolites of the lower volcanic sequence (Elston, 1957). Elston (1957) states the local thickness varies from 200 to 400 ft because of erosion after deposition.

The Mimbres Peak Formation consists of genetically-related rhyolite flows and their intrusive equivalents, pumiceous tuffs, sandy tuffs, and perlites (Elston, 1957). Flow rocks and intrusive rocks have identical lithologies, trend northwest, occur within 1 mi of a major fault and exhibit definite alignment along faults (Elston, 1957). Three miles northeast of Mimbres Peak; Mimbres Peak tuffs, pumiceous

tuffs, perlite and rhyolite flows crop out for 6 mi along the northwest-trending Mimbres fault. Two perlite exposures in this area are of interest to this current study. Elston (1957) mapped a rhyolite plug at Mimbres Peak and he states at this location, bedded pumiceous tuffs occur below 100 ft of perlite breccia and are capped in a few spots by perlite flows. Elston (1957) estimates the Mimbres Peak Formation reaches a maximum thickness of 2500 ft in the northeast corner of Dwyer quadrangle.

The Box Canyon rhyolite tuff is a gray, massive ignimbrite that reaches a maximum thickness of 75 ft and has exposure limited to the upper 4 mi of the Box Canyon (Elston, 1957). Box Canyon rhyolite tuff conformably overlies the Mimbres Peak and Kneeling Nun Formations (Elston, 1957).

Rustler Canyon basalt occurs as thin flows and flow breccias that reach a maximum thickness of 50 ft and are limited to the western part of Dwyer quadrangle (Elston, 1957).

The Caballo Blanco rhyolite tuff is the youngest formation of Elston's lower volcanic sequence. Elston (1957) states this gray ignimbrite caps the lower volcanic sequence at almost all locations in the Dwyer quadrangle. The Caballo Blanco tuff reaches a maximum thickness of 325 ft at Caballo Blanco.

The lowest units of the upper volcanic sequence are flow-layered andesite and overlying rhyolite members of the Razorback Formation (Elston, 1957). The andesite occurs as alternating flows and breccias and overlies Caballo Blanco rhyolite or, in some places, the Mimbres Peak Formation. A possible source for the andesite is a 1 mi long, northwest-trending dike in the western part of Dwyer quadrangle (Elston, 1957). The Razorback rhyolite has a basal breccia of black perlitic glass succeeded by a spherulitic zone and an upper flow-layered rhyolite (Elston, 1957). No rhyolite source has been found. A combined thickness of 800 ft for both members occurs in Donahue Canyon (Elston, 1957).

The overlying Bear Springs basalt is composed of flows, breccias, agglomerates, conglomerates, and rare sandy tuffs (Elston, 1957). Possible source dikes occur in the west half of Dwyer quadrangle where Bear Springs basalt covers large areas (Elston, 1957). Elston (1957) states a thickness of 650 ft measured at the mouth of Tom Brown Canyon must be considered a conservative estimate of total thickness.

The Swartz rhyolite, the last Tertiary volcanic of the upper volcanic sequence has an exposure limited to the mouth of Tom Brown Canyon (Elston, 1957). The rhyolite occurs as flows, tuffs, and breccias associated with local domelike

rhyolitic intrusive bodies and small dikes (Elston, 1957).

Santa Fe fanglomerates overlie most of the Tertiary upper volcanic sequences in the northeastern corner of Dwyer quadrangle.

Elston (1957) states that between the Precambrian and Cretaceous times the Dwyer quadrangle and surrounding areas were relatively stable. Laramide deformation included normal faulting and intrusion by stocks and sills (Elston, 1957). Several periods of post-Laramide faulting occurred in the Dwyer quadrangle along the same fault lines established by Laramide deformation (Elston, 1957). The Sugarlump-Rubio Peak contact provides evidence for this movement (Elston, 1957). Elston (1957) contends that some of the local faulting controlled a limited amount of local Tertiary intrusion and eruptive activity. Alignment of Mimbres Peak flow rhyolites and sources along major northwest-trending faults and the large Razorback andesite feeder dike in the western part of the quadrangle may support this idea (Elston, 1957).

Elston's (1957) cross section of Dwyer quadrangle shows several high-angle, northwest-trending normal faults and fault blocks typical of the Basin and Range Province. The regional dip to the southwest and local mountains are the

result of fault block movement along the northwest-trending Mimbres Hot Springs, Mimbres, and Cooks Range high-angle, normal faults (Elston, 1957). Vertical offset along the Mimbres fault reaches 4000 ft at the Rubio Peak-Razorback fault contact near the northern boundary of the quadrangle (Elston, 1957). Several northeast-trending normal faults break the fault bocks into segments but this does not affect the regional dip (Elston, 1957). The local dip of Tertiary volcanic rocks is a result of flow folding of viscous lavas, subsidence of volcanic basins and doming around local intrusive bodies (Elston, 1957).

The Wallace Ranch Area. The local geology of the Wallace Ranch area is described in Finnell (1987) and Elston (1960). Hahman (1989), the most detailed geologic map of the area to date is a result of his geologic assessment of the local perlite occurrence. The area surrounding Wallace Ranch is dominated by many interfingered Tertiary extrusive rocks ranging in composition from andesite flows and basalt flows, to quartz latite ash flows, and rhyolite tuffs, flows and their intrusive equivalents. Middle Proterozoic gneiss and granites, Cretaceous Beartooth quartzite and Colorado shale are mapped 9.3 mi south of Wallace Ranch (Finnell, 1987). These formations are not exposed in the immediate vicinity of the Wallace Ranch, they probably lie beneath the thick pile of local Tertiary volcanics.

Elston (1960) divides local Tertiary volcanics into four groups. The oldest is the Datil Formation which has 9000 ft of rhyolite flows, tuffs, and welded tuffs interbedded with gray andesite and latite porphyry. The Datil Formation is exposed east of Wallace Ranch and covers a much larger area to the south and west. Miocene purple-gray latite is exposed 13 mi to the west of Wallace Ranch. This latite grades upward into a widespread, overlying basalt and basaltic andesite (Elston, 1960). The basaltic flow is locally interbedded with the Gila Conglomerate and crops out in a broad belt around the Wallace Ranch area (Elston, 1960). An upper rhyolite lies unconformably above the basalt and forms a northwest-trending zone 7 mi long and 1.5 mi wide. Rhyolite flows, tuffs, and plugs with perlite facies occur in this formation. The Wallace Ranch perlite occurrence is associated with this rhyolite formation. Locally, the upper rhyolite reaches a maximum thickness of 200 ft. A high-angle, normal fault forms the southwest boundary between the downthrown rhyolite and the adjacent, upthrown basalt formation (Elston,1960).

Finnell (1987) differentiated Elston's four Tertiary volcanics into many individual units based on composition and lithology. Units of interest in the Wallace Ranch area belong to the Sycamore Camp Rhyolite Series (Finnell, 1987). Basaltic andesite of the Sycamore Camp correlates with

the same broad belt of identical lithology mapped by Elston (1960) near Wallace Ranch. A light gray, thin-bedded, air-fall tuff containing perlite, pumice, and basalt fragments overlies the basaltic andesite (Finnell, 1987). An overlying rhyolite with perlitic zones (Finnell, 1987) correlates with Elston's (1960) perlitic, Upper Rhyolite. Finnell (1987) states that the rhyolite has a maximum thickness of 210 ft and the perlitic zones are exposed in Pine Canyon. Local perlitic zones were investigated for possible commercial value before Hahman (1989). Hahman (1989) mapped a basaltic andesite in the Wallace Ranch area that is equivalent to Finnell's (1987) local, olivine basalt. Hahman (1989) combined Finnell's (1987) air-fall tuff and tuffaceous sandstone (Tst) with granular perlite breccia of the overlying rhyolite and calls the unit undifferentiated perlite. Hahman (1989) mapped the black, classical perlite, perlitic rhyolite tuff, and overlying pink, flow-banded rhyolite of Finnell's rhyolite (Tsr) as separate units. Finnell (1987) mapped a rhyolite plug with a black glass border and northwest-trending dikes 1.5 mi southeast of Pine Canyon. Finnell does not speculate if this is the source of the Wallace Ranch area Tertiary rhyolites. Finnell (1987) describes local fan deposits (Qf) overlying the Tertiary rhyolites as Holocene bouldery, gravel deposits.

Finnell's (1987) cross section of the southwest corner of the Cliff quadrangle illustrates seven high-angle, northwest trending, normal faults typical of Basin and Range terrane. Brushy Mountain, southeast of Wallace Ranch, is a fault block bounded on both sides by high-angle normal faults. An east-west trending normal fault at the south end of Brushy Mountain brings downdropped Tertiary quartz-latite ash-flow tuff (Tmt) in contact with Middle Proterozoic granite (Finnell, 1987). A relation between faulting and Tertiary volcanism is not discussed by Finnell (1987) or Elston (1960).

RESULTS

THE McDONALD RANCH AREA

FIELD MAPPING. An outcrop map of the east margin of the Burro Cienaga was made at the scale of 1:12,000 (Plate 1). Locations of samples, foliation, and strike and dip measurements are on the map (Plate 1). The outcrop trends N40W and has a lower rhyolite (Trl), an intermediate perlite (Tp), and an overlying rhyolite (Tr) that are of primary interest to this study. The lower rhyolite is white or yellow, lithic-rich, and silicified adjacent to the overlying perlite zone. The perlite separates the lower rhyolite (Trl) from the overlying rhyolite (Tr) in most areas. At several points along the rhyolite outcrop,

perlite is not present and the two rhyolites are in contact. Strike and dip measurements of perlite foliations and flow-bands indicate a general northwest strike; and, except at several locations, a dip of 22 to 33° NE. The shape and thickness of the perlite is extremely variable and highly irregular (Plate 1). Ballman (1960) states that the perlite near McDonald Ranch resembles a "malformed lens". The perlite horizon reaches a thickness of 300 ft at the north and south ends of the study area. The north end is 2 mi southeast of the center of Hedlund's (1978) "rhyolite dome of Burro Cienaga". The cross section of Hedlund's rhyolite dome shows a dome radius of 1.5 mi that is truncated by a high-angle normal fault to the east (Hedlund, 1978).

Perlite outcrops thin to the southeast along the Burro Cienaga. Perlite thickness ranges from 50 ft in the north to 4 ft to the southeast; 1.2 mi to the southeast, the south outcrop is 300 ft thick. A prospect pit is at the base of this outcrop. Unlike the thick, north outcrop, the south outcrop has a pink, devitrified, felsic core and numerous felsic stringers that range in thickness from 0.3 to 5 ft. The felsic core thickens to the southeast to nearly 40 ft before it is covered by colluvium. The underlying perlite zone is buried by Quaternary alluvium of the Burro Cienaga. The perlite horizon above the felsic

core is overlain by a black, dense, glassy vitrophyre. Hedlund (1978) mapped a local formation designated the upper vitrophyre (Truv) and places it at the top of the rhyolite dome-flow complex of Burro Cienaga. The upper vitrophyre (Truv) crops out 350 ft to the east and stratigraphically above the thick, south perlite outcrop. An ash-flow tuff, which overlays the upper vitrophyre, is the Kneeling Nun Formation (Hedlund, 1989). Dip directions in local glass foliation range from N70W to N60E. No faults are visible in the study area.

PETROGRAPHY. Thin sections of eight samples from the McDonald Ranch area are described in Appendix B. Samples MR-3, MR-4, MR-7, MR-10, and MR-21 are perlites. Samples MR-6 and MR-29 are welded tuffs. Sample MR-28 is from the lower, lithic rhyolite. Hand samples and thin sections of local perlites are 99% glass with pervasive perlitic fractures (Fig. 3). No traces of vesicles or glass shards are present in the glassy groundmass. The 1 to 3% phenocrysts present in decreasing order of abundance include anhedral to euhedral plagioclase, sanidine, and biotite. Magnetite is present in all McDonald Ranch thin sections. Two welded tuffs, MR-6 and MR-29 have welded glass shards in their groundmasses. MR-6 is composed of volcanic lithics and is silicified; both samples are from the lower rhyolite formation (Trl). Sample MR-28 contains volcanic lithics and

is a vitric lithic rhyolite from the lower rhyolite formation (Trl). The welded tuff (MR-6) and the vitric lithic rhyolite (MR-28) were taken directly above the perlite horizon. This implies perlite interfingers with the top of the lower rhyolite formation at these sample locations (Plate 1).

THE SWARTZ AREA

FIELD MAPPING. An outcrop map of the hills and drainages along the southwest margin of Tom Brown Canyon was made at the scale of 1:12,000 (Plate 2). The locations of samples and foliation strike and dip measurements are noted on the map. Three major perlite outcrops occur in the area and trend N30W, N72W, and N55E (plate 2). Two of the perlite horizons (N72W and N55E) appear to be genetically associated with an adjacent lithology (Mimbres Peak rhyolite) and exhibit similar physical, lithologic, petrographic, and geochemical characteristics. These perlite horizons occur in the southwest part of the study area. The third outcrop (N30W) appears to be genetically associated with a different adjacent lithology (lithic tuff) and exhibits unique characteristics compared to the other two outcrops.

The two perlite outcrops in the southwest part of the study area (N72W and N55E) are black, angular, vitreous, glass with clear, feldspar phenocrysts. The glass does not have

visible perlitic fractures in hand sample. The outcrops occur on opposite sides of a hill and are the single outcrop of a perlite lens that underlies a rhyolite cap (Plate 2). The perlite thickness varies from 6 to 250 ft and overlies a bedded, red, lithic tuff, and a white, lithic tuff of the Mimbres Peak Formation. The 250 ft of perlite exposed on the southeast margin of the field area appears to rapidly pinch out beneath the hilltop. Outcrops down strike and on the opposite side of the hill are substantially thinner. Locally, several areas of the perlite horizon grade up into silicified, spherulitic zones that are 5 to 15 ft thick. Individual spherulites are gray or red and range from 0.5 to 3 in. in diameter. A pink and gray, flow-banded, fine-grained rhyolite flow of the Tertiary Mimbres Peak Formation overlies the perlite horizon and spherulitic zones. Locally, perlite and spherulitic zones grade upward, into the overlying flow-banded rhyolite. The overlying rhyolite formation varies from 50 to 200 ft thick. Locally, rhyolite composition grades to dacite. The rhyolite has an inferred normal fault contact along its entire southwest margin with an upthrown block of Tertiary Rubio Peak andesite.

Along the southeast margin, the lower contact of the Mimbres Peak rhyolite is covered at most places by colluvium. The lower contact with underlying perlite is visible at several outcrops (Plate 2). A bedded, cream, lithic tuff is visible

at the bottom of landslide scars that cut through colluvium along the southeast margin of the rhylolite. Although contacts between rhyolite and tuff are covered, a lower perlite-tuff contact is exposed. This tuff is either an underlying member of the Mimbres Peak Formation or a member of the older Sugarlump Formation (Elston, 1957). To the southeast, the tuff has an inferred normal fault contact with older Rubio Peak andesite.

Along the northern margin of the study area, the Mimbres Peak Formation is truncated and normal faulted against younger Razorback rhyolite and Bear Springs basalt (Plate 2). Faulting occurs along a series of subparallel, northwest-trending, normal faults that form the Mimbres fault zone (Elston, 1957). The perlite outcrop in the north part of the field area trends N30W and is composed of black, vertically jointed, blocky glass that contains abundant, altered, white, phenocrysts. Pebbles and boulders of red felsite commonly occur in the glass matrix. The southeast end of the glass zone grades into a bedded, red, lithic-rich, tuff of the Mimbres Peak Formation. This tuff occurs above and below the entire glass horizon. The lower glass-tuff contact is gradational and the upper contact is very sharp. The glass zone is a welded lithic tuff horizon of the adjacent lithic-rich Mimbres Peak tuff. Mimbres Peak tuff is in contact with overlying flow-banded Mimbres Peak

rhyolite for a distance of 0.3 mi; this contact is then truncated by the Mimbres Fault. The lithic tuff below the glass zone is in contact with a bedded, white, vitric, lithic tuff of the Mimbres Peak Formation. The nature of this contact and the stratigraphic relationship between these tuffs is not apparent in the field. To the southwest, Rubio Peak andesite is in fault contact with a bedded, white, vitric lithic tuff of the Mimbres Formation (Elston, 1957).

PETROGRAPHY. Thin sections of 12 samples from the Swartz field area are described in Appendix B. Hand samples S-2, S-4, S-5, and S-8 are perlites from the two physically similar outcrops (N72W and N55E, Plate 2). Sample S-42 is from the felsic formation overlying the western end of the N72W perlite outcrop. Samples S-10, S-13, S-16, and S-17 are glass from the welded tuff horizon (N30W). Samples S-38 and S-39 are from the red lithic tuff below the welded tuff horizon. Sample S-40 is from the overlying red lithic tuff.

Hand samples S-2, S-4, S-5, and S-8 are black, vitreous, highly fractured glass with biotite and clear feldspar phenocrysts. Perlitic fractures are not visible. Red felsic veinlets are visible in S-4 and S-5. Thin sections of the four samples range from 95 to 97% highly fractured

glass that exhibits poorly developed or no perlitic fracture development. Samples S-4 and S-5 exhibit flow textures around phenocrysts in the glass groundmass. The 3 to 5% phenocrysts present in decreasing order of abundance include anhedral to euhedral plagioclase, sanidine, biotite, and quartz with rare zircon, sphene, and hornblende accessories. Swirls and streaks of hematite or randomly distributed opaque specks of magnetite are present in all thin sections. Feldspar-rich, asymmetrical, radial devitrification structures are present in S-5. No trace of relict glass shards or large concentrations of vesicles are visible in the glass groundmass.

Hand sample S-42 is a flow-banded felsite with quartz and biotite phenocrysts, and red felsic lithics. The thin section has a microcrystalline matrix containing abundant feldspar laths and subhedral plagioclase, sanidine and biotite. Rare sphene and zircon accessories are present. This sample has the same major phenocryst assemblage and accessory minerals as the underlying glass. S-42 is a dacite and reflects the variable composition of the overlying Mimbres Peak rhyolite.

Hand samples S-10, S-13, S-16, and S-17 are fractured, black, vitreous, glass with clear feldspar phenocrysts, red spherulites and red felsic veins. Numerous phenocrysts and

lithics are altered to white clay. Thin sections of these samples are 70 to 85% glass groundmass composed of horizontally oriented fiamme pumice fragments in a glass matrix. Pumice fragments are bent and crushed around adjacent volcanic lithics and phenocrysts. The entire groundmass has perlitic fracture development, not evident in hand samples. All samples contain 5 to 10% volcanic lithics; plagioclase-rich, oxide-stained andesite lithics are most common. Brown alteration rims of clay or zeolite commonly surround the volcanic lithics. Phenocrysts present in the groundmass in order of decreasing abundance include anhedral to euhedral plagioclase (zoned and unzoned), biotite, sandine, and rare, accessory zircon and hornblende. Glomerocrysts of plagioclase, sanidine, and biotite are present in S-13 and S-17. Randomly distributed opaque specks of magnetite are present in all thin sections. Samples S-10, S-13, S-16, and S-17 have horizontally aligned fiamme pumice with vesicles crushed parallel to the alignment direction.

THE WALLACE RANCH AREA

FIELD MAPPING. An outcrop map of the Wallace Ranch perlite occurrence was made at the scale of 1:12,000 (Plate 3). The map and lithologic units are based on the geologic map of Hahman (1989). Outcrops of a basal lithic tuff (Tlt), an overlying granular perlite breccia (Tpbx), and classical

perlite (Tpcs) are exposed below flow-banded rhyolite (Tr) on hillsides surrounding Pine Canyon. The basal lithic tuff (Tlt) and overlying granular perlite breccia (Tpbx) are mapped as separate units in this study. Hahman (1989) mapped both units as one and classified it as undifferentiated perlite (Tpu). Locally, lithic tuff (Tlt) overlies dark-gray, olivine basalt (Finnel, 1987). This contact is visible at the east and south margin of the study area. Finnell (1987) states the lithic tuff has a maximum thickness of 220 ft. Exposures of lithic tuff occur throughout the entire study area; its contact with overlying granular perlite breccia (Tpbx) is distinct (Plate 3).

Locally, exposures of granular perlite breccia (Tpbx) vary in thickness from 15 to 60 ft. The breccia consists of gray, banded, granular-perlite, cobbles and boulders in a white, sandy matrix. The breccia contact with overlying black, classical perlite (Tpcs) is distinct. The top 2 to 3 ft of granular perlite breccia adjacent to the overlying, black, classical perlite zone are completely welded. Below this welded horizon, breccia blocks occur in a white, sandy matrix. Thickness of the overlying black, classical perlite is quite consistent and averages 6 to 10 ft. The upper part of the perlite horizon grades into a spherulitic zone. Scattered red and brown, feldspar-rich, spherulites become more abundant up-section; they eventually

intergrow and form a dense, devitrified zone. The devitrified zone at the Wallace Ranch area interfingers with and grades into overlying, flow-banded rhyolite (Tr). The flow-banded rhyolite is gray to pink, dense, and contains cavities lined with vapor-phase, crystalline, quartz (R. Chamberlin, 1992, personal comm.). Rhyolite always overlies the classical perlite (Tpcs) and reaches a thickness of 320 ft in the southwest corner of the study area. Classical perlite (Tpcs) is absent in the north part of the study area. Siliceous, perlitic rhyolite tuff ((Tprt); Hahman, 1989) overlies granular perlite breccia (Tpbx) and grades upward into overlying flow-banded rhyolite. The siliceous, perlitic rhyolite tuff (Tprt) may be equivalent to the black classical perlite ((Tpcs); Hahman, 1989).

PETROGRAPHY. Thin sections of eight samples from the Wallace Ranch field area are described in Appendix B. Thin sections W-9, W-10, and W-17 are classical perlite. Thin sections W-19 and W-21 are from overlying, flow-banded rhyolite. Thin section W-1 is a spherulite and W-5 is a granular perlite. Thin section W-8 is from the basal lithic tuff (Tlt). Hand samples of the black, classical perlite are vitreous and exhibit pervasive perlitic fractures (Appendix A). Thin sections of the classical perlite contain 99% flow-textured glass. Sample W-10 has

asymmetrical devtrification structures aligned along flow bands. Phenocrysts and glomerocrysts of anhedral to subhedral sanidine, plagioclase, biotite, and rare hornblende are aligned in subparallel manner typical of a well-developed, trachytic texture (Fig. 4). All perlite and rhyolite samples have randomly distributed opaque specks of magnetite in the groundmass. The spherulite thin section (W-1) shows in detail, asymmetrical, radiating, fibrous bundles of microcrystalline feldspar and quartz growths (Lofgren, 1971). Rhyolite samples (W-19 and W-21) have miarolitic cavities lined with vapor phase quartz (Lofgren, 1971; R. Chamberlin, 1992, personal comm.). Microscopic textures include cryptocrystalline quartz and radiating devitrification structures.

Vitric lithic tuff (W-8) underlies the granular perlite breccia and contains andesite and basalt lithics, fiamme pumice fragments, and a variety of perlite fragments. Phenocrysts of plagioclase, sanidine and quartz occur in a cryptocrystalline silica matrix.

PHYSICAL TESTING. Physical tests using the methods of Barker and Hingtgen (1985), were conducted on perlite samples from the McDonald Ranch, Swartz, and Wallace Ranch field areas. GREFCO No Agua Peaks standards (referred to as the "GREFCO standard" or "standard" in the text) were

included at the start and finish of each series of field sample expansions. Expanded characteristics of field samples are compared to expanded standards. The compiled data are listed in Appendix C.

McDONALD RANCH PHYSICAL TESTING DATA. The 22 McDonald Ranch samples have an average yield of 94.1%. The 10 GREFCO standards have an average yield of 97.1%. McDonald Ranch expanded densities range from 2.66 to 25.5 lb/ft^3 (Fig. 5). A group of 12 samples ranges from 2.5 to 3.5 lb/ft^3. Omitting two outliers of 23.4 and 25.5 lb/ft^3, the remaining 20 samples have an average expanded density of 5.2 lb/ft^3. Standards range from 2.58 to 3.48 lb/ft^3 and average 3.1 lb/ft^3 (Fig. 5). Relative brightness of McDonald Ranch samples ranges from 46.2 to 63.6% and averages 57.9% (Fig. 6). Relative brightness of standards ranges from 64.6% to 71.2% and averages 68.9% (Fig. 6). The nonexpansible content of McDonald Ranch perlite samples ranges from 3.0 to 83.5% (Fig. 7). Omitting two outliers of 74.6 and 83.5%, the remaining 20 samples have an average nonexpansible content of 13.8%. The standards range from 1.9 to 5.9% nonexpansibles and have an average value of 4.8%. McDonald Ranch compacted densities range from 3.09 to 12.6 lb/ft^3 and average 5.6 lb/ft^3 (Appendix C). Compacted density of the standards ranges from 2.87 to 3.94 lb/ft^3 and averages 3.67 lb/ft^3. Sieve analysis data

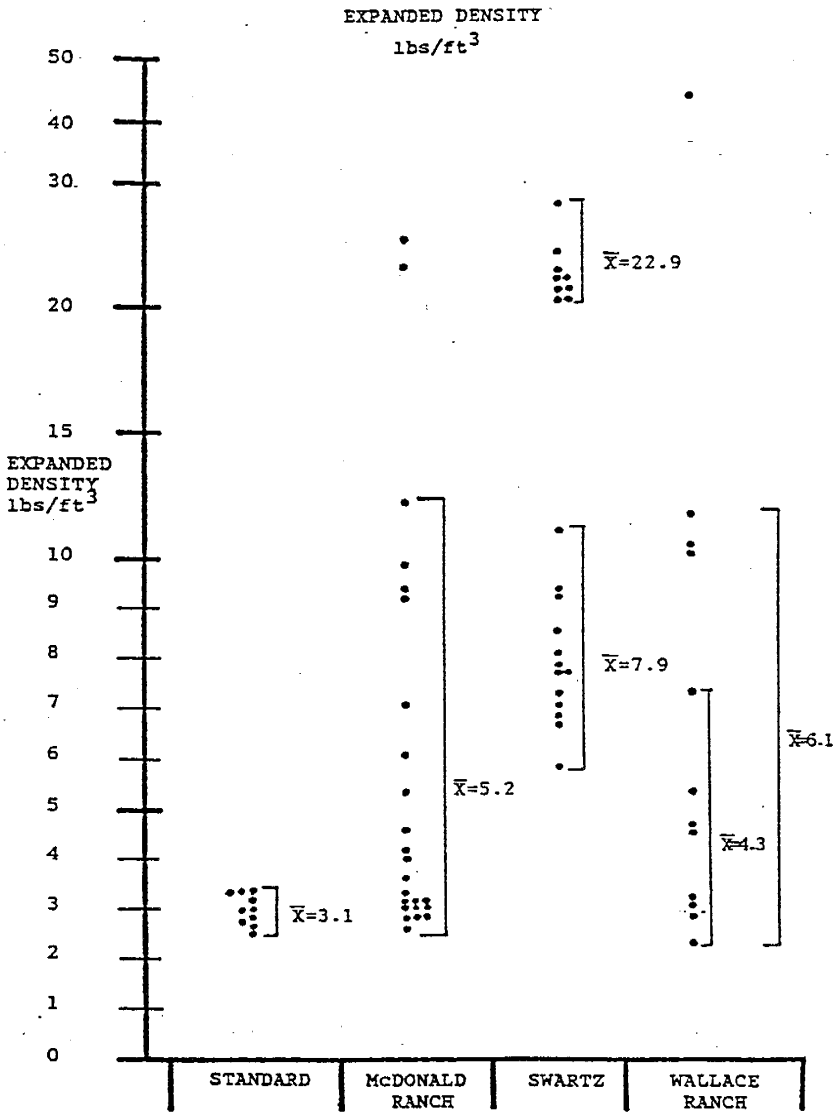

FIG. 5. Physical testing data. Expanded density of GREFCO standard, McDonald Ranch, Swartz, and Wallace Ranch perlite.

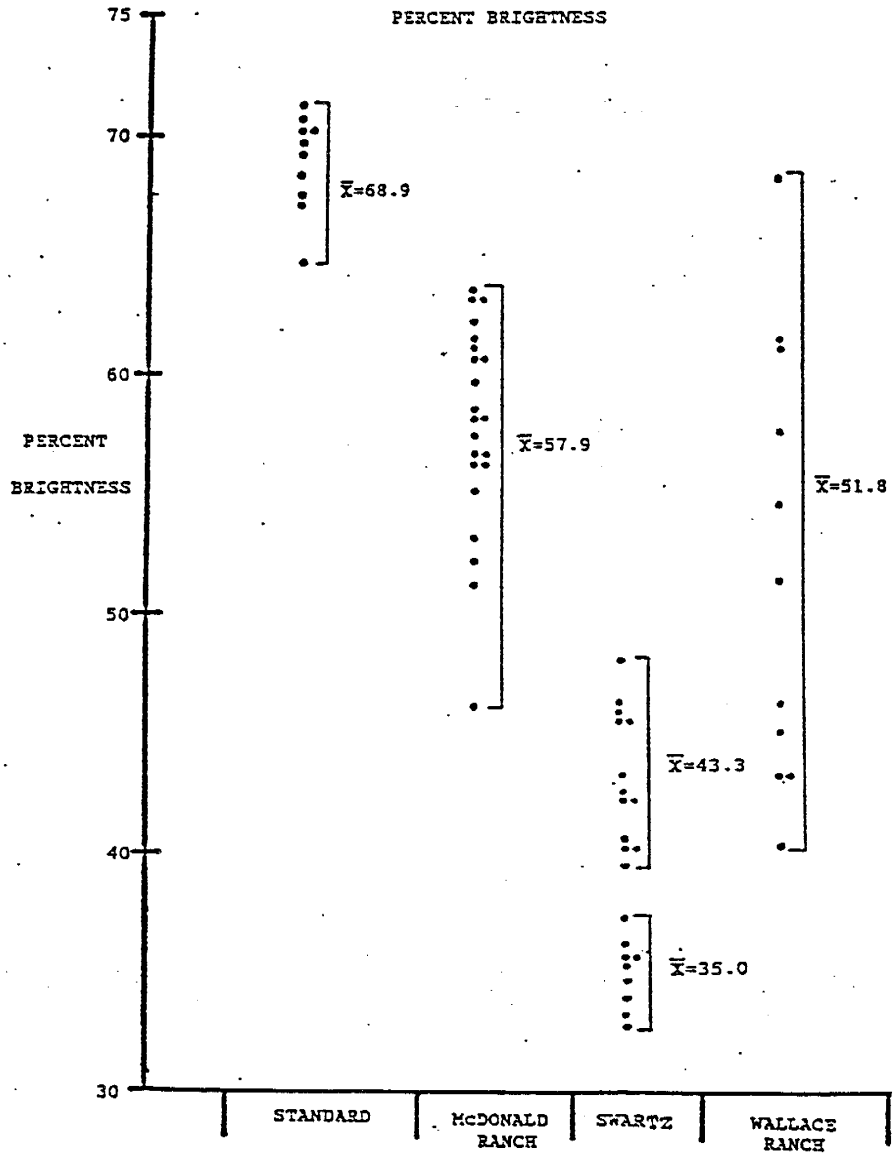

FIG. 6. Physical testing data. Percent brightness of GREFCO standard, Mcdonald Ranch, Swartz, and Wallace Ranch expanded perlite.

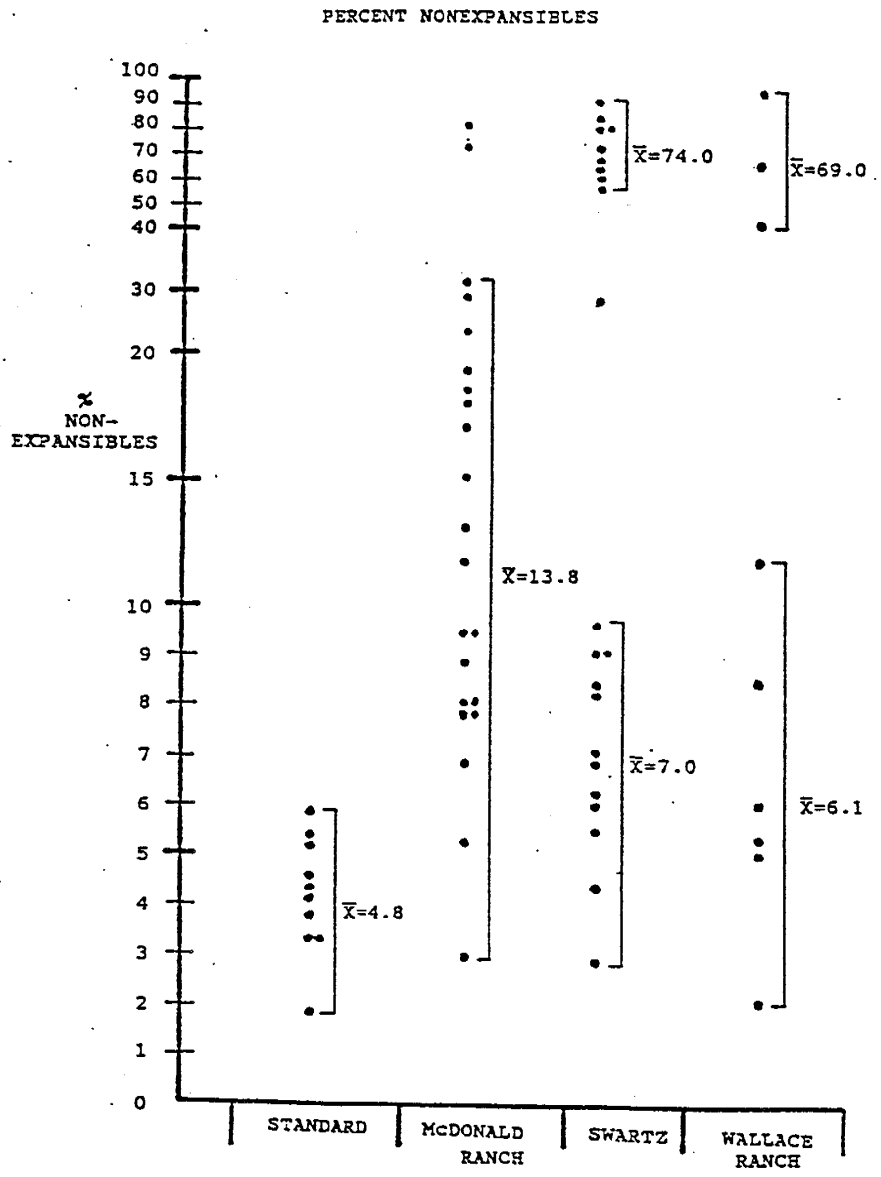

FIG. 7. Physical testing data. Percent nonexpansibles of GREFCO standard, McDonald Ranch, Swartz, and Wallace Ranch expanded perlite.

of expanded McDonald Ranch perlite and GREFCO standards are listed in Appendix C. Average percent retained values are in Table 1.

TABLE 1.

Sieve data showing average percent retained on each screen for expanded McDonald Ranch perlite.

MESH SIZE	20	30	50	70	100	140	PAN
STANDARD (% retained)	3.0	29.7	52.8	10.0	3.2	0.89	0.4
McDONALD R (% retained)	1.4	23.5	56.8	11.6	3.9	1.4	1.4

McDonald Ranch perlite sieve analyses data similar to the GREFCO standard except in the coarse fractions (+20 and +30 mesh) and in the fine fractions (+140 and pan). Less McDonald Ranch perlite expands to the two coarser fractions. McDonald Ranch perlite generates more -100 mesh fines due to breaking of expanded particles upon vesiculation.

SWARTZ AREA PHYSICAL TESTING DATA. The Swartz area data exhibit a distinct difference between expanded welded tuff

and perlite samples. Although both data sets appear on the same figure (Figs. 5, 6, and 7), each will be discussed separately.

SWARTZ PERLITE SAMPLES. The 13 Swartz perlite samples (outcrops N72W and N55E) have an average yield of 97.2%. The 10 GREFCO standards average 97.1% yield. Swartz perlite expanded densities range from 5.95 to 11.03 lb/ft^3 (Fig. 5). A group of 13 samples has an average expanded density of 7.9 lb/ft^3. Standards range from 2.58 to 3.48 lb/ft^3 and average 3.1 lb/ft^3. Brightness of Swartz perlite ranges from 40.1 to 48.1% and averages 43.3% (Fig. 6). Standards range from 64.6 to 71.2% brightness and average 68.9% (Fig. 6). Swartz perlite has a nonexpansible content of 2.9 to 9.7% and averages 7.0% (Fig. 7). Standards range from 1.9 to 5.9% nonexpansibles and average 4.8%. Compacted densities of Swartz perlite range from 8.67 to 9.56 lb/ft^3 and average 9.27 lb/ft^3. Standards range from 2.87 to 3.94 lb/ft^3 and have an average compacted density of 3.67 lb/ft^3. Sieve analyses data of expanded Swartz perlite and GREFCO standards are in Appendix C. Average percent retained values are in Table 2.

TABLE 2.

Sieve data showing average percent retained on each screen for expanded Swartz perlite.

MESH SIZE	20	30	50	70	100	140	PAN
STANDARD (% retained)	3.0	29.7	52.8	10.0	3.2	0.89	0.4
SWARTZ (% retained)	0.1	5.3	80.7	11.6	1.8	0.29	0.2

Expanded Swartz perlite sieve analyses differ from the GREFCO standard in the coarse and fine fractions. Although less fines are being generated by Swartz perlite, most of the expanded material is in the +50 mesh fraction and very little in the +30 and +20 mesh fractions.

SWARTZ WELDED TUFF. Nine Swartz welded tuff samples have an average yield of 96.2%. The 10 GREFCO standards have an average yield of 97.1%. Swartz welded tuff expanded densities range from 20.6 to 28.1 lb/ft^3 (Fig. 5) and average 22.9 lb/ft^3. Standards range from 2.58 to 3.48 lb/ft^3 and average 3.1 lb/ft^3 (Fig. 5). Brightness of welded tuff samples ranges from 32.9 to 37.3% and

averages 35.0% (Fig. 6). Standards range from 64.6 to 71.2% brightness and average 68.9% (Fig. 6). The nonexpansible content of Swartz welded tuff samples ranges from 58.2 to 90.4% and averages 74.0% (Fig. 7). Standards range from 1.9 to 5.9% nonexpansibles and average 4.8% (Fig. 7). Compacted densities of Swartz welded tuff samples were not calculated due to their high initial expanded densities. Compacted densities of standards range from 2.87 to 3.94 lb/ft^3 and average 3.67 lb/ft^3. Sieve analysis data of expanded Swartz welded tuff and GREFCO standards are in Appendix C. Average percent retained values are in Table 3.

TABLE 3.

Sieve data showing average percent retained on each screen for expanded Swartz welded tuff.

MESH SIZE	20	30	50	70	100	140	PAN
STANDARD (% retained)	3.0	29.7	52.8	10.0	3.2	0.89	0.4
SWARTZ (% retained)	0.2	0.2	42.9	43.0	12.5	1.1	0.4

Swartz welded tuff sieve analysis data differ from the

standard in the coarse size fraction (+20 and +30 mesh) and in the +70 and +100 mesh range. These differences reflect the poor expansibility of the welded tuff.

WALLACE RANCH AREA PHYSICAL TESTING DATA. Eleven expanded Wallace Ranch samples have an average recovery of 93.9%. Ten expanded GREFCO standards average 97.1%. Wallace Ranch perlite expanded densities form two groups, one group of three samples averages 10.9 lb/ft^3. The second group averages 4.3 lb/ft^3 (Fig. 5). Both groups combined range from 2.4 to 11.9 lb/ft^3 and have an average expanded density of 6.1 lb/ft^3. An outlier of 44.8 lb/ft^3 is omitted from the data. Brightness of Wallace Ranch perlite ranges from 40.5 to 68.4% and averages 51.8% (Fig. 6). The nonexpansible content of Swartz samples has a bimodal distribution. The first group ranges from 2.2 to 11.9% nonexpansibles and averages 6.1%. The second group has three members that range from 43 to 96.8% and average 69.0% (Fig. 7). Average compacted density of Wallace Ranch perlite is 5.69 lb/ft^3. Sieve analysis data of Wallace Ranch expanded perlite and GREFCO standards are in Appendix C. Average percent retained values are in Table 4.

TABLE 4.

Sieve data showing average percent retained on each screen for expanded Wallace Ranch perlite.

MESH SIZE	20	30	50	70	100	140	PAN
STANDARD (% retained)	3.0	29.7	52.8	10.0	3.2	0.89	0.4
WALLACE R. (% retained)	0.62	12.3	55.2	18.0	8.12	3.5	2.3

Wallace Ranch perlite sieve analyses indicate a lack of expansion into the coarse (+20 and +30 mesh) fraction and a higher percent of fines in the -100 mesh fraction.

NONEXPANSIBLES. Visual classification of the nonexpansible material recovered from the furnace during perlite expansion was conducted with a binocular microscope. A compilation of these observations is in Appendix E.

GREFCO NO AGUA PEAKS STANDARD NONEXPANSIBLES. The nonexpansible fraction of all GREFCO standards consists of 80 to 90% clear, unexpanded or partially expanded, vitreous, glass particles in the +100 mesh range. Lesser constituents

include: glass shards; rare, clear quartz and feldspar phenocrysts; and rare, biotite phenocrysts.

McDONALD RANCH NONEXPANSIBLES. The most common constituent of the nonexpansible fraction of all samples is clear, slightly melted, unexpanded or partially expanded, vitreous glass particles in the +100 mesh range. These glass particles are filled with small white bubbles that make the glass appear white. These glass particles account for 50 to 93% of the unexpanded fraction of each sample. Other common unexpanded particles include: opaque white and gray glass fragments; clear glass shards and fragments; broken glass vesicle walls; biotite, clear feldspar, and quartz fragments and phenocrysts; and rare amber sphene fragments.

SWARTZ PERLITE NONEXPANSIBLES. The most common constituent of the nonexpansible fraction of Swartz perlite is unexpanded, opaque white, granular, vitreous, glass particles in the +100 mesh range. These glass particles account for 50 to 95% of the unexpanded fraction of each sample. Lesser common unexpanded particles include: partially expanded clear glass particles; black biotite and clear feldspar phenocrysts; clear quartz fragments; opaque pink glass fragments; and amber sphene fragments.

SWARTZ WELDED TUFF NONEXPANSIBLES. The most common constituent of the nonexpansible fraction of all samples is unexpanded, opaque white, vitreous, granular glass in the +100 mesh range. These glass particles account for 70 to 97% of the unexpanded fraction of each sample. Other common unexpanded particles include: black-andesitic and red-basalt volcanic lithics; opaque gray or pink glass shards; rare biotite and clear feldspar phenocrysts; and rare, clear, quartz fragments.

WALLACE RANCH PERLITE NONEXPANSIBLES. The most common constituent of the nonexpansible fraction of most samples is unexpanded and partially expanded, clear or opaque white, vitreous glass particles in the +100 mesh range. The clear glass particles are filled with minute white bubbles that give the glass a white hue. The opaque white glass particles have a distinctly granular texture. Both particles account for nearly 80% of the unexpanded fraction of most samples. Other unexpanded particles that commonly occur with the glass particles include: biotite, feldspar, and quartz phenocrysts; glass shards; and rare, euhedral hornblende phenocrysts and amber sphene fragments. Sample W-18-A (Tlt) has a nonexpansible fraction composed of 80% basalt and andesite volcanic lithics with lesser, partially expanded white glass particles and rare biotite and feldspar phenocrysts.

SCANNING ELECTRON MICROSCOPY (SEM).

GREFCO SOCORRO PIT PUMICEOUS PERLITE SEM PHOTOMICROGRAPHS: Figure 8 shows abundant, flattened, vesicles typical of pumiceous, perlite texture. Note the lack of classical perlitic fracture development. Figure 9 shows the bulbous form of expanded perlite caused by vesiculation of molecular water when perlite particles reach the softening range. Note the presence of broken particle walls and abundance of particle fragments. These features result from bursting of particles during rapid expansion. Figure 10 is a magnified view (X250) of a burst particle wall. Note the interior honeycomb texture formed by adjacent vesicle walls. Figure 11 shows a variety of unexpansible particles recovered from the furnace. Euhedral plagioclase phenocrysts, phenocryst fragments, glass shards, and unexpanded glass particles are visible in the photomicrograph.

McDONALD RANCH SEM PHOTOMICROGRAPHS. Figure 12 shows the concentric, onionskin fracture pattern typical of classical perlite. Fractures form at the boundary of hydrated and unhydrated glass as a result of tensional strain associated with a volume increase of the hydrated glass (Friedman and Smith, 1958). Figure 13 shows the bulbous form of expanded perlite caused by vesiculation of molecular water while the glass is in the softening range. Broken vesicle walls

photomicrograph.

SWARTZ WELDED TUFF SEM PHOTOMICROGRAPHS. Figure 20 shows the lack of visible perlitic fracture, vesicles or fracture texture in Swartz welded tuff. The fracture pattern can best be described as hackly. Figure 21 shows expanded welded tuff particles and the total lack of expansion typical of Swartz welded tuff particles. Only the particle in the center of Figure 21 displays partial expansion. The surrounding particles are glass shards.

Figure 22 is a magnified view (X250) of the partially expanded particle. Partial melting occurred but no signs of vesiculation are visible. Figure 23 is a photomicrograph of unexpansible glass shards and phenocryst fragments.

WALLACE RANCH GRANULAR PERLITE SEM PHOTOMICROGRAPHS. Figure 24 is a magnified view (X200) of the frothy texture of granular perlite; note the absence of perlitic fractures. Figure 25 shows the bulbous form of expanded granular perlite. The particle walls may rupture during expansion. Figure 26 shows the interior of a ruptured, expanded particle; note the thin outer walls and the honeycomb interior structure. Figure 27 shows unexpansible particles of partially expanded glass, glass shards, and broken vesicle walls.

WALLACE RANCH CLASSICAL PERLITE SEM PHOTOMICROGRAPHS. Figure 28 shows the concentric, perlitic fracture of Wallace Ranch classical perlite. This texture is typical of classical perlite. Figure 29 shows the bulbous shape of expanded classical perlite and the occurrence of burst, expanded particles. Figure 30 shows the interior of a burst particle; note the thin outer wall and the interior, honeycomb texture. Burst particles and broken vesicle walls may result from over-expansion or handling during SEM mount preparation. Figure 31 shows a variety of nonexpansible particles from expanded Wallace Ranch classical perlite. A feldspar phenocryst, glass shards, broken vesicle walls and phenocryst fragments are visible in the photomicrograph.

GEOCHEMISTRY

PENNFIELD TEST. The Pennfield test (Jenkins, 1972) was used to determine the total water content of selected McDonald Ranch, Swartz, and Wallace Ranch perlite samples. Figure 32 shows the distribution of water content in weight percent among individual samples from each perlite occurrence. Perlite water content ranges from 1.73% (WR-1) to 5.78% (MR-4). All McDonald Ranch samples are perlites, with water contents that range from 3.63% to 5.78%. Swartz samples include perlite (S-2, 4, and 7), welded tuff (S-10 through 25) and a spherulite (S-2B). Water contents of the perlite and welded tuff are nearly equal (Fig. 32). The spherulite

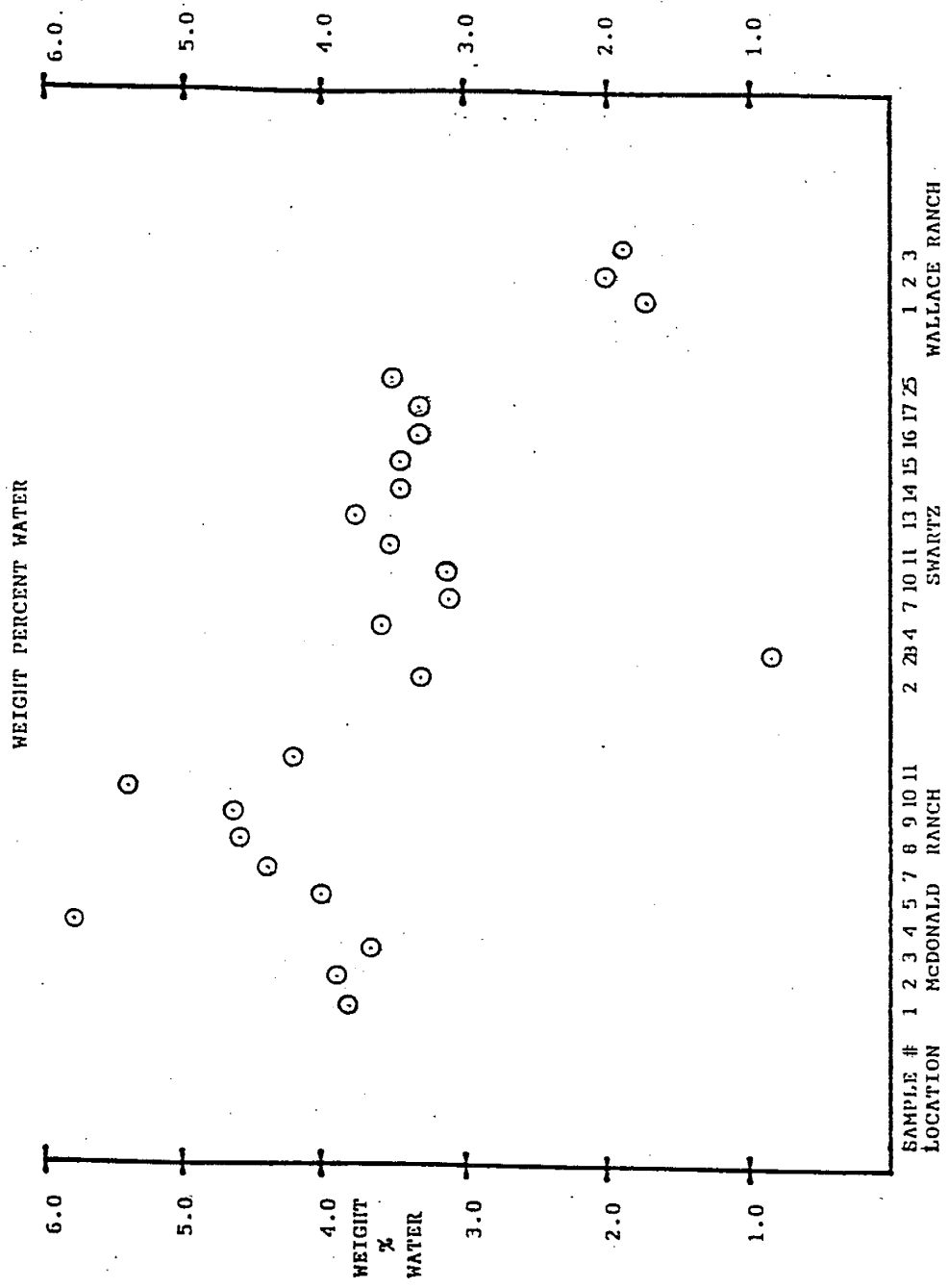

FIG. 32. Pennfield test results. Wt % water content of McDonald Ranch, Swartz, and Wallace Ranch perlite and welded tuff samples.

water content is very low, 0.82%. Water content of Wallace Ranch granular perlite (WR-3) is nearly equal to the two classical perlite samples WR-1 and WR-2. All three samples range from 1.73 to 2.00 wt %.

X-RAY FLUORESCENCE SPECTROMETRY (XRF). A complete compilation of XRF analyses of McDonald Ranch, Swartz, and Wallace Ranch perlites and rhyolites is in Appendix D. Major and trace element analyses were conducted on selected perlite and rhyolite samples. The analytical method of elemental parameters used during XRF analysis assumes the analytical standard and unknowns have the same chemical composition (C. Mckee, 1992, personal comm.). This assumption does not account for volatiles and produces compositions that total greater than 100%. Oxide data were recalculated to anhydrous composition before the data were plotted. The relative wt % of oxides in perlites and adjacent rhyolites or tuffs are used to determine if a genetic relationship between adjacent lithologies exists. Due to secondary hydration and related movement of large quantities of meteoric water through the perlite, wt % of immobile elements are plotted against wt % SiO_2. Selected trace elements are plotted against Nb, because niobium is unlikely to be mobilized during hydration and devitrification (Spell, 1987).

McDONALD RANCH XRF DATA. A distinct difference in oxide content exists between the lower rhyolite and the overlying perlite and rhyolite. The lower rhyolite has a higher SiO_2 content than the two overlying horizons. A decreasing Al_2O_3 and Fe_2O_3 trend occurs as the SiO_2 content of both rhyolites increases (Figs. 33 and 34). This trend occurs with perlite Al_2O_3 content (Fig. 33). A small degree of overlap occurs between perlite and overlying rhyolite oxide data. Although the rhyolite has a slightly greater SiO_2 content than the perlite, both exhibit very similar Al_2O_3 and Fe_2O_3 concentrations (Figs. 33 and 34). The standard has an Al_2O_3 content that plots among the perlite group but the Fe_2O_3 content is less than either the perlite or overlying rhyolite. Lower rhyolite, oxide data are isolated from the other groups as a result of its higher SiO_2 and lower oxide contents. All three groups exhibit a decreasing abundance of Al_2O_3 with increasing SiO_2.

Figure 35 is a plot of wt % MgO vs wt % SiO_2. No distinct correlation between MgO and SiO_2 content is visible in the groups. The lower rhyolite MgO content falls in the same range as the overlying perlite. No overlap of data occurs. The standard has less MgO content than the perlite and plots in the rhyolite range.

Figure 36 is a plot of wt % TiO_2 vs wt % SiO_2. No

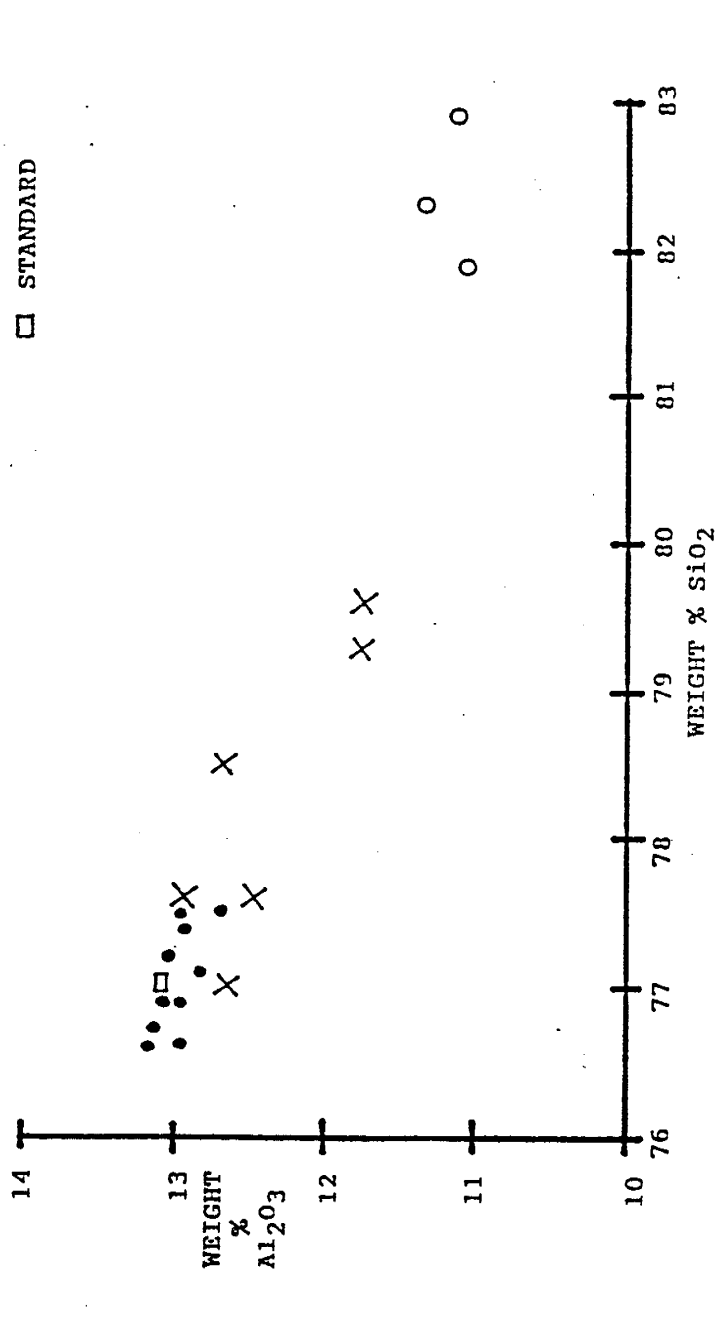

FIG. 33. McDonald Ranch XRF data. Al_2O_3 vs SiO_2. All oxides are expressed in wt %.

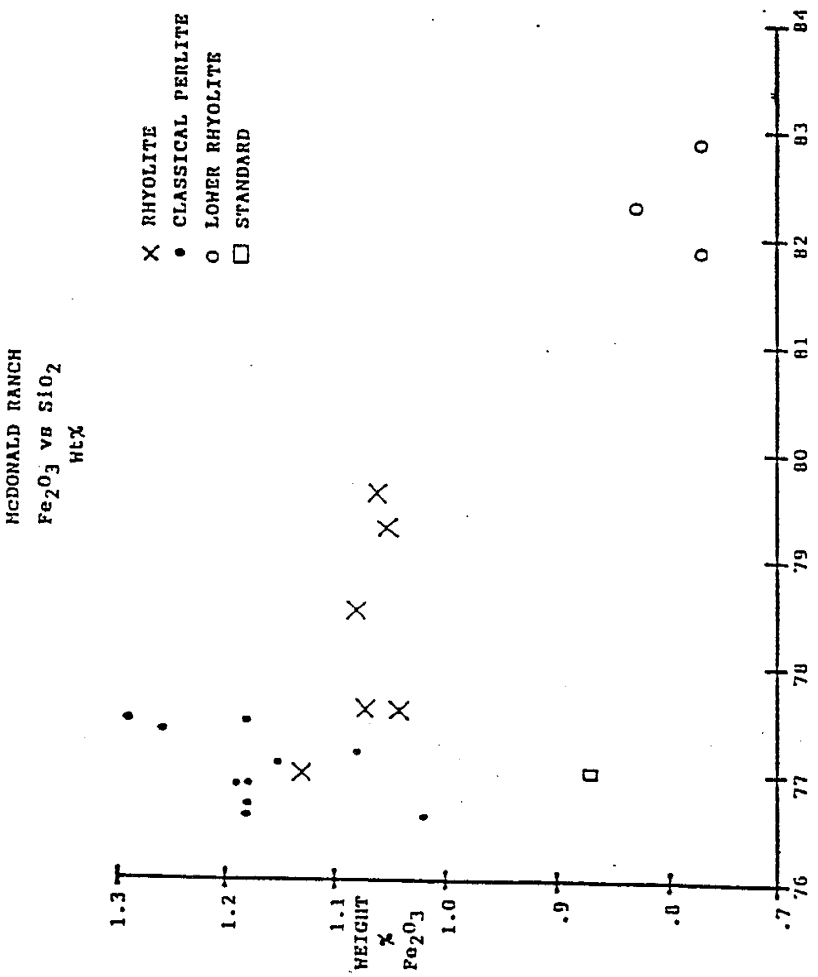

FIG. 34. McDonald Ranch XRF data. Fe_2O_3 vs SiO_2. All oxides are expressed in wt %.

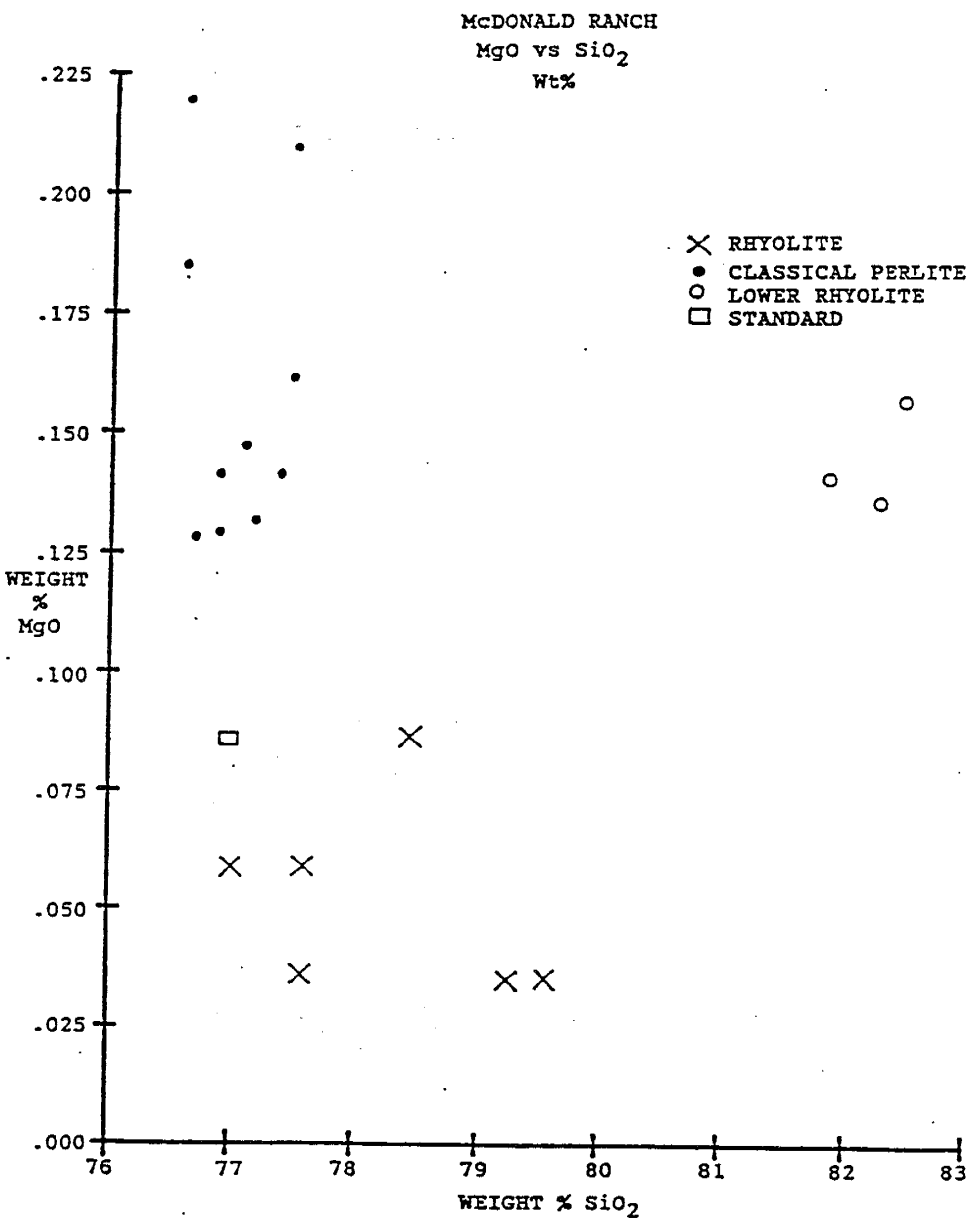

FIG. 35. McDonald Ranch XRF data. MgO vs SiO_2. All oxides are expressed in wt %.

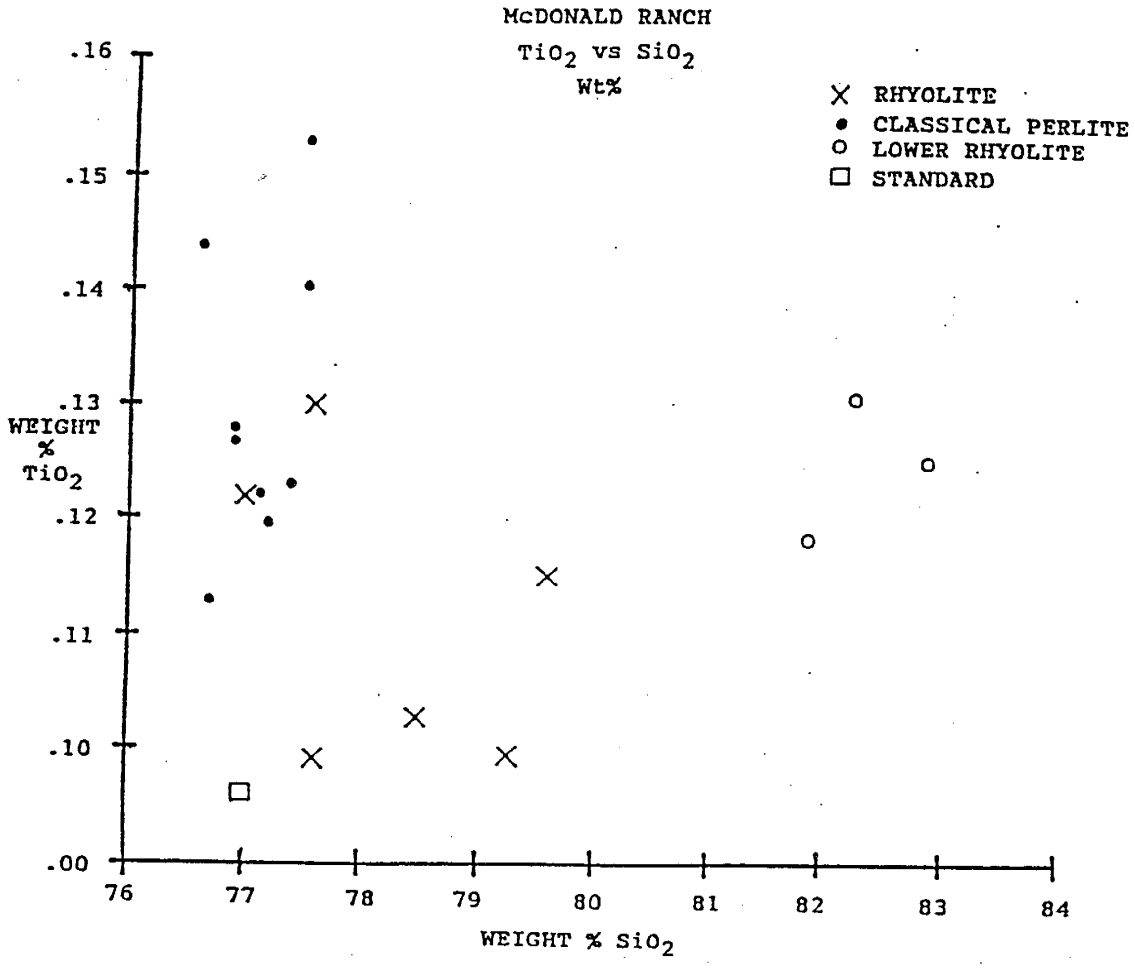

FIG. 36. McDonald Ranch XRF data. TiO_2 vs SiO_2. All oxides are expressed in wt %.

distinct correlation between TiO_2 and SiO_2 content is visible in the groups. A slight overlap of perlite and overlying rhyolite data occurs. The lower rhyolite data are within the perlite and rhyolite TiO_2 content range, but is in the richer SiO_2 field. The standard has a lower TiO_2 wt % than the perlite or the two rhyolites.

Trace element data from the McDonald Ranch area is in Figure 37. The ppm values of Ti, V, and Cr are combined and divided by the Nb ppm value; the result is plotted against the Nb ppm value. This procedure takes advantage of the common association of Ti, V, and Cr and will lessen any existing analytical error. Differences in Ti, V, and Cr concentrations between lithologies and similar Nb concentrations prevent induced correlation of the data sets. A slight correlation between the perlite Ti, V, and Cr values and increasing Nb content exists. A similar correlation is absent in the two rhyolites. The standard has an Nb content of 103.68 ppm and plots off the data field. Perlite and overlying rhyolite data group within the same range of total values but the perlite is richer in Nb. The lower rhyolite has less combined Ti, V, and Cr, and a lower Nb content than both overlying units.

SWARTZ XRF DATA. Major element oxide and trace element data from Swartz perlite, overlying rhyolite, welded tuff, lithic

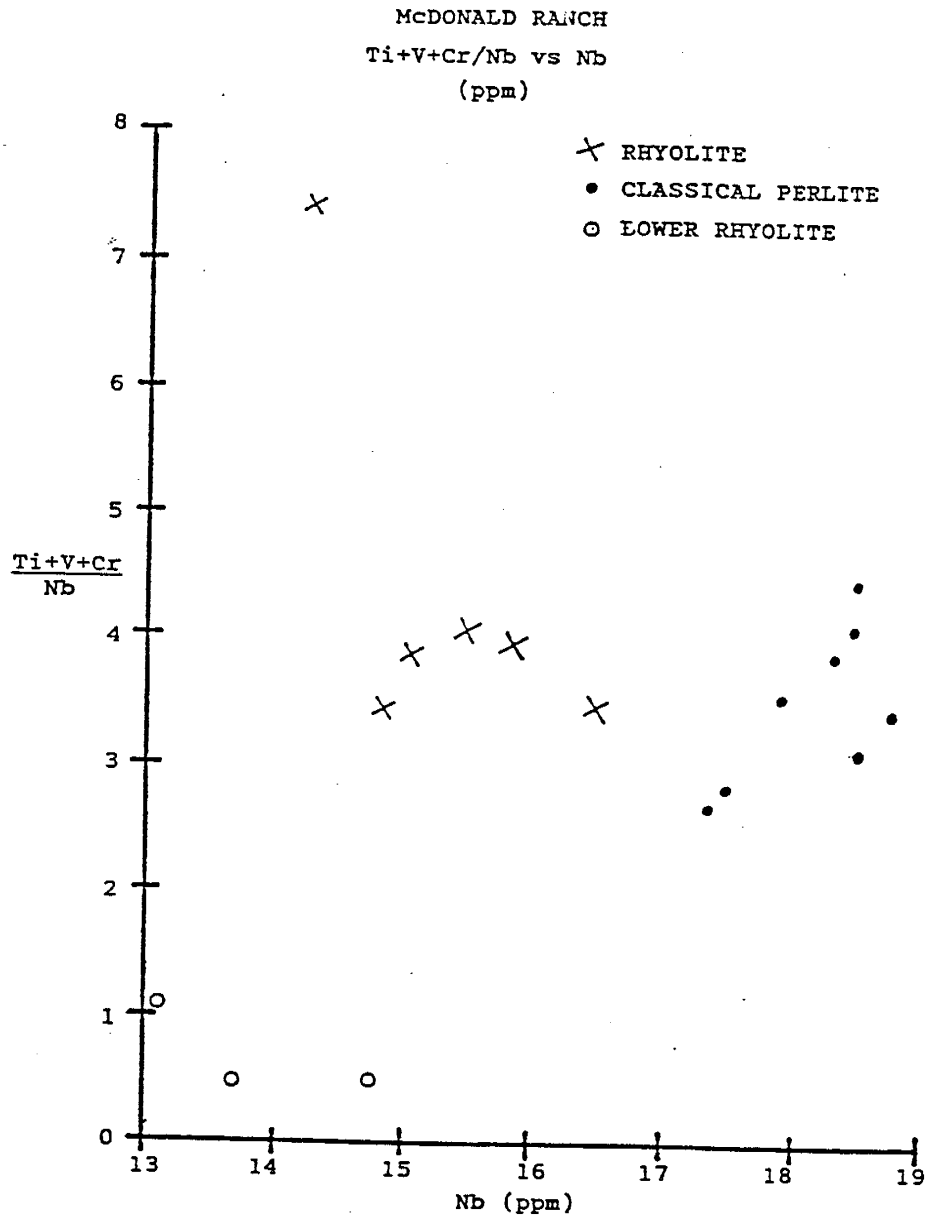

FIG. 37. McDonald Ranch XRF data. Ti+V+Cr/Nb vs Nb. All trace elements are expressed in ppm.

tuff and a standard are plotted on corresponding diagrams. Figure 38 shows a distinct correlation between decreasing Al_2O_3 and increasing SiO_2 for each data group. Considerable overlap occurs with all data groups except for the welded tuff and rhyolite.

Figure 39 shows a correlation between decreasing Fe_2O_3 and increasing SiO_2 in the rhyolite and lithic tuff data groups. No trend is visible in perlite and welded tuff data. Lithic tuff data overlap perlite, welded tuff and rhyolite data. The perlite data plot below welded tuff data and above rhyolite data with respect to Fe_2O_3 content. The standard plots in the lower rhyolite Fe_2O_3 concentration range.

All data groups exhibit a decreasing TiO_2 content with increasing SiO_2 (Fig. 40). Lithic tuff displays the widest range of TiO_2 wt % values. Lithic tuff, perlite, and rhyolite data overlap. Perlite data plot above and overlap into the rhyolite data field. The welded tuff has a higher TiO_2 concentration than perlite and rhyolite but does not overlap into either data field. The GREFCO standard has 0.063 wt % TiO_2 and plots below the data field in Figure 40.

Figure 41 displays wt % MgO versus SiO_2 data. Perlite

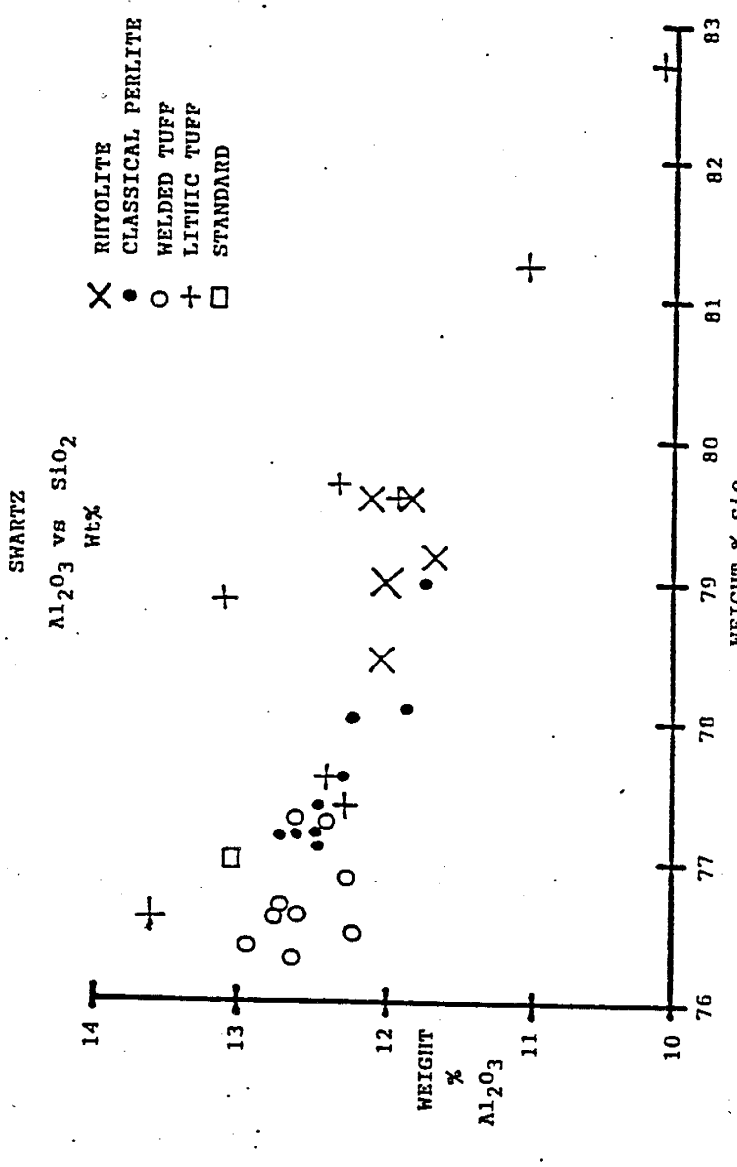

FIG. 38. Swartz XRF data. Al_2O_3 vs SiO_2. All oxides are expressed in wt %.

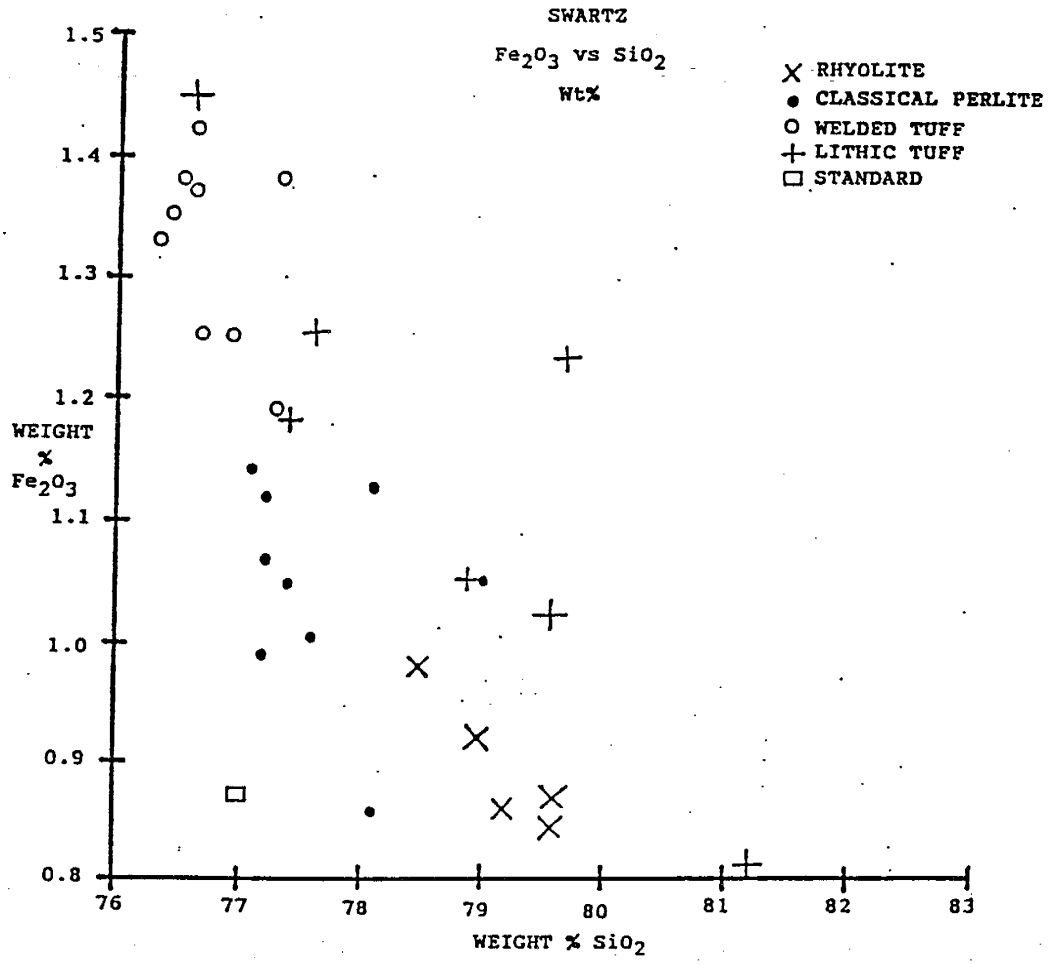

FIG. 39. Swartz XRF data. Fe_2O_3 vs SiO_2. All oxides are expressed in wt %.

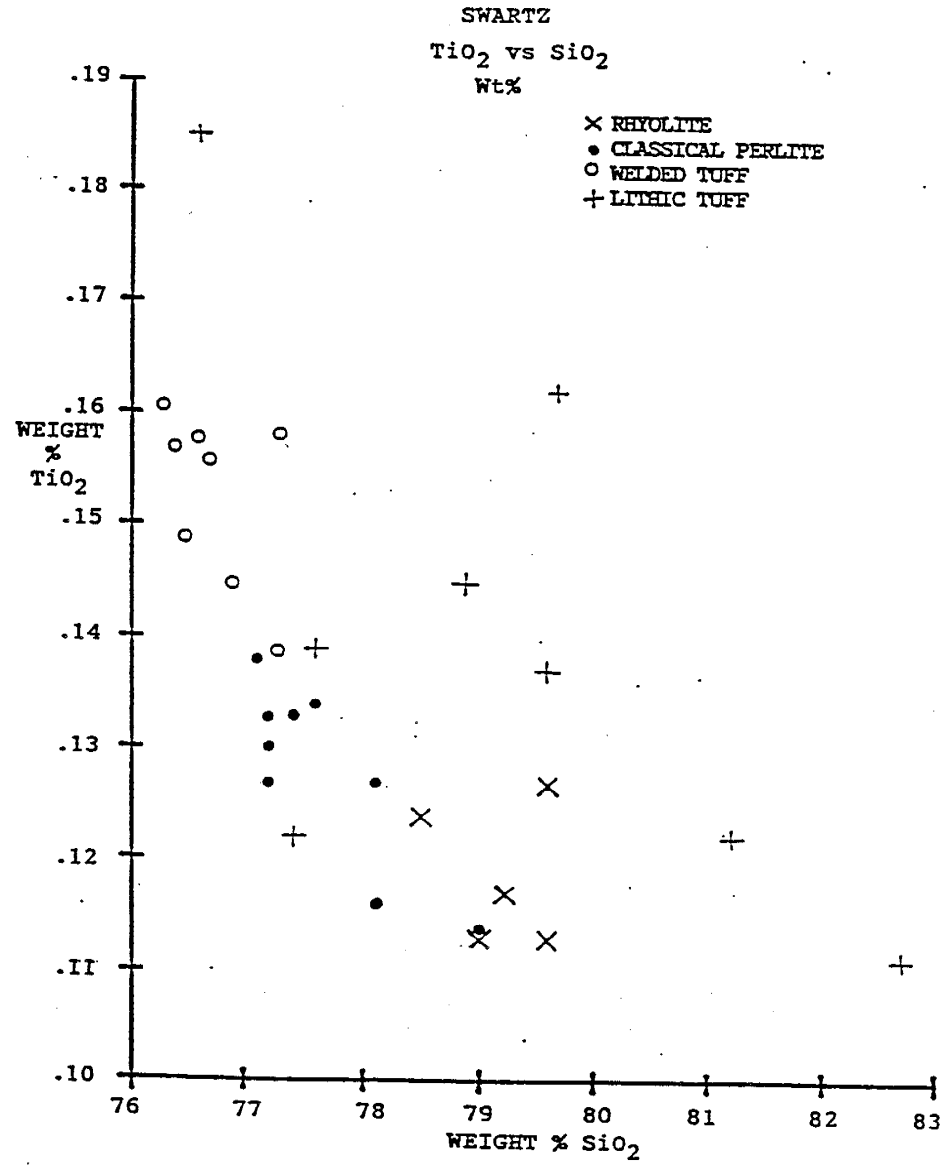

FIG. 40. Swartz XRF data. TiO_2 vs SiO_2. All oxides are expressed in wt %.

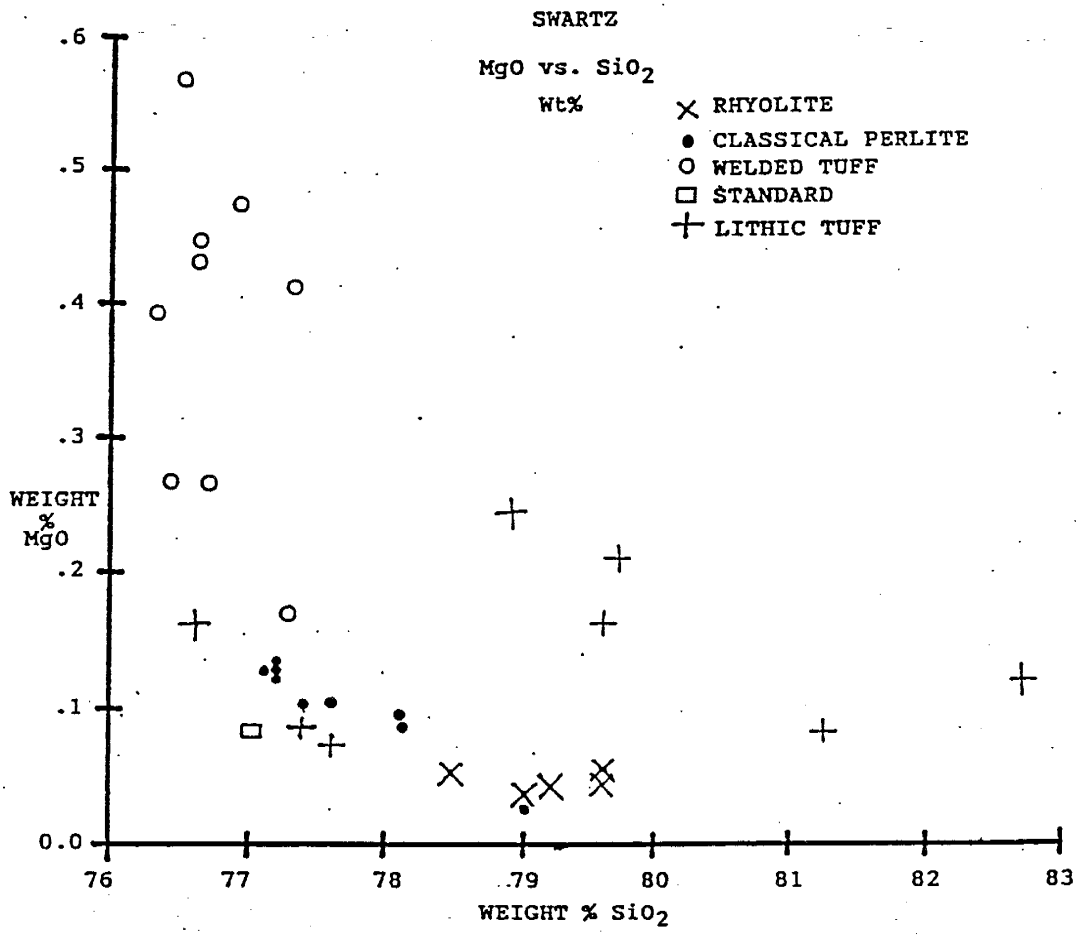

FIG. 41. Swartz XRF data. MgO vs SiO_2. All oxides are expressed in wt %.

shows a distinct decreasing MgO concentration with increasing SiO_2. Other data groups show little or no visible correlation. Overlap of perlite, rhyolite, and lithic tuff data is evident. Welded tuff MgO data plot above the other data with no overlap. The standard plots in the perlite-lithic tuff-rhyolite range (0.87 wt %).

Selected trace element data include Ba vs Nb and Sr vs Nb diagrams (Figs. 42 and 43). Figure 42 shows the narrow and nearly equal range of Ba values for the perlite and overlying rhyolite. No correlation between Ba concentration and Nb is visible in any of the data sets. The lithic tuff has the widest range of Ba values and overlaps the other three data groups. The welded tuff is richer in Ba than perlite and rhyolite. All data occur within a 15 ppm range of Nb concentration. The standard has a concentration of 103.68 ppm Nb and 24.07 ppm Ba. Consequently, the standard plots below and to the right of the Figure 42 data field.

Figure 43 is an Sr vs Nb diagram; no correlation between Sr and Nb concentrations is demonstrated by the data sets. The lithic tuff has the widest range of Sr values and overlaps the other three data groups. Perlite and overlying rhyolite Sr data occur within the same narrow range of Sr values. Rhyolite samples display a particularly tight grouping of both Nb and Sr values. The welded tuff is

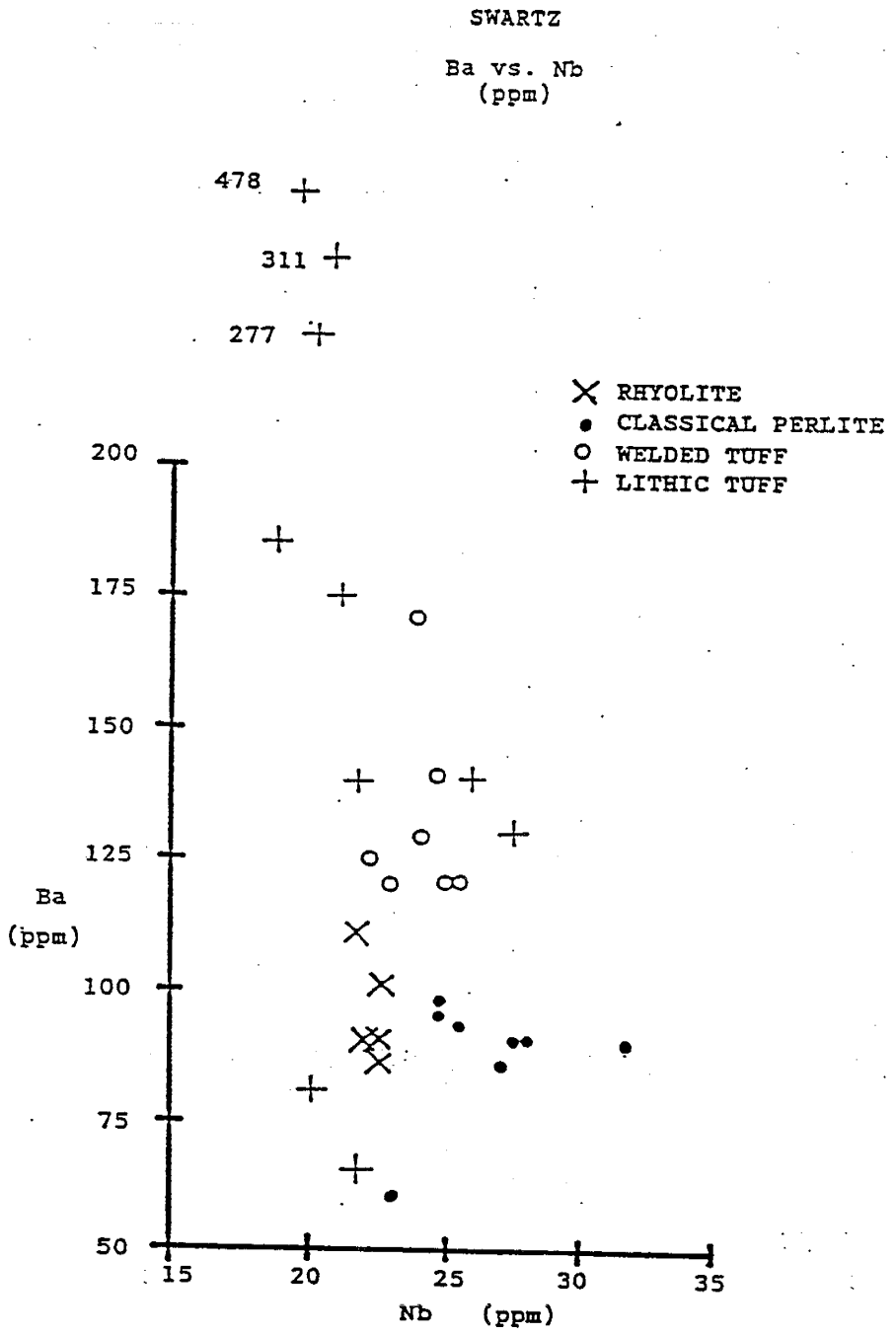

FIG. 42. Swartz XRF data. Ba vs Nb. All trace elements are expressed in ppm.

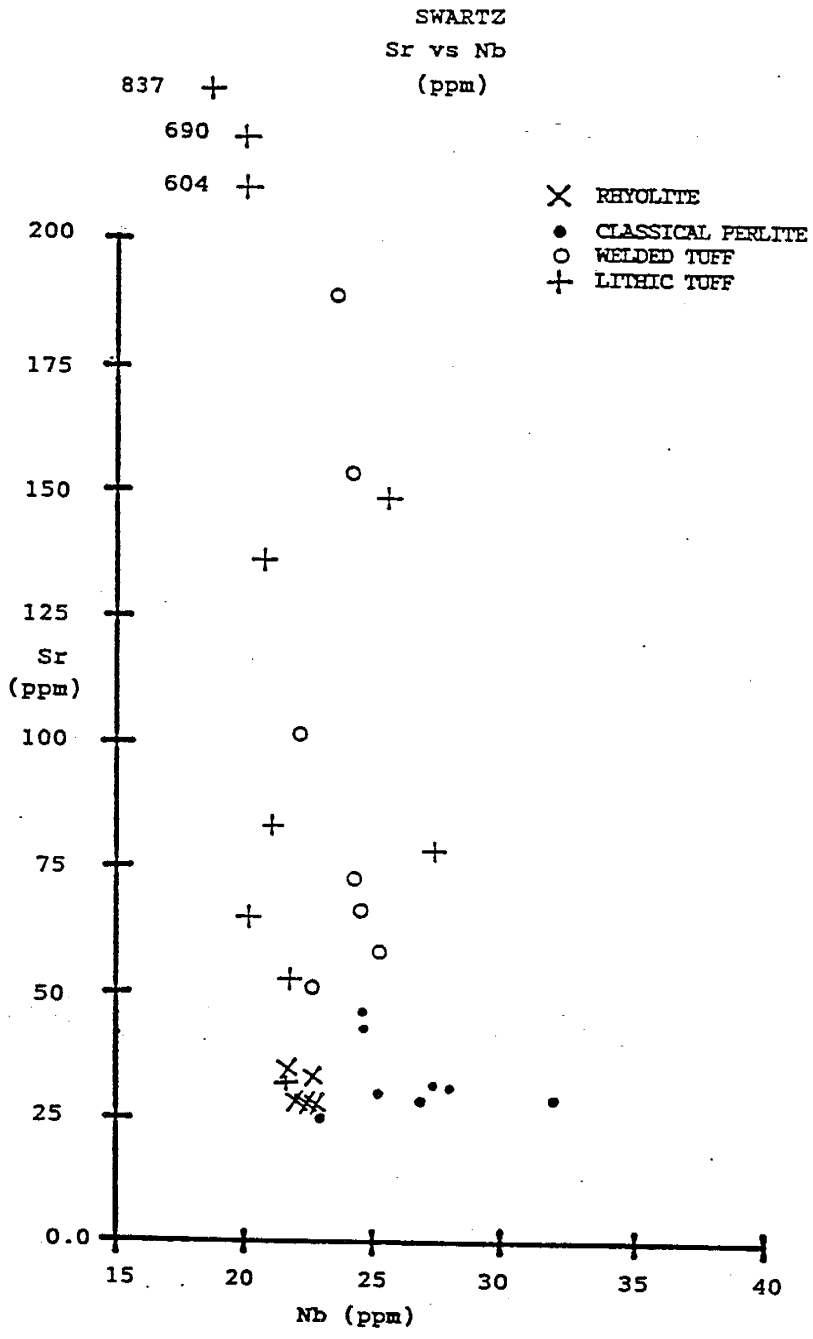

FIG. 43. Swartz XRF data. Sr vs Nb. All trace elements are expressed in ppm.

richer in Sr and has a wider range of Sr values than perlite and rhyolite samples. All data groups occur within a 15 ppm range of Nb values. The standard has Nb and Sr concentrations of 103.68 ppm Nb and 2.39 ppm Sr. These values plot below and to the right of the Figure 43 data field.

WALLACE RANCH XRF DATA. Figure 44 shows a decrease of granular perlite Al_2O_3 content with an increase of SiO_2. Granular perlite has the widest range of Al_2O_3 values. No correlation between Al_2O_3 content and SiO_2 is evident among the other data groups. The classical and granular Al_2O_3 vs SiO_2 data overlap. The overlying rhyolite has the lowest concentration of Al_2O_3 of the data groups in Figure 44.

Figure 45 shows wt % TiO_2 vs SiO_2 data. The granular perlite group has the widest range of TiO_2 data values and overlaps the other two groups. A correlation between decreasing TiO_2 and increasing SiO_2 is visible in granular perlite data. No correlation is visible among the other two groups. The GREFCO standard has a TiO_2 concentration of 0.063 wt % and plots below the Figure 45 data field.

Wt % MgO versus SiO2 is plotted on Figure 46. No

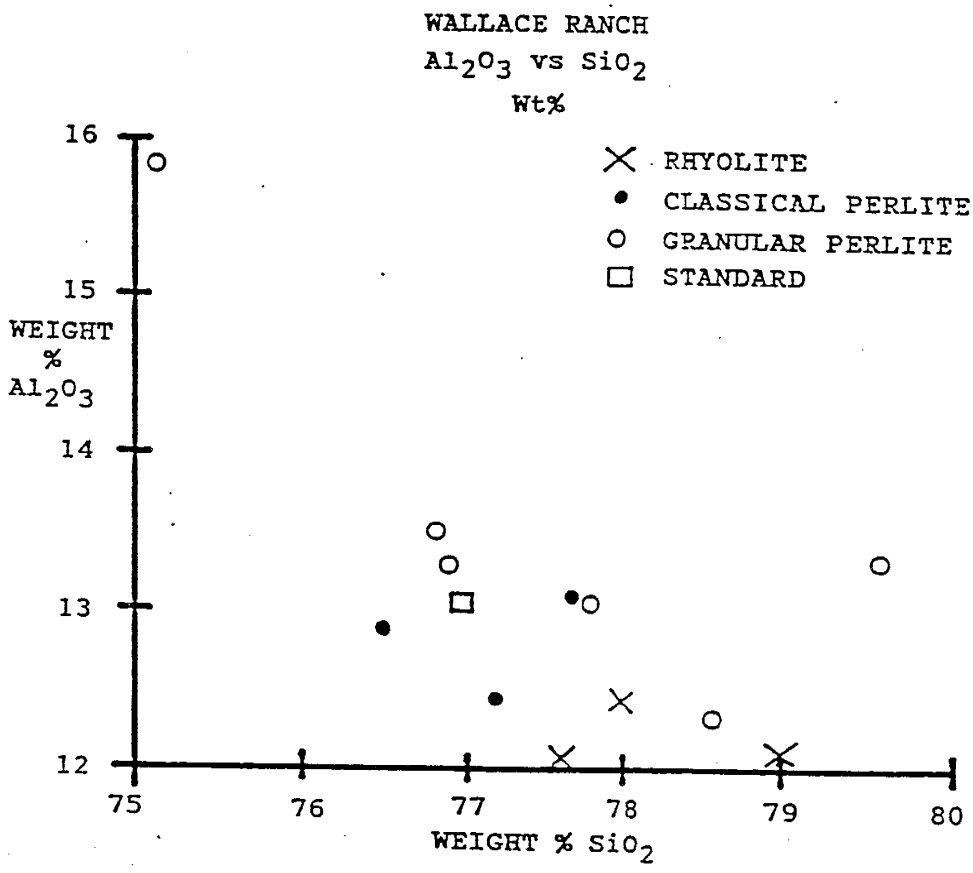

FIG. 44. Wallace Ranch XRF data. Al_2O_3 vs SiO_2. All oxides are expressed in wt %.

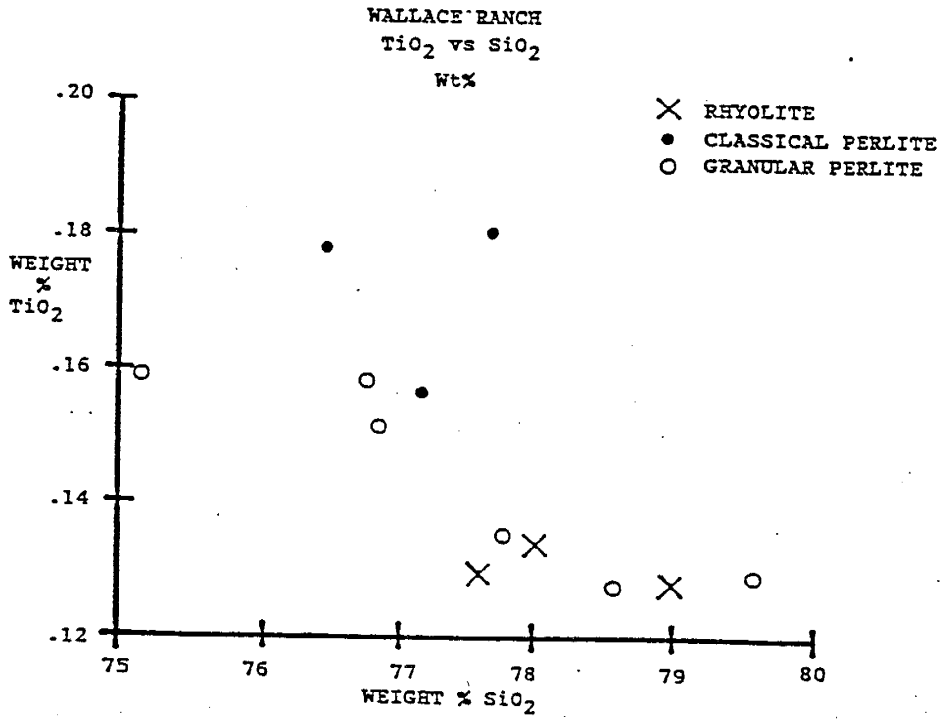

FIG. 45. Wallace Ranch XRF data. TiO_2 vs SiO_2. All oxides are expressed in wt %.

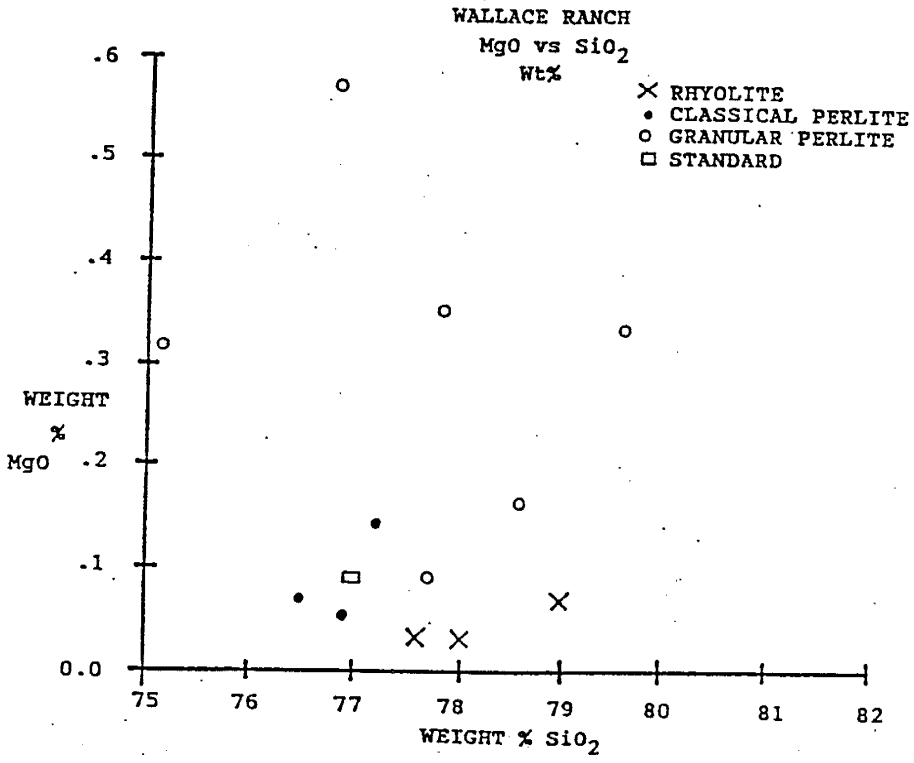

FIG. 46. Wallace Ranch XRF data. MgO vs SiO_2. All oxides are expressed in wt %.

correlation between MgO and SiO_2 is visible in any of the data sets.

The sum of Ti, V, and Cr concentrations divided by the Nb concentration is plotted against the Nb value in Figure 47. The granular perlite group displays a correlation of an increasing Ti, V, and Cr coefficient with increasing Nb. No correlation is visible in the other two data groups. The standard has an Nb value of 103.68 ppm and a Ti, V, and Cr coefficient of 6.29. These values plot to the right of the data field in Figure 47. No correlation between data groups is visible.

ISOTOPE DATA. Six hydrated glass samples from the Swartz area were analyzed for δO^{18} and D/H. Three are perlite (S-4, 7, and 27) and three are welded tuff (S-11, 13, and 15). Sample locations are on Plate 2. Plagioclase phenocrysts were hand picked from each glass sample and analyzed for δO^{18}. The δO^{18} values of glass samples range from 14.6 to 17.0 o/oo and plagioclase values range from 6.3 to 7.6 o/oo with respect to SMOW (Table 5). Corrected D/H ratios of glass samples range from -113 to -120 o/oo; no difference in D/H ratios between perlite and welded tuff glasses occurs (Table 5). A delta D outlier of -131 o/oo is omitted from the data (S-4).

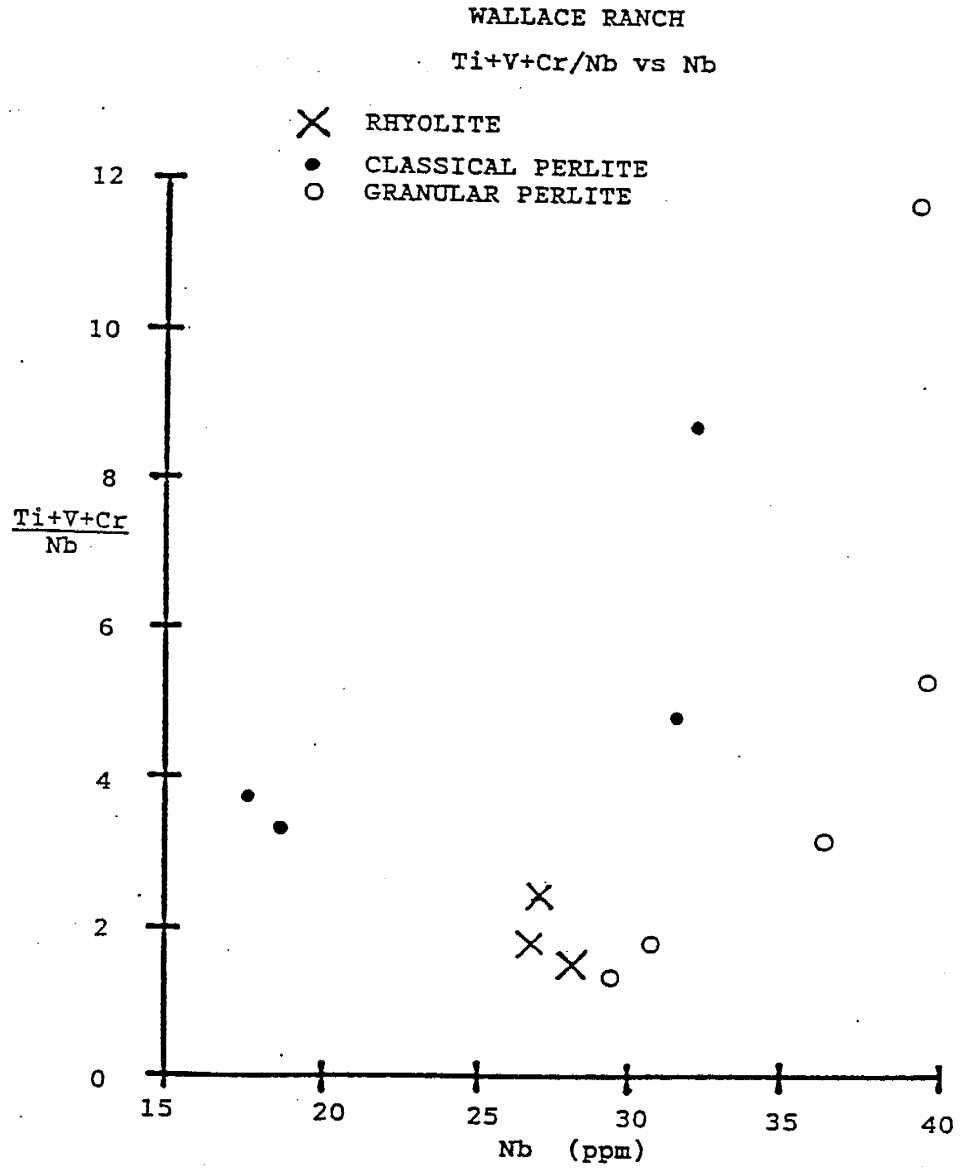

FIG. 47. Wallace Ranch XRF data. Ti+V+Cr/Nb vs Nb. All trace elements are expressed in ppm.

TABLE 5.

Oxygen and Hydrogen Isotope Data for Swartz Perlite and Welded Tuff

Sample	CO_2 % Yield	--- Del O-18 ---- Glass	Feldspar	Corrected Del D (o/oo) Glass Only
Perlite				
S-2	---	---	---	-131
S-4	99.6	17.0	6.74	-120
S-5	---	---	---	-114
S-7	102.2	16.2	6.50	---
S-27	102.0	14.6	6.32	---
W-10	---	---	---	-114
Welded Tuff				
S-11	103.0	15.4	7.5	-113
S-13	101.7	15.8	7.1	-120
S-15	60.5	16.0	7.6	-116

The CO_2 % Yield is applicable to feldspar phenocrysts only and it is based on the molecular weight of $NaAlSi_3O_8$ (262g/mole).

Table 5 depicts the δO^{18} values for plagioclase phenocrysts, perlite, and welded tuff. Phenocrysts picked from perlite range from 6.3 to 6.7 o/oo. Phenocrysts picked from welded tuff range from 7.130 to 7.496 o/oo. The perlite and welded tuff glasses show no distinct difference in δO^{18} values.

DISCUSSION

THE McDONALD RANCH AREA

FIELD MAPPING. The perlite horizon is nearly 300 ft thick at the north and south ends of the McDonald Ranch field area (Plate 1). Perlite pinches and swells in thickness for 1.25 mi along strike between these two thick outcrops. The thick north perlite outcrop may represent: 1) A portion of a rhyolite chill margin or rhyolite glass flow derived from the rhyolite dome of Burro Cienaga, 1.25 mi to the northwest (Hedlund, 1978), or 2) A portion of a rhyolite chill margin or rhyolite glass-flow derived from a closer extrusive center of the local, dome-flow complex mapped by Hedlund (1978) and discussed by Weber and Austin (1982).

Elements of the the dome-flow complex crop out for 10 km along Burro Cienaga (Weber and Austin, 1982). Flow laminations in local perlite dip northeast, away from the dome of Burro Cienaga center. This may result from the

original dome being a local topographic high during extrusion or subsequent fault-block rotation (Ballman, 1960).

The thin, undulating perlite horizon between the two thick outcrops appears to conform with the upper surface of underlying rhyolite. No zones of glass brecciation exist along the strike length of the outcrop. The continuous lateral extent of this perlite horizon suggests it is a chill margin of the overlying rhyolite flow.

The origin of the thick perlite outcrop at the southern margin of the study area is related to a local extrusion of the Burro Cienaga dome-complex. There are no local glass breccia zones or field evidence of glass brecciation. It is unlikely that a viscous mass of rhyolite glass nearly 300 ft thick could flow a great distance without brecciation. The center of the rhyolite dome of Burro Cienaga (Hedlund, 1978) is 3.8 mi to the northwest; therefore, a local extrusive source is most likely for this thick local perlite outcrop. A black vitrophyre nearly 30 ft thick overlies the south perlite outcrop. It was mapped by Hedlund (1978) as an overlying element of the rhyolite dome-flow complex. A pink felsic core occurs between local, lower perlite and upper perlite horizons (Plate 1). This felsic core thickens to the southeast; indicating the possible location of a

local extrusive center for this outcrop. Local glass foliation orientations are varied but tend to dip away from the thickening felsic core.

PETROGRAPHY. Thin sections of McDonald Ranch perlite are 99% glass and contain no traces of large vesicles or glass shards. This implies the perlite is the product of a hydrated rhyolite glass chill margin or glass flow, not a welded tuff. Lack of abundant, flattened vesicles suggests the glass did not originate from a water-rich, frothy pumiceous extrusion (Naert, 1974). Pumiceous perlite occurs at the Socorro and No Agua Peaks deposits; it is composed of up to 20% vesicles (Naert, 1974; Whitson, 1982).

Thin sections of adjacent tuffs and rhyolite (MR-6, 28, and 29) are taken from locations stratigraphically above and below perlite in the north part of the field area (Plate 1). This indicates that the tuffs and rhyolite are intercalated with perlite in what may be the margin of the flow. The large north outcrop has many felsic stringers intercalated with the perlite. The thin perlite horizon that continues to the southeast does not have these features. The thick perlite outcrop to the south has many felsic layers, stringers and laminations within the glass body. None of these features are lithic tuffs; they represent devitrified felsic zones within the perlite mass.

THE SWARTZ AREA

FIELD MAPPING. The field map and samples indicate the two perlite outcrops in the southwest part of the study area (N72W and N55E) are exposures of the same continuous perlite horizon (Plate 2). Glass-flow lamination dips range from horizontal to 20° and generally dip inward toward the hill. Locally, several areas of the perlite zone grade upward into a siliceous, spherulitic horizon that is succeeded by the overlying, flow-banded, Mimbres Peak Rhyolite. The upward succession of glass, spherulitic zone, and flow-banded rhyolite suggests the perlite is a chill margin of the rhyolite. The spherulitic horizon represents a zone that cooled slower than the outer perlite (Lofgren, 1978; Whitson, 1982). Hand samples of perlite (S-2, 3, and 4) have no lithics whereas the two underlying vitric lithic tuffs (S-41 and S-44) have abundant visible lithics.

The welded tuff outcrop (N30W) in the north part of the study area occurs within a vitric, lithic, tuff zone. The southeast end of the welded tuff horizon grades laterally into the lithic tuff unit. The welded tuff comprises a welded zone of the adjacent lithic tuff. Hand samples of both have the same visible lithic composition, although phenocrysts and lithics of the welded zone have been altered to a white, clay and commonly display red alteration rims. Fractures are filled with white or red, hematitic

chalcedony and alteration products. The physical appearance, lithic composition, and welded tuff origin distinguish this glass zone from the perlite horizon (N72W and N55E, Plate 2).

PETROGRAPHY. Perlite thin sections from outcrops N72W and N55E range from 95 to 97% glass. The remaining 3 to 5% consists of phenocrysts; no volcanic lithics or fiamme pumice fragments are present (S-2, 4, and 8; Appendix B). Accessories of sphene are present in the perlite and overlying felsic unit. Glass forms a homogeneous groundmass with no traces of glass shards or abundant, flattened vesicles. Glass flow-texture is common around phenocrysts. Lack of relict glass shards or flattened vesicles in the glass groundmass implies the hydrated glass is the product of a rhyolite flow margin or a rhyolite glass extrusion (Naert, 1974). A welded tuff or frothy, water-rich, pumiceous origin are not likely to produce a glass groundmass of such optical homogeneity.

Thin sections of the welded tuff horizon N30W (S-10, 13, 16, and 17) contain 70 to 85% glass groundmass composed of horizontally oriented fiamme pumice fragments in a glass matrix. Pumice fragments are bent around adjacent volcanic lithics and phenocrysts. Pumice vesicles are flattened parallel to fiamme alignment direction. The

presence of crushed, horizontally oriented fiamme pumice fragments, volcanic lithics and lack of flow textures in the groundmass indicate a welded tuff origin for the glass. The andesitic volcanic lithics are accidental but the aligned fiamme pumice fragments are juvenile. Fiamme pumice form when more than 90% of the magmatic water is exsolved during vesiculation upon extrusion of these melts at temperatures in excess of 700°C (Naert, 1974). If the pumiceous fragments rapidly accumulate and remain soft, latent heat is retained and primary vesiculation is destroyed by compression from the weight of overlying layers.

THE WALLACE RANCH

FIELD MAPPING. Field mapping reveals the bulk of perlite reserves at the Wallace Ranch area are associated with the granular perlite breccia. The source of this horizon has not been determined and no unbrecciated, homogeneous, granular, gray perlite body is exposed locally. Overlying, black, classical perlite is the only laterally continuous, local perlite horizon. The classical perlite zone grades upward into a spherulitic horizon that is succeeded by overlying flow-banded rhyolite. The spherulites develop in a zone that has a slower cooling rate and a higher temperature than the underlying, glassy chill-margin (Lofgren, 1971; Whitson, 1982). The classical perlite horizon appears to grade laterally into the siliceous,

glassy, rhyolite tuff mapped by Hahman (1989). Hahman (1989) mapped two northwest-trending rhyolite dikes (Plate 3) as the source of the local rhyolite extrusive mass. Finnell (1987) mapped a large rhyolite plug and associated northwest-trending rhyolite dikes 0.5 to 1.25 mi to the southeast. These features are included in Finnell's (1987) Miocene Sycamore Camp Rhyolite Group, and may be a likely source of the Wallace Ranch perlite occurrence.

The morphology of this perlite occurrence is unlike Whitson's dome model (Fig. 48) because there are no wide margins of glass with steeply dipping or vertical flow-banding to indicate the dome margin. Two modes of formation are possible: 1) Granular perlite was extruded first and solidified as a dome or a flow. Subsequent extrusion of overlying rhyolite from the same vent brecciated the granular perlite body, pushed the breccia fragments along and covered the debris. The black, classical perlite horizon forms the lower chill margin of the overlying rhyolite flow. The top 2 to 3 ft of granular perlite breccia adjacent to the classical perlite zone are completely welded. Below this zone, the breccia blocks occur in a white, sandy matrix.

2) The three lithologies formed contemporaneously during a single endogenous extrusive event. The granular perlite

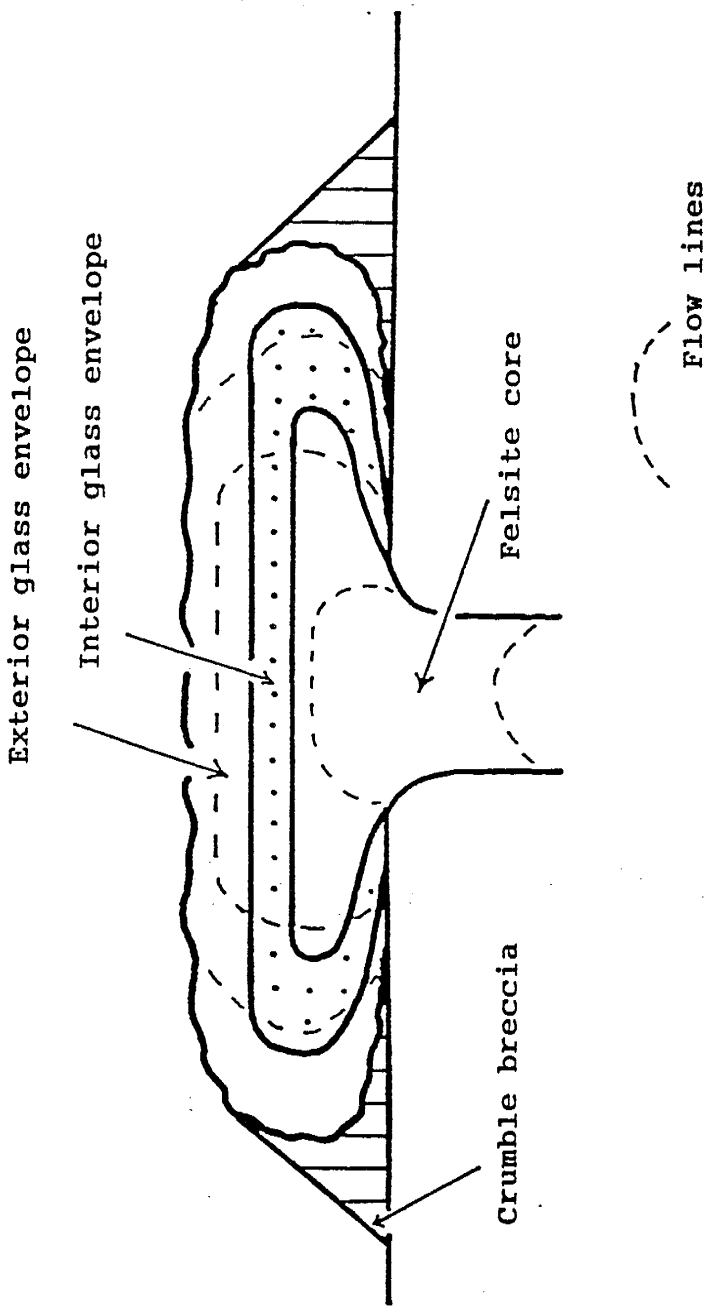

FIG. 48. Schematic cross section of an endogenous dome showing idealized lithologic zonation as seen at No Agua Peaks, New Mexico (after Whitson, 1982).

breccia represents an auto-brecciated remnant of a brittle, expanding, exterior margin of an extrusive mass (Whitson, 1982). Granular perlite texture is a result of vesiculation at the extrusion's outer margin (Breese and Piper, 1985). The outwardly expanding endogenous dome continually flows over the marginal breccia. Incipient to complete welding of breccia blocks occurs (Whitson, 1982). The black classical perlite horizon represents a separate cooling unit (Whitson, 1982). The overlying rhyolite would represent the interior devitrified felsite exposed by complete erosion of the uppermost chill margins (Fig. 48).

The perlite deposit at Brushy Mountain is a breccia with blocks of highly vesicular perlite and dense, perlitic glass in a matrix of pulverized glass and clay alteration products (Weber and Austin, 1982). A sequence of devitrified and highly spherulitic rhyolite flows overlies the perlite block breccia (Weber and Austin, 1982). This perlite deposit has a morphology similar to the Wallace Ranch occurrence.

PETROGRAPHY. Thin sections of classical perlite (W-9, 10, and 17) consist of up to 99% flow-textured glass. Well developed trachytic texture in W-10 and growth of radial devitrification structures along possible shear planes are evidence of glass flow during emplacement. The microscopic

texture of a spherulite is described by Lofgren (1971) and Whitson (1982) as feldspar crystal groups arranged in divergent radial clusters that grow as a result of glass devitrificaton, not primary crystallization. Devitrification is a primary process that occurs at a much higher temperature than the temperature at which secondary hydration of the glass occurs (R. Chamberlin, 1992, personal comm.). Lack of relict glass shards in the glass indicates the glass does not have a welded tuff origin. The granular texture of the breccia suggests some degree of vesiculation occurred during extrusion of the glass. The source of water can be either magmatic or meteoric water incorporated into the melt at a shallow depth prior to, or during emplacement in the upper to middle cooling temperatures (Weber and Austin, 1982).

Microscopic textures visible in the flow-banded rhyolite include cryptocrystalline quartz bands and radiating, feldspar-rich, devitrification structures. The local viscosity of the melt will determine which micro-texture forms. Assuming melt composition and temperature are constant at the local microscopic level, local variation of volatiles in the melt will affect viscosity (R. Chamberlin, 1992, personal comm.).

PHYSICAL TESTING DATA

McDONALD RANCH. All samples have furnace yields nearly equal to the standard. Analyses indicate expanded density of McDonald Ranch perlite is variable and related to sample location. Samples from the thick, north outcrop have the highest expanded densities and are unsuitable for commercial use (MR-10, 20 to 24). Five samples were taken on 25 ft centers perpendicular to strike of the thick north outcrop (MR-20 to 24). Descriptions of the samples indicate felsic bands or vitrophyre layers are common in the perlite.

The data display a group of values less than 3.5 lb/ft^3 (Fig. 5). These data represent samples taken south of the thick, north outcrop. A sample line of seven samples on 50 ft centers was taken at the thick, south outcrop (MR-13 to 19). These samples and others taken in the same area have expanded densities suitable for commercial use (Fig. 5).

Average brightness data presented in Figure 6 show variability within a range of values that have no correlation to sample location. The variability occurs within a range of consistent values. This range of values has an average brightness nearly 10% below the GREFCO standard average. This value can be increased by omitting the outlier of 46.2%. Average brightness of the expanded

perlite may be affected by impurities such as iron oxides. Greater concentrations of these oxides are present in McDonald Ranch samples than in the GREFCO standard (Appendix D). Locally, the perlite is light-gray and does not vary in color across the study area.

The percent nonexpansibles of samples varies across the study area. A distinctly greater percent occurs in perlite samples from the thick, north outcrop and local area. The most common constituent of the nonexpansible fraction is unexpanded or partially expanded glass in the +100 mesh fraction. These particles account for 50 to 93% of the unexpanded fraction of each sample. These particle's lack of expansion is not related to poor or variable furnace performance because standards expanded during the same run consistently produce excellent expansion characteristics. Lack of glass particle expansion may be related to local microscopic variations of volatiles in the glass or lack of an adequate local micro-fracture or vesicle network. An increase of expansion temperature or furnace draft adjustment may produce expansion in these particles also. No adjustment of furnace parameters will force phenocrysts, lithics, unhydrated glass, or felsic fragments to expand.

McDonald Ranch expanded perlite sieve analyses are similar to the GREFCO standard. Less perlite expands into the +20

and +30 mesh size fraction. Higher expansion temperatures may improve the yield in these size fractions. More fines are being generated than the standard. This may be the result of vesicle walls bursting during expansion or breakage during handling and lab preparation. An increase in expansion temperature may cause additional fines to be produced by bursting. This expanded perlite size distribution indicates the perlite may have a wider range of end-uses that depend on the expanded particle size.

SWARTZ AREA. All Swartz samples have furnace yields nearly equal to the GREFCO standard values. The remaining Swartz physical testing data exhibit a bimodal distribution split between perlite and welded tuff samples (Figs. 5, 6, and 7). Expanded perlite densities average 7.9 lb/ft^3; welded tuff expanded densities average 22.9 lb/ft^3. SEM photomicrographs show excellent perlite expansion. The expanded density may be suitable for some commercial applications if kept below 11 lb/ft^3. Lower expanded densities may be produced by adjusting furnace parameters during expansion. SEM photomicrographs of "expanded" welded tuff show no appreciable expansion and very little particle vesiculation. This is the primary reason for the high expanded densities. Lack of an interconnecting network of fractures or vesicles may prevent vesiculation and consequent expansion of the glass. The welded tuff also

has a high percentage of nonexpansible particles that contribute to high expanded density. Adjustment of furnace parameters during expansion will not improve welded tuff expansibility. No commercial applications exist for a partially expanded product with such a high density.

Brightness of the expanded perlite averages 43.3%, 22% below the GREFCO standard. The values are distributed over a 10% range and exhibit no distinct grouping (Fig. 6). Expanded welded tuff has the lowest percent brightness of all samples in this study. The average value of 35% is 34% below the average standard percent brightness value. Low brightness values may be caused by impurities such as iron oxides. Swartz perlite has higher concentrations of iron oxides than the standard, Wallace Ranch and McDonald Ranch perlites (Appendix D). Color intensity of these impurities may be enhanced by heating during the expansion process.

The nonexpansible fraction of Swartz perlite consists of 50 to 95% unexpanded glass in the +100 mesh size fraction (Fig. 19). These opaque white, granular glass particles exhibit slight vesiculation and have undergone partial melting. This process is related to physical properties of the glass, not furnace performance. Lack of adequate volatiles at a local, microscopic level may cause this poor

expansibility. Lack of a local network of microscopic fractures or vesicles may inhibit vesiculation and consequent glass expansion.

Swartz welded tuff nonexpansible content ranges from 58.2 to 90.4% (Fig. 7). White opaque, unexpanded glass accounts for 70 to 97% of this fraction. An inherent physical property of the glass prevents expansion, not inadequate furnace performance. Lack of expansion may be related to local, microscopic deficiencies in volatiles. Lack of interconnected fractures or vesicles at a microscopic level may prevent vesiculation and consequent glass expansion. Volcanic lithics are present in the tuff and add to the amount of nonexpansible material present. Manipulation of furnace operating parameters will not improve expansibility of the welded tuff.

Sieve analyses of Swartz perlite indicate very poor expansion into the +20 and +30 mesh fractions. Most expanded particles are retained on the 50 mesh screen (80.7%). Adjustment of furnace parameters during expansion may produce a wider distribution of expanded fractions. Expanding a different perlite size fraction will yield an expanded product with a different size distribution. These options may produce a sized expanded product of commercial value.

Swartz welded tuff sieve analyses indicate very little expansion occurs. This reflects the poor inherent expansibility of the welded tuff that cannot be improved by manipulating furnace parameters.

WALLACE RANCH. Furnace yield of Wallace Ranch samples averages 93.9%, 4% less than the GREFCO standard value. Expanded densities have a variable range of values that do not correlate with sample location. Granular and classical perlite samples have similar expanded densities. Several classical perlite samples have higher densities in the range unsuitable for commercial use (Fig. 5). Lithic tuff (Tlt) samples (W-18-A, B) have the highest expanded densities; a result of unexpansible volcanic lithics.

Figure 6 shows percent brightness data of the standard and three study areas. Wallace Ranch samples have the widest range of values. A granular perlite sample has the highest value of 68.4%; classical perlite samples have values between 45.0 and 61.4%. Classical and granular perlites have similar oxide concentrations. Variation of iron oxide content may affect average brightness of expanded perlite. Lithic tuff (Tlt) samples have the lowest percent brightness due to the presence of iron oxide-rich volcanic lithics.

The nonexpansible fraction of Wallace Ranch perlite has

a bimodal distribution (Fig. 7). The lithic tuff (Tlt) has the highest percent of nonexpansibles because it is composed of 90% basalt fragments. Granular and classical perlite have a range of 2.2 to 11.9% nonexpansibles that are composed of 80% unexpanded and partially expanded glass. The nonexpansible nature of these glass particles is related to a physical property of the glass, not furnace performance. Lack of volatiles at a local, microscopic level may inhibit expansion of the glass particles. Lack of a local, microscopic network of fractures or vesicles may prevent vesiculation and consequent glass expansion. These particles are partially expanded; adjustment of furnace operating parameters during expansion may improve expansibility of these particles. Percent nonexpansibles is related to the lithologic unit sampled at the Wallace Ranch. The lithic tuff (Tlt) has a distinctly higher percent nonexpansibles due to abundant volcanic lithics. The perlite units have less nonexpansibles; unexpanded glass particles and rare phenocrysts are most common.

Wallace Ranch sieve analyses indicate a lack of expansion into the coarse, +20 and +30 mesh fraction and a greater fines content in the -100 mesh fraction. Fines may be generated by vesicle wall bursting during expansion. Expanding to a coarser fraction can be accomplished by using a coarser furnace feed.

Physical testing data from drill hole samples obtained by Hahman (1989, Appendix C) suggest perlite units at depth have variable expansion qualities. These samples are from rotary-percussive drill cuttings, not core. Many samples were completely pulverized and the potential for contamination from previously drilled horizons exists. Thirty-four samples representing composite drill intervals of 10 ft were analyzed.

The 34 samples have furnace yields that range from 2 to 17% below the standard. Expanded densities vary widely between adjacent 10 ft drill intervals. Expanded density values range from 3.62 to 62.4 lb/ft^3. The variation can be attributed to volcanic lithics in the lithic tuff (Tlt) or cross-contamination by unexpansibles from overlying horizons. The granular perlite breccia may have unexpansible horizons, if this unit exists at depth.

Average brightness values range from 23.40 to 60.43%; the values vary widely between drill holes and adjacent 10 ft composite intervals. Values around 45% are common and may reflect the presence of iron oxide-rich glass zones or volcanic lithics.

Percent nonexpansible values vary widely between drill holes and adjacent 10 ft intervals. Values range from 4.3

to 96.9% and appear to correlate with expanded density and brightness values. Percent nonexpansible values are commonly between 17 and 23% and are always greater than the standard. Composition of the nonexpansibles is not known. The large percent values indicate the presence of material other than nonexpansible or partially expanded glass. This other material may be volcanic lithics from the basal lithic tuff horizon (Tlt).

Sieve analyses of expanded perlite from drill cuttings indicate a lack of expansion into the +20 and +30 mesh size range for all samples. Nominal expansion into the +30 mesh size occurs at less than 1/3 the weight percent of the standard. More fines (-100 mesh) are produced; 50% of the sample expands to the mesh and 20 to 40% of the sample expands to the +70 mesh fraction. These analyses indicate the drill hole samples expand to a lesser degree than samples collected and expanded for this study. These values indicate the samples are composed of a high percent of nonexpansible or poorly expansible material. The samples may contain a large volume of volcanic lithics from the basal lithic tuff (Tlt). Perlite fragments in the lithic tuff will contribute to the expansible fraction of the drill samples.

SCANNING ELECTRON MICROSCOPY

Perlite from the study areas displays a variety of micro-textures. A concentric, onionskin fracture pattern is evident in classical perlite from the McDonald Ranch, Swartz, and Wallace Ranch occurrences. Wallace Ranch granular perlite has a distinct, frothy, texture composed of swirled vesicles. The GREFCO sample (Socorro pit) is a pumiceous perlite that displays numerous, flattened, aligned vesicles. These perlites have a distinct, visible, interconnecting system of fractures or vesicles. Swartz welded tuff does not have a visible interconnecting system of fractures or vesicles. Fractures and vesicles must be important in determining the expansibility of the perlite. The welded tuff's poor expansibility is related to the lack of these features; although, the tuff has a water content in the perlite range (Fig. 32).

Expanded perlite particles form bulbous, rounded, balloon shapes supported by an intricate network of interior vesicle walls. Maintaining the integrity of the outside walls is important to expanded perlite quality. Over-expansion of interior vesicles will burst the exterior walls, impair the ability to achieve consistent expanded specifications, and cause a reduction of strength and insulating properties of the expanded product. The degree of vesiculation is a direct consequence of furnace operating parameters. It is

of utmost importance in a commercial venture to find furnace operating parameters that optimize expansion of a particular perlite feed. The perlite feed must be of consistent quality to assure continuous expansion to consistent physical specifications.

There is little difference in the morphologies of expanded perlites from the three occurrences and the GREFCO Socorro pit. Each suffers a small degree of outer wall bursting; Swartz classical perlite displays the least amount of bursting. All samples have interior vesicles of nearly equal diameter. Wallace Ranch classical perlite has interior vesicles of a slightly smaller diameter.

Swartz welded tuff displays evidence of minor amounts of vesiculation and consequent expansion. Intricate interior cell structures do not form; most particles show no sign of vesiculation. The nonexpansible fraction is composed of glass fragments, broken vesicle walls, phenocrysts, unexpanded perlite particles and partially expanded perlite particles. These unexpansibles are characterized optically and listed in Appendix E.

GEOCHEMISTRY

PENNFIELD TEST. The total water content of perlite and welded tuff samples from the three study areas ranges from 1.73 to 5.78 wt %. Figure 32 shows Wallace Ranch granular perlite (W-3) has a water content of 1.86% (obsidian range). This sample has among the best expansion characteristics of the documented samples (Appendix C). Swartz perlite and welded tuff have the same range of water content but display extremely different expansion characteristics (Appendix C). The welded tuff has extremely high expanded density (20.6 to 28.1 lb/ft^3) and a high percentage of nonexpansibles (58.2 to 90.4%). Data indicate that the degree of expansibility (furnace yield, expanded density, and percent nonexpansibles) is not directly related to total water content of the glass.

X-RAY FLUORESCENCE SPECTROMETRY (XRF)

McDONALD RANCH XRF. Al_2O_3 and Fe_2O_3 contents of the perlite and overlying rhyolite are similar and their ranges overlap to a small degree (Figs. 33 and 34). The lower rhyolite has lower Al_2O_3 and Fe_2O_3 contents than both overlying units. A correlation between increasing SiO_2 content and decreasing Al_2O_3 and Fe_2O_3 is visible in the perlite and overlying rhyolite (Figs. 33 and 34). Similarity in Al_2O_3 and Fe_2O_3 contents of perlite and overlying rhyolite suggest the two lithologies are

genetically related.

Figures 35 and 36 display wt % TiO2 and MgO vs SiO2. TiO_2 and MgO data display more scatter than Al_2O_3 and Fe_2O_3 data. A small degree of overlap occurs with perlite and overlying rhyolite TiO_2 data. Lower rhyolite TiO_2 and MgO contents are in the same range as the overlying lithologies but a higher SiO_2 content offsets the data to the right. Higher mobility of these oxides may contribute to data scatter. No conclusions concerning genetic relations of adjacent lithologies can be reached using TiO_2 and MgO data.

Figure 37 displays the Ti+V+Cr/Nb ratio plotted against Nb content. Except for one value, the overlying rhyolite group displays the same range of values as the perlite data. Rhyolite outlier MR-27 has a Cr value of 101.9 ppm which is nearly double other rhyolite Cr values. This may be due to contamination from the metal pulverizer. The lower rhyolite group has less Nb and lower ratio values than both overlying units. Trace element data suggest the perlite and overlying rhyolite are genetically related. Both differ from the lower rhyolite with respect to the trace element ratio and Nb content.

SWARTZ XRF. Wt % Al_2O_3 and Fe_2O_3 vs SiO_2 data are plotted separately on Figures 38 and 39. Perlite, welded tuff, lithic tuff, and rhyolite samples are within a 3% range of Al_2O_3. A difference in Fe_2O_3 content of the groups is evident. A genetic relationship among sample groups cannot be determined from data presented in Figures 38 and 39.

Wt % TiO_2 and MgO versus SiO_2 are plotted separately on Figures 40 and 41. Perlite and overlying rhyolite data overlap. The welded tuff contains higher concentrations of both oxides that plot over a wider range of values. Although perlite and rhyolite data occur in the same value range, no genetic relationship between the units can be determined from this data.

Sr versus Nb data on Figure 43 display very similar Sr concentrations for the perlite and overlying rhyolite. The other two groups have greater Sr concentrations occurring over a wider range of values. These data indicate the perlite and rhyolite units are genetically related.

The narrow range of similar Ba concentrations exhibited by the perlite and rhyolite in Figure 42 suggest the units are genetically related.

WALLACE RANCH XRF. Figures 44 and 45 show wt % Al_2O_3 and TiO_2 vs SiO_2. The three lithologies have the same Al_2O_3 content and similar TiO_2 contents. Analyses indicate the three units are genetically related. MgO vs SiO_2 data in Figure 46 show granular perlite breccia has a wider range of enriched MgO values. This may be due to material in the breccia matrix.

Trace element data presented in Figure 47 indicate a close similarity between overlying rhyolite and granular perlite breccia. Ti+V+Cr/Nb versus Nb data in Figure 47 indicate a wide variation of values for all lithologies except the rhyolite. These data indicate the three units are genetically related.

ISOTOPE DATA. Swartz glass and plagioclase phenocryst δO^{18} values agree with Taylor's (1968) δO^{18} analyses of glass and sodic andesine from hydrated obsidian samples obtained near Silver City, New Mexico (Table 5). Taylor's glass δO^{18} value is 15.5 o/oo and sodic andesine δO^{18} value is 7.2 o/oo. He attributes greater glass values to the ability of water to pass through the glass along the myriad cracks and imperfections present in perlitic glass (Taylor, 1968). Figure 49 represents a straight line drawn through a plot of Taylor's hydrated volcanic glass samples from the Western United States. Taylor's hydrated glass

line is derived from Craig's meteoric water line. Both are related by assumed constant fractionation factors of 0.965 for D/H and 1.0245 for O^{18}/O^{16} (Fig. 49). Constant fractionation factors are reasonable assumptions if hydration occurred over a narrow temperature range and if the hydration represents an approach to a type of metastable isotopic equilibrium (Taylor, 1968).

Three hydrated welded tuffs (S-11, 13, and 15) and one perlite (S-4) are plotted on Figure 49. These samples fall to the right of Taylor's hydrated volcanic glass line. Taylor concluded that during low temperature hydration ($50^{o}C$), volcanic glass takes on an O^{18}/O^{16} ratio controlled by the composition of local meteoric water, and roughly 25 o/oo higher in O^{18} than the water (Taylor, 1968). Swartz samples exhibit this trend.

Swartz welded tuff plagioclase phenocrysts are consistently 1 o/oo higher in O^{18} than plagioclase from the perlite. The welded tuff has interacted with greater amounts of meteoric water and undergone more secondary alteration than the perlite outcrop. This is evident in alteration of phenocrysts and lithics to white clay and the presence of fractures filled with silica and alteration products visible in hand sample (Appendix A). The δO^{18} difference is attributed to water associated with the alteration

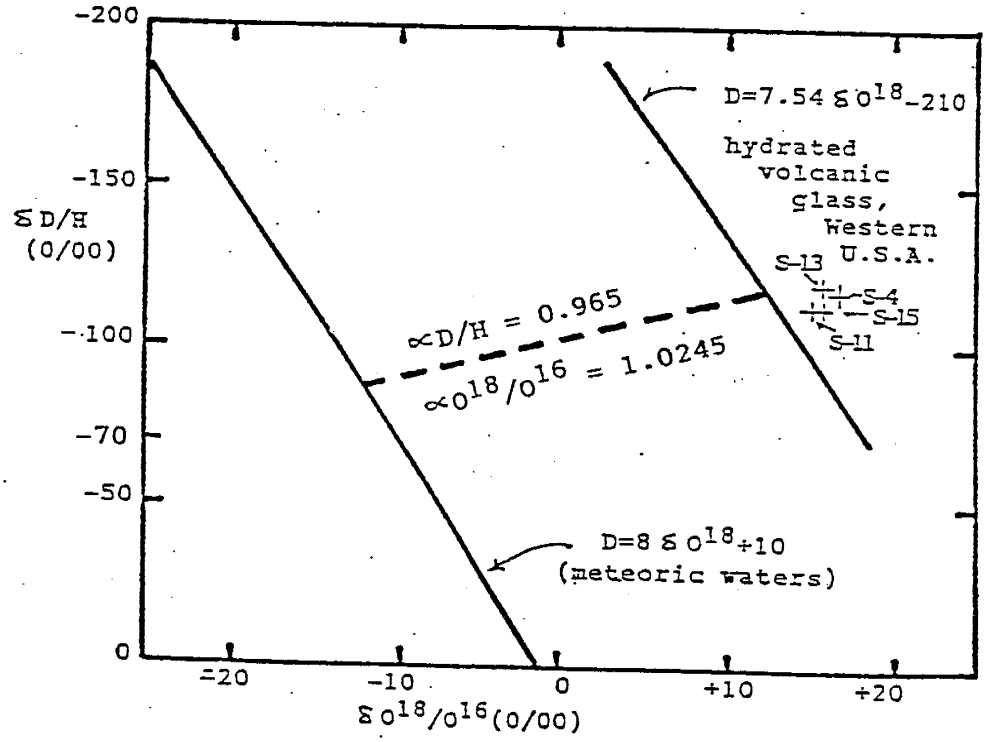

FIG. 49. Relationship between selected Swartz D/H and O^{18}/O^{16} data and Taylor's hydrated volcanic glass line and the meteoric water line (after Taylor, 1968).

process (Taylor, 1968). This effect is neither present in the Swartz glass O^{18} analyses nor in the D/H data.

ECONOMIC CONSIDERATIONS

Perlite has a low unit value. An economic evaluation of a perlite occurrence must consider other criteria in addition to deposit size, grade and overburden thickness. These other criteria include: location, access, physical and chemical characteristics of expanded perlite, market, transportation, and competition. In this section, these items are addressed for each occurrence. Reserve and overburden estimates are given for each occurrence. These estimates are based on field maps and cross-sections; no drill data are used in the calculations.

THE GREFCO PIT AT SOCORRO, NEW MEXICO This world-class deposit will compete with any new perlite deposits brought into production in the western United States. Near Socorro, this pit has a dedicated rail spur and siding and access to Route 60 and I-25. The GREFCO pit has sufficient proven reserves to last into the middle of the next century (Jenkins, 1989). Mining is conducted by scrapers; no drilling and blasting is necessary. No overburden exists; therefore, stripping is not required to expose ore. The reserves are well above the local water table and pumping will never be required.

The GREFCO pit is a homogeneous dome of pumiceous perlite. Unlike the No Agua Peaks depcsit, the Socorro dome has no zonation, cooling layers, or spherulitic zones. Microscopic obsidian nodules have been identified (Chamberlin, 1992, personal comm.) but they do not hinder production or commercial quality. Since extrusion as a pumiceous glass, no devitrification has occurred and no resultant felsic cores, horizons, or spherulitic zones exist. The in-situ perlite has a light-tan color that may result from the low oxide content (XRF data, Appendix D). Expanded characteristics are excellent and have provided consistent physical results over a long history of past production. Expansion to consistent physical specifications is a crucial criteria for long-term marketing of sized perlite. GREFCO has many years of perlite industry expertise.

McDONALD RANCH

Location. The McDonald Ranch perlite occurrence is 15 mi north of I-10 and 16 mi south of NM Highway 90 (Fig. 1). The nearest rail siding is adjacent to I-10. Access from I-10 and NM Highway 90 is via NM Highway 189, a graded dirt road. NM Highway 189 is not designed to sustain heavy truck traffic (38 t) and is not passable when wet. An adequate source of electricity for a mill does not exist nearby.

Perlite Impurities. Rhyolite bands, lithic bands, vitrophyre layers and phenocrysts are visible in the perlite outcrop. Thin section analyses show 1 to 3% phenocrysts and oxides in the glass groundmass. The presence of felsic and vitrophyre bands and layers render the thick, north outcrop unacceptable for expansion and mining. The thick, south outcrop has a thick, felsic core that can be selectively removed during the mining process. The perlite quality is acceptable for production of a marketable, expanded product. The percent brightness is lower than the GREFCO standard due to a higher oxide concentration. This may limit the expanded product's market.

Occurrence Size and Form. Minable reserves are restricted to the thick, south outcrop and are estimated to contain 6.8 million tons of perlite. This reserve base is not large enough to justify capital investment for a large, high capacity mill. A portable crushing and screening plant can be used for rough sizing prior to shipment to a finish mill. The felsic core will have to be selectively removed during mining. The south outcrop is lens shaped and most reserves can be recovered without stripping or mining to a depth greater than 80 ft. Mining below current ground level (+5160 ft above MSL) will require going below the local water table. Burro Cienaga represents the top of the local water table during the wet fall and spring seasons. Pumping

water from the pit may disrupt local water wells and reduce profitability of the operation.

To the north, outcrop thickness varies and has an irregular, unpredictable form. Thin chill margins and thicker lenses occur but no minable thicknesses are present until the north outcrop is reached. Medium and thick layers of rhyolite and vitrophyre zones intercalated with the thick, north perlite horizon render this outcrop unminable even if selective mining is considered.

SWARTZ AREA

Occurrence Location. Perlite crops out 1.1 mi west of NM Highway 61 at Swartz. Access is by a trail that follows Tom Brown Canyon upstream to the study area. A heavy-duty road able to sustain truck traffic will have to be constructed from NM Highway 61 to the perlite outcrop. US 180 is 15 mi to the southwest. A rail siding may be accessible at Bayard or Deming. If needed, power will have to be brought in a short distance from the main line along NM Highway 61.

Perlite Impurities. Abundant volcanic lithics and phenocrysts render the welded tuff outcrop unsuitable for expansion. The perlite has 3 to 5% phenocrysts and oxides in the glass groundmass. Many of the perlite outcrops have an overlying spherulitic zone which on occasion exceeds the

thickness of the perlite horizon. Spherulites are not expandable and form a dense, siliceous overburden that must be removed. The thick perlite horizon noted on Plate 2 does not have a thick overlying spherulitic horizon. Perlite in this outcrop is of commercial quality. The percent nonexpansibles is low and represents an acceptable level of impurities composed of phenocrysts and unexpansible glass. Average brightness is 20% below average standard values and may limit commercial use of the expanded product. The presence of iron oxides indicated by XRF analyses causes low brightness values.

Occurrence Size and Form. Minable reserves of 1.85 million tons are accessible without stripping at the large perlite outcrop noted on Plate 2. An additional 617,700 t of perlite can be mined by stripping 1.6 million t of rhyolite for an overall stripping ratio of 0.65:1. The bulk of the reserves are on a hillside; mining can be conducted without intersecting the top of the local water table. Total reserves of 2.48 million t will not justify capital expenditure for a large, high capacity mill. A small, portable crushing and screening plant would be used to rough-size perlite prior to shipment to a finish mill.

This outcrop has an asymmetrical, lens-shape and rapidly thins-out beneath the hill. No other outcrops of minable

thickness occur at the Swartz area. The remaining perlite horizon is a thin, chill margin that swells to lens-shaped zones but rarely exceeds 12 ft in thickness.

WALLACE RANCH

Occurrence Location. The Wallace Ranch is northwest of Riverside, 16 mi west of NM Highway 180 (Fig. 1). Access to the area is gained by leaving NM Highway 180 and traveling west for 16 mi on a graded dirt road. The dirt road has several steep grades, passes through several arroyos; it is not designed to sustain heavy truck traffic. The nearest rail siding is adjacent to NM Highway 180. An adequate supply of electricity for a large mill is not readily available.

Perlite Impurities. Granular perlite breccia blocks occur in a sandy, white matrix with clay impurities. Matrix abundance varies within this unit. Breccia blocks contain a few percent phenocrysts manifest in the nonexpansible fraction. The classical perlite zone has a ubiquitous overlying spherulitic horizon that is extremely detrimental to perlite quality. Oxide concentrations in the classical perlite are greater than the granular perlite; both have variable percent brightness values. The few percent nonexpansible fraction of the classical perlite consist of nonexpansible glass and phenocrysts. These two lithologies

exhibit satisfactory expansion characteristics; their variable percent brightness values may limit the end-use of the expanded product. The basal lithic tuff (Tlt) contains perlite fragments; but, physical test data indicate this unit is unsatisfactory for commercial expansion. The poor expanded density, low brightness and high percent nonexpansibles are due to volcanic lithics and a siliceous matrix.

Occurrence Size and Form. Total estimated granular perlite breccia and classical perlite reserves are 68.15 million t. Basal lithic tuff (Tlt) is not considered perlite ore and tonnage calculations do not include this unit. Total estimated rhyolite overburden is 45.4 million t. Much of the perlite reserve base is above ground elevation (+5600 ft above MSL); an open pit will have to be excavated to recover all reserves. The floor of Pine Canyon has an intermittent stream that flows during the fall and spring seasons. Water will have to be pumped from the pit as mining continues below the 5600 ft level. A perlite reserve of this size does justify capital expenditure for a high capacity mill. Such an expenditure is not justified for the Wallace Ranch occurrence because: 1) the remote location, 2) lack of an adequate access road or rail siding, 3) lack of an adequate source of electrical power, 4) inconsistent expanded physical characteristics limit end-use of the expanded

product.

The form of the perlite occurrence is best described as a massive breccia of granular perlite blocks with an overlying classical perlite horizon. The classical perlite horizon has an upper spherulitic zone that grades into an overlying flow-banded rhyolite. Contemporaneous extrusion of the three units as an endogenous dome has not been determined in this study. Separate extrusion of granular perlite before the classical perlite and rhyolite are a possibility. Speculation exists as to the source of the three units. Is the source beneath the volcanic pile or is it a vent mapped by Finnell (1987) southeast of Pine Canyon? This uncertainty has not been resolved by this study.

CONCLUSIONS

Field mapping and petrographic studies of the three perlite occurrences have shown:

1. The thick perlite lenses of the McDonald Ranch area are isolated features of rhyolite glass extrusion associated with local elements of Hedlund's (1978) rhyolite dome complex of Burro Cienaga.
2. The large felsic core and steeply dipping glass flow-banding at the west margin of the south outcrop at McDonald Ranch suggest it is the remnant of a large glass lobe.

3. Thin perlite horizons at the McDonald Ranch area are chill margins of the overlying rhyolite flow.
4. The N30W glass outcrop at Swartz is a welded tuff horizon associated with the adjacent lithic tuff unit. This glass zone is not genetically related to the perlite outcrops N72W and N55E.
5. Swartz perlite outcrops N72W and N55E are exposures of the same perlite lens and are a chill margin of overlying flow-banded, Mimbres Peak rhyolite.
6. Two modes of formation are possible for the Wallace Ranch perlite occurrence: a) Granular perlite breccia, classical perlite and overlying flow-banded rhyolite are products of the same endogenous, extrusive event. b) A granular perlite body was extruded first then subsequent extrusion of rhyolite from the same vent brecciated the granular perlite body and covered it. The classical perlite is a lower chill margin of the overlying rhyolite.

Physical testing of perlite and welded tuff samples from the three occurrences has shown:
1. Perlite from the McDonald Ranch thick, south outcrop has expanded physical characteristics of a marketable, commercial perlite.
2. Perlite from the McDonald Ranch thick, north outcrop has expanded physical characteristics different from the south outcrop. The north outcrop perlite does not have expanded

physical properties of a marketable, commercial perlite.
3. Welded tuff from the Swartz area does not have expanded physical properties of a marketable, commercial perlite.
4. Swartz perlite from the thick lens of outcrop N55E has expanded physical properties of a marketable, commercial perlite with an end-use limited by variable expanded densities and low brightness values.
5. Granular perlite breccia and classical perlite from the Wallace Ranch area have expanded physical properties of a marketable commercial perlite with an end-use limited by variable expanded density and brightness values.
6. Basal lithic tuff (Tlt) in the Wallace Ranch area does not have expanded physical properties of a marketable commercial perlite.

Microscopic examination of the nonexpansible fraction of expanded perlite furnace yield has shown:
1. An inherent physical property of all perlite samples causes partial or no expansion in a fraction of the furnace feed. This property may be related to: a) An inadequate amount of volatiles in the perlite at a local, microscopic level. b) Inadequate or lack of an interconnecting network of fractures or vesicles at a local microscopic level.
2. Swartz welded tuff does not exhibit vesiculation or incipient expansion. This may be related to inherent

physical properties of the glass previously discussed above.
3. Furnace performance is not a contributing factor to the percent nonexpansibles of the field samples. Standards expanded with samples exhibit consistently low nonexpansible percent values.

Scanning electron microscope photographs of perlite samples, expanded perlite, and nonexpansibles has shown:
1. Classical perlite has an interconnecting network of concentric fractures. Granular perlite has an interconnecting network of swirled vesicles. Pumiceous perlite has an interconnecting network of flattened vesicles.
2. Swartz welded tuff has concentric fractures visible in thin section. These fractures have been filled with secondary silica (Appendix B). SEM photographs show no evidence of this fracture network.
3. Expansibility of a perlite is related to the presence of an interconnecting network of fractures or vesicles. These voids allow incipient vesiculation and subsequent expansion to occur. Lack of these features in the welded tuff prevents this hydrated glass from expanding.
4. The bulbous form of expanded perlite is supported by an interior network of vesicle walls. The exterior of the expanded particle bursts when the particle over-expands. This phenomenon degrades the physical properties of expanded

particles. Over-expansion may be related to expansion temperature and can controlled by adjusting furnace operating parameters.

Determination of perlite and welded tuff water content (weight percent basis) with the Pennfield test has shown:
1. Swartz welded tuff is a hydrated glass with a water content in the perlite range (2 to 6 wt %).
2. Water content of a hydrated volcanic glass is not an important parameter that determines expansibility or physical characteristics of the expanded glass because some perlites that expand well have less H_2O than unexpansible welded tuffs.

X-ray fluorescence spectrometry (XRF) of perlites, welded tuffs, lithic tuffs, and rhyolites from the three field areas has shown:
1. McDonald Ranch perlite displays a correlation between increasing SiO_2 content and decreasing Al_2O_3 and Fe_2O_3. This correlation also exists in overlying rhyolite samples. Similarities in Al_2O_3 and Fe_2O_3 contents of the perlite and overlying rhyolite suggest the two adjacent lithologies are genetically related.
2. The Ti+V+Cr/Nb ratio versus Nb concentration data suggest the McDonald Ranch perlite and overlying rhyolite are genetically related. Data indicate these two units are

not genetically related to the rhyolite occurring below the perlite horizon.

3. Sr versus Nb data indicate Swartz perlite and overlying rhyolite are genetically related.

4. The narrow range of similar Ba concentrations in the perlite and overlying rhyolite samples indicate these two adjacent units are genetically related.

5. Trace element analyses of Wallace Ranch granular perlite breccia, classical perlite and overlying rhyolite indicate the three units are genetically related.

δO^{18} and D/H ratio isotope analyses of Swartz perlite and welded tuff have shown:

1. Swartz perlite and welded tuff δO^{18} and D/H ratio values agree with values produced by Taylor (1968) from a hydrated obsidian sample obtained 6 mi north of Silver City, New Mexico.

2. δO^{18} values in the hydrated glasses are greater than δO^{18} values from plagioclase phenocrysts contained within the glasses. Taylor (1968) attributes this to the exchange of oxygen in the silica with oxygen from large amounts of meteoric water during secondary hydration of the glass.

3. Plagioclase phenocrysts from Swartz welded tuff are 1 per mil higher in O^{18} than plagioclase from the perlite. This indicates an exchange with greater amounts of meteoric water during secondary alteration. The welded tuff has

been subjected to a greater degree of secondary alteration than the perlite.

Economic considerations indicate:

1. The remote location and poor access of the three perlite occurrences detract from their economic value.
2. Expanded perlite physical characteristics from the three occurrences are variable, do not yield consistent specifications, and limit the end-use marketability.
3. Perlite reserves at Swartz, McDonald Ranch, and Wallace Ranch are sufficient to mine but economic factors render them uneconomical at the present time.
4. Current production at Socorro and No Peaks will continue to dominate the perlite industry of the United States.

APPENDIX A

Hand Sample Descriptions

This appendix contains field descriptions of hand samples collected for this study.

MR = McDonald Ranch sample

S = Swartz sample

W = Wallace Ranch sample

APPENDIX A (continued)

MR-1: Porphyritic perlite; approximately 2% phenocrysts of biotite. Gray glass with pervasive perlitic fractures and vitreous luster. Rare red felsic veinlets.

MR-2: Porphyritic perlite; 1% phenocrysts of biotite. Gray glass with pervasive perlitic fractures and vitreous luster.

MR-3: Porphyritic perlite; approximately 2% phenocrysts of biotite. Light-gray glass with pervasive perlitic fractures and vitreous luster.

MR-4: Siliceously altered glass; highly fractured glass that has been silicified. White with a dull luster

MR-5: Perlite; gray glass with pervasive perlitic fractures and vitreous luster. No visible phenocrysts.

MR-6: Silicified breccia; red felsic pebbles and yellow silicified glass clasts (0.2-1mm). 2% biotite phenocrysts in a siliceous matrix.

MR-7: Porphyritic perlite; gray glass with pervasive perlitic fractures and a vitreous luster. 1% biotite phenocrysts. Chalcedony veinlets.

MR-8: Porphyritic perlite; dark-gray glass with pervasive perlitic fractures, a vitreous luster, and red felsic veinlets. Rare biotite phenocrysts.

MR-9: Identical to MR-8

APPENDIX A (continued)

MR-10: Porphyritic perlite; dark-gray glass with pervasive perlitic fractures, a vitreous luster, and red glass veinlets. 1% biotite phenocrysts.

MR-11: Porphyritic perlite; dark-gray glass with pervasive perlitic fractures, vitreous luster, and numerous red, siliceous, spherulites (1-3mm). 1% biotite phenocrysts.

MR-12: Porphyritic perlite; gray glass with perlitic fractures, black flow laminae, red flow bands and red felsic lenses. 2% biotite phenocrysts.

MR-13: Porphyritic perlite; gray glass with pervasive perlitic fractures, vitreous luster, and red felsic veinlets. 2% biotite phenocrysts.

MR-14: Porphyritic perlite; gray glass with pervasive perlitic fractures and a vitreous luster. 2% biotite phenocrysts.

MR-15: Porphyritic perlite; gray glass with pervasive perlitic fractures, vitreous luster, and red felsic veinlets. 2% biotite phenocrysts.

MR-16: Porphyritic perlite; gray glass with pervasive perlitic fractures, vitreous luster, red felsic veinlets, and red siliceous spherulites (1-3mm). 2% biotite phenocrysts.

MR-17: Porphyritic perlite; light-gray glass with pervasive perlitic fractures, vitreous luster, and red glass veinlets. 2% biotite phenocrysts.

APPENDIX A (continued)

MR-18: Porphyritic perlite; light-gray glass with pervasive perlitic fractures, vitreous luster, black glassy flow bands, and rare, red felsic veinlets. 2% biotite phenocrysts.

MR-19: Porphyritic perlite; gray glass with pervasive perlitic fractures, vitreous luster, red glass bands, and red felsic bands. 3% biotite phenocrysts.

MR-20: Perlite; gray glass with pervasive perlitic fractures, vitreous luster, and black flow-bands. No visible phenocrysts.

MR-21: Porphyritic perlite; gray, flow-banded glass with pervasive perlitic fractures, and a vitreous luster. 2% biotite phenocrysts.

MR-22: Porphyritic perlite; gray glass with pervasive perlitic fractures, vitreous luster, black flow-bands and rare, red, felsic bands. 3% biotite phenocrysts.

MR-23: Porphyritic perlite; gray glass with pervasive perlitic fractures, vitreous luster, red felsic bands and red felsic pebbles (2-4mm). 2% biotite phenocrysts.

MR-24: Identical to MR-23.

APPENDIX A (continued)

MR-25: Dense, red and white, flow-banded, porphyritic rhyolite; 6% phenocrysts of dominantly quartz and subordinate biotite.

MR-26: Dense, pink, sparsely porphyritic rhyolite; 5% phenocrysts of dominantly quartz with lesser biotite. Minor red, rhyolite lithics.

MR-27: Dense, pink and white, flow-banded, porphyritic rhyolite; 4% phenocrysts of dominantly quartz with lesser biotite. Red rhyolite lithics.

MR-28: Dense, pink, flow-banded, lithic rhyolite; 3% phenocrysts of biotite, quartz fragments, and rhyolite lithics in a red microcrystalline matrix.

MR-29: Lithic tuff; approximately 2-5% phenocrysts of biotite and lesser quartz with flow-banded rhyolite lithics (1-2mm) in a pink microcrystalline matrix.

MR-30: Dense, pink, porphyritic, rhyolite; 7% phenocrysts of dominately biotite, lesser quartz, and subordinate, clear, feldspar in a pink, microcrystalline matrix.

MR-31: Identical to MR-30.

MR-32: Lithic, porphyritic, light-pink, rhyolite; 5% phenocrysts of dominant biotite and lesser quartz. White rhyolite lithics (1-3mm). Silicification and bleaching of this sample is quite prevalent.

APPENDIX A (continued)

MR-33: Identical to MR-32.

S-1: Vitric, lithic, tuff; 4% phenocrysts of dominant biotite and lesser quartz with black elongated fiamme fragments (1-4mm) in a red, felsic, microcrystalline matrix.

S-2: Porphyritic perlite; black, highly fractured glass with a vitreous luster. 2% phenocrysts of biotite and clear feldspar. Rare, red, felsic, veinlets.

S-2-B: Siliceous spherulites; red, siliceous, spherulites (1-5cm) encased in black perlite.

S-3: Porphyritic perlite; black, highly fractured glass with a vitreous luster. 3% phenocrysts of clear feldspar. Red felsic veins and veinlets.

S-4: Porphyritic perlite; black, highly fractured glass with a vitreous luster. 3% phenocrysts of clear feldspar.

S-5: Porphyritic perlite; black, highly fractured glass with a vitreous luster. 4% phenocrysts of biotite and lesser clear feldspar. Red silicic veinlets and red siliceous spherulites (2-4mm).

S-6: Porphyritic perlite; black, highly fractured glass with a vitreous luster. 2% phenocrysts of clear feldspar.

APPENDIX A (continued)

S-7: Porphyritic perlite; black, highly fractured glass with a vitreous luster. 5% phenocrysts of biotite and lesser, clear feldspar.

S-8: Identical to S-7.

S-9: Vitric, lithic, porphyritic, tuff; 8% phenocrysts of biotite, lesser clear feldspar, and subordinate quartz. Black fiamme fragments and red felsic lithics in a red microcrystalline felsic matrix. Numerous lithics and phenocrysts altered to a white clay.

S-10: Lithic perlite; black glass with perlitic fractures and a vitreous luster. Red felsic lithics, quartz fragments, and white quartz veinlets. Brown-rimmed vugs filled with white clay and cryptocrystalline quartz. Phenocrysts altered to white clay.

S-11: Porphyritic, spherulitic perlite; black glass with perlitic fractures and a vitreous luster. 2% phenocrysts of clear feldspar. Red siliceous spherulites (1-4mm). Vugs filled with white clay.

S-12: No sample.

S-13: Welded lithic tuff; highly fractured black glass with a vitreous luster. Numerous vugs lined with brown alteration rims and filled with chalcedony. Red spherulites (1-3mm) and altered lithics(1-5mm).

APPENDIX A (continued)

S-14: Welded crystal tuff; highly fractured black glass with a vitreous luster. 2% phenocrysts of clear feldspar. Red siliceous spherulites (1-5mm) and red felsic veins. Some phenocrysts altered to white clay.

S-15: Welded crystal tuff; highly fractured black glass with a vitreous luster. 1-2% phenocrysts of clear feldspar. Numerous Phenocrysts altered to white clay. Red siliceous spherulites(1-5mm). Vugs filled with white clay.

S-16: Welded crystal tuff; highly fractured black glass with a vitreous luster. 2% phenocrysts of clear feldspar and lesser quartz. Vugs filled with white or green clay. Phenocrysts altered to white clay.

S-17: Welded crystal tuff; highly fractured black glass with a vitreous luster. 2% phenocrysts of clear feldspar. Red siliceous spherulites (1-4mm), vugs filled with white clay and phenocrysts altered to white clay.

S-18: Identical to S-17.

S-19: Identical to S-17.

S-20: Welded crystal tuff; highly fractured black glass with a vitreous luster. 3% phenocrysts of clear feldspar and lesser quartz. Vugs filled with white clay and phenocrysts altered to white or green clay. Red siliceous spherulites (2-15mm).

APPENDIX A (continued)

S-21: Vitric lithic tuff; Red, siliceous, microcrystalline or glassy matrix. Rare quartz phenocrysts. Black, flattened fiamme fragments, red rhyolitic and black volcanic lithics (1-5mm). Phenocrysts or lithics altered to white clay.

S-22: Vitric, lithic, crystalline, tuff; siliceous, microcrystalline or glassy matrix. 4% phenocrysts of dominantly clear feldspar, lesser biotite, and subordinate quartz. Black, flattened fiamme fragments, and red rhyolitic lithics.

S-23: No sample.

S-24: Siliceous spherulites; red siliceous spherulites with biotite phenocrysts. The spherulites (2-50mm) are encased in a matrix of black, highly fractured glass.

S-25: Crystalline, vitric tuff; black, highly fractured glass matrix with a vitreous luster. Rare phenocrysts of clear feldspar, red siliceous spherulites (1-5mm), and vugs filled with white clay. Phenocrysts altered to white clay.

S-26: Porphyritic perlite; black glass with perlitic fractures and a vitreous luster. 4% phenocrysts of clear feldspar, and lesser biotite. Red felsic veinlets.

S-27: Identical to S-26.

APPENDIX A (continued)

S-28: Porphyritic perlite; black glass with perlitic fractures and a vitreous luster. 3% phenocrysts of clear feldspar and lesser biotite.

S-29: Porphyritic perlite; black glass with perlitic fractures and a vitreous luster. 2% phenocrysts of clear feldspar. Red felsic spherulites (1-5mm).

S-30: Porphyritic perlite; black glass with perlitic fractures and a vitreous luster. 2% phenocrysts of clear feldspar. Red felsic veinlets.

S-31: Identical to S-30

S-32: Altered, vitric, lithic, tuff; red, siliceous, microcrystalline or glassy matrix with black, flattened fiamme fragments, quartz fragments, and red rhyolite lithics. Many lithics are altered to white clay.

S-33: Dense, flow-banded, rhyolite; maroon and white flow bands. White siliceous bands and lenses. Rare biotite phenocrysts.

S-34: Identical to S-33. Rare quartz phenocrysts.

S-35: Identical to S-33. Rare clear feldspar phenocrysts.

S-36: Altered, porphyritic, flow-banded, rhyolite; maroon and white flow-bands, white siliceous lenses and white bands of clay alteration products. Rare quartz fragments and rare phenocrysts of biotite.

APPENDIX A (continued)

S-37: Vitric, lithic, tuff; pink microcrystalline or glassy matrix with 2% phenocrysts of biotite and lesser quartz. Red rhyolite lithics, pink tuff lithics, and quartz fragments. Lithics and/or phenocrysts altered to white clay.

S-38: Identical to S-37.

S-39: Identical to S-37. No alteration .

S-40: Vitric, lithic, tuff; pink microcrystalline or glassy matrix with 3% phenocrysts of biotite, clear feldspar, and lesser quartz. Flow-banded rhyolite and pink tuff lithics.

S-41: Identical to S-40.

S-42: Flow-banded, maroon and white, rhyolite; Rare biotite phenocrysts, red felsic lithics, and quartz fragments. Brown-rimmed, chalcedony-filled vugs. Vugs filled with white clay.

S-43: Silicified, lithic, tuff; Pink microcrystalline matrix with black, fiammme fragments, and white quartz veins. Fractures in the matrix are filled with silica. The entire sample is silicified.

S-44: Vitric, lithic, tuff; pink microcrystalline or glassy matrix with rare biotite phenocrysts. Red and black glass fragments, black volcanic lithics, and quartz fragments.

APPENDIX A (continued)

S-45: Vitric, lithic, tuff; Black, fractured glass matrix with pink rhyolite lithics, white quartz fragments, and black glass fragments. No visible phenocrysts.

W-1: Perlite; black glass with pervasive perlitic fractures and a vitreous luster. Rare red felsic veinlets. No visible phenocrysts.

W-2: Identical to W-1.

W-3: Perlite; light-brown to gray, granular glass with dark-gray bands and a vitreous luster. No visible phenocrysts.

W-4 to W-7: No sample.

W-8: Volcanoclastic; pebble-size fragments of basalt, rhyolite, altered volcanic lithics, and various perlites in a sandy, white, siliceous matrix. Vugs filled with chalcedony.

W-9: Perlite; black glass with pervasive perlitic fractures and a vitreous luster. Rare, red, siliceous spherulites (1-4mm). No visible phenocrysts.

W-10: Vitrophyre: Red and gray glass with a vitreous luster. 3% phenocrysts of biotite and lesser quartz.

APPENDIX A (continued)

W-11: Volcanic breccia; gray granular and black classical perlite pebbles and cobbles in a white siliceous, sandy, matrix.

W-12: Volcanic breccia; gray granular and black classical perlite pebbles and cobbles in a gray glassy matrix.

W-13-A: Volcanic breccia; gray granular perlite and vitrophyre pebbles and cobbles in a purple, vitreous, glass matrix.

W-13-B: Volcanic breccia; gray granular perlite and vitrophyre pebbles and cobbles in a purple, devitrified, glass matrix.

W-14: Altered vitrophyre; silicified, black-banded, glass with some bands altered to white clay.

W-15: Volcanoclastic; fragments of basalt, glass and rhyolite in a sandy, siliceous matrix. Numerous vugs filled with chalcedony and many lithics altered to white clay.

W-16: Perlite; black glass with pervasive perlitic fractures and a vitreous luster. Rare red, felsic, veinlets. No visible phenocrysts.

W-17: Volcanic breccia; pebble to cobble size clasts of classical perlite, granular perlite, and vitrophyre fragments in a punky, white matrix.

APPENDIX A (continued)

W-18-A: Volcanoclastic; pebbles of basalt, perlite, rhyolite, and vitrophyre in a sandy, siliceous matrix. Numerous clasts are altered to white clay. Vugs filled with chalcedony.

W-18-B: Identical to W-18-A.

W-19: Dense, flow-banded, rhyolite; pink and white, microcrystalline, flow-bands. Vugs lined with silica.

W-20: Volcanic breccia; gray granular and black classical perlite pebbles and cobbles in a punky, sandy, white siliceous matrix.

W-21: Dense, flow-banded, rhyolite; Gray flow-bands, vugs lined with chalcedony.

W-22: Dense, flow-banded, rhyolite; pink and white, microcrystalline, flow bands. Vugs lined with silica.

APPENDIX B

Petrographic Descriptions

Petrographic descriptions of sample thin sections are given in this appendix. Phenocrysts are listed in order of decreasing abundance.

MR = McDonald Ranch samples

S = Swartz samples

W = Wallace Ranch samples

APPENDIX B (continued)

MR-3: Perlite: 99% glass, 1% phenocrysts.

Groundmass: pervasive perlitic fractures, rare asymmetric, radial, siliceous, devitrification structures, .2-.8mm. Phenocrysts: Plagioclase, euhedral to anhedral, core-rim zoned and unzoned, polysynthetic and carlsbad twinning common, .3-.5mm; Biotite, subhedral, brown, pleochroic, .3-1.4mm; Glomerocrysts of plagioclase and biotite phenocrysts and fragments, .8-1.3mm; Oxides: Magnetite, opaque specks randomly distributed in the groundmass, also distributed as linear features in the groundmass.

MR-4: Perlite: 97% glass, 3% infilled fractures.

Groundmass: glass, pervasive perlitic fractures and numerous random fractures. Oxides: Magnetite, rare, anhedral, opaque specks. No visible phenocrysts. Large fractures are filled with cryptocrystalline quartz, clay alteration products, and/or zeolites.

MR-6: Silicified, Welded, Lithic, Tuff: 60% glass, 40% phenocrysts and lithics. Groundmass: glass shards, glass and fiamme fragments. Veins of cryptocrystalline quartz and clay alteration products. Lithics: Andesite, plagioclase-rich, .8-2.8mm, several lithics altered to clay. Phenocrysts: Plagioclase, subhedral to anhedral, fractured and altered to clay, polysynthetic twinning common, .2-.4mm; Biotite, subhedral, brown, pleochroic, .05-.6mm. Oxides: Hematite, anhedral, stains.

MR-7: Perlite: 98% glass, 2% phenocrysts.

Groundmass: glassy, pervasive perlitic fractures, fractures filled with cryptocrystalline quartz and/or an alteration product. Flow bands of opaque minerals or microvesicles in the groundmass. Phenocrysts: Sanidine,

APPENDIX B (continued)

subhedral to anhedral, spotty alteration, .4-1.3mm; Plagioclase, subhedral to anhedral, fractured, carlsbad and polysynthetic twinning common, .2-.7mm; Biotite, subhedral, brown, pleochroic, .4-2.3mm; Oxides: Magnetite, anhedral, opaque specks randomly distributed in the groundmass, also as linear features; Glomerocrysts of subhedral plagioclase, sanidine, and biotite. Phenocrysts and glomerocrysts are aligned parallel to flow-bands of opaque mineral specks.

MR-10: Perlite: 98% glass, 2% phenocrysts.

Groundmass: glass, pervasive perlitic fractures. Fractures filled with cryptocrystalline quartz and/or an alteration product. Phenocrysts: Plagioclase, subhedral to anhedral, sector-zoned and unzoned, fractured, clay alteration, .4-1.1mm; Sanidine, subhedral, fractured, clay alteration products form parallel wisps and streaks in the groundmass, .3-1.1mm; Biotite, subhedral, fragments, brown, pleochroic, .1-1.0mm; Oxides: Magnetite, anhedral, opaque specks randomly distributed in the groundmass. Glomerocrysts of subhedral sanidine and plagioclase, .5-1.6mm.

MR-21: Perlite: 98% glass, 2% phenocrysts.

Groundmass: glass, pervasive perlitic fractures. Phenocrysts: Plagioclase, subhedral to anhedral, sector-zoned and unzoned, carlsbad twinned, fractured, .4-1.2mm; Sanidine, subhedral, sector-zoned, fractured, .2-1.4mm; Biotite, subhedral, brown, pleochroic, .3-1.2mm; Oxides: Magnetite, anhedral, opaque specks randomly distributed in the groundmass. Glomerocrysts of subhedral plagioclase and biotite, 2-4.0mm.

APPENDIX B (continued)

MR-28: Vitric, Lithic, Rhyolite.

Groundmass: microcrystalline to glassy, veins of cryptocrystalline quartz. Phenoncrysts: Plagioclase, subhedral, fractured, carlsbad twinned, .4-2.2mm; Sanidine, subhedral, fractured, .3-1.8mm; Biotite, subhedral, brown and green, pleochroic, .2-.6mm; Zircon, subhedral, v.high relief, colorless, .01-.07mm; Oxides: Magnetite, anhedral, opaque specks randomly distributed in the groundmass. Lithics: Andesite, plagioclase-rich, clay alteration products,.1-1.2mm.

MR-29: Welded Tuff: 99% glass, 1% phenocrysts.

Groundmass: glass, welded glass shards, visible local alteration to clay or zeolites; Phenocrysts: Biotite, subhedral, brown, pleochroic, .4-2.2mm; Plagioclase, subhedral, fractured, carlsbad twinned, .2-.6mm; Sanidine, subhedral, fractured, altered spots, .3-.7mm; Oxides: Magnetite, anhedral, opaque specks randomly distributed in the groundmass.

S-2: Perlite: 97% glass, 3% phenocrysts.

Groundmass: glass, highly fractured with poorly developed perlitic fractures, fractures filled with an alteration product; Phenocrysts: Plagioclase, euhedral to anhedral, fractured, carlsbad twinned, .2-.9mm; Biotite, euhedral, brown, strongly pleochroic, .3-.5mm; Sphene, subhedral, h. relief, .1-.25mm; Oxides: Magnetite, opaque specks randomly distributed in the groundmass.

S-4: Perlite: 95% glass, 5% phenocrysts.

Groundmass: glass, highly fractured with poorly developed perlitic fractures, fractures filled with an

APPENDIX B (continued)

alteration product; Phenocrysts: Plagioclase, subhedral, fractured, carlsbad twinned, .5-1.3mm; Sanidine, subhedral, fractured, .7-1.2mm; Biotite, euhedral, brown, pleochroic, .5-1.0mm; Oxides: Hematite, anhedral, streaks in the groundmass.

S-5: Perlite: 97% glass, 3% phenocrysts.

Groundmass: glass, pervasive perlitic fractures, fractures filled with cryptocrystalline quartz and/or an alteration product, siliceous radial, asymmetrical, devitrification structures; Phenocrysts: Plagioclase, subhedral, fractured, polysynthetic twinning, spots altered to sericite, core-rim zoned and unzoned, .5-1.25mm; Sanidine, subhedral, fractured, .2-1.2mm; Biotite, euhedral, brown, pleochroic, .2-1.2.mm; Hornblende, subhedral, .4-.9mm; Oxides: Magnetite, anhedral, opaque specks randomly distributed in the groundmass; Hematite, anhedral, swirls and streaks randomly distributed in the groundmass.

S-8: Perlite: 97% glass, 3% phenocrysts.

Groundmass: glass, highly fractured, pervasive perlitic fractures, fractures filled with cryptocrystalline quartz and/or an alteration product; Phenocrysts: Plagioclase, euhedral to subhedral lathes, .05-.2mm; Sanidine, subhedral, fractured, .5-1.6mm; Biotite, euhedral, brown, pleochroic, .2-.6mm; Hornblende, euhedral, green, .2-.7mm; Sphene, euhedral, gray, .1-.3mm; Oxides: Magnetite, anhedral, opaque specks randomly distributed in the groundmass.

S-10: Vitric, Lithic, Tuff: 70% glass, 30% lithics and phenocrysts. Groundmass: Glass and fiamme pumice, highly fractured, pervasive perlitic fractures, fractures

APPENDIX B (continued)

filled with cryptocrystalline quartz and an alteration product; Phenocrysts: Sanidine, subhedral, fractured, .25-.6mm; Plagioclase, euhedral to subhedral, fractured, carlsbad twinned, .11-.6mm; Quartz, subhedral, undulatory extinction, fractured, .2-1.5mm; Biotite, euhedral to subhedral, brown, pleochroic, .1-.5mm; Hornblende, subhedral, brown, .3-.75mm; Lithics: Andesite, plagioclase-rich with a black or dark brown mafic matrix; phenocrysts of sanidine, plagioclase lathes, and biotite in a black mafic matrix, .5-8.0mm; Fiamme pumice fragments, 1-4.0mm.

S-13: Welded, Lithic, Tuff: 85% glass, 10% phenocrysts, and 5% vein-fill material. Groundmass: glass and fiamme pumice fragments, highly fractured, pervasive perlitic fractures, fractures are filled with alteration products and/or cryptocrystalline quartz, a large vein (2-4mm) cross-cuts the thin-section and is filled with microcrystalline quartz, alteration products, and plagioclase phenocrysts. Phenocrysts: Plagioclase, euhedral to subhedral, fractured, polysynthetic twinning, .4-1.3mm; Sanidine, euhedral to subhedral, fractured, .4-1.3mm; Biotite, euhedral to subhedral, brown, pleochroic, .2-.7mm. Glomerocrysts: subhedral plagioclase, sandine, and biotite, .6-1.3mm; Lithics: Andesite, altered rims, plagioclase lathes with lesser opaque minerals, 1-2.5mm; Fiamme pumice fragments, 2-8.0mm.

S-16: Welded, Lithic, Tuff: 70% glass, 20% lithics, and 10% phenocrysts. Groundmass: glass and fiamme fragments, pervasive perlitic fractures, fractures filled with cryptocrystalline quartz and/or an alteration product. Phenocrysts: Sanidine, euhedral to subhedral, .2-.7mm; Plagioclase, subhedral, .3-.5mm; Biotite, euhedral to

APPENDIX B (continued)

subhedral, brown, pleochroic, .1-.5mm; Quartz, subhedral, undulatory extinction, fractured, .1-.3mm; Hornblende, subhedral, green, .2-.4mm; Hornblende, subhedral, .2-.4mm; Zircon, subhedral, .1-.2mm; Oxides, Magnetite, anhedral, opaque specks randomly distributed in the groundmass. Lithics: Andesite, plagioclase-rich with altered sanidine, broken biotite, and opaque minerals, lithics exhibit alteration rims of clay and/or zeolite, 1-2.5mm; Fiamme pumice, 1-4mm.

S-17: Welded, Lithic, Tuff: 85% glass, 10% lithics, and 5% phenocrysts. Groundmass: glass and fiamme pumice fragments, pervasive perlitic fractures, fractures filled with cryptocrystalline quartz and/or an alteration product; Phenocrysts: Plagioclase, euhedral to subhedral, polysynthetic twinning, .1-1.4mm; Biotite, euhedral to subhedral, brown, pleochroic, .2-.7mm; Sanidine, subhedral, .2-1.2mm; Quartz, subhedral, undulatory extinction, .3-.6mm; Hornblende, subhedral, brown, .1-.3mm; Glomerocrysts: subhedral plagioclase, sanidine, biotite, and hornblende, .4-1.5mm; Oxides: Magnetite, anhedral, opaque specks randomly distributed in the groundmass; Lithics: Andesite, plagioclase lathes, zoned plagioclase, biotite, and opaque minerals in a dark mafic matrix, 2-5.0mm; Fiamme pumice fragments, 2-8.0mm.

S-38: Vitric, Lithic, Tuff. 95% glass, 5% phenocrysts, and lithics. Groundmass: Glass and Fiamme pumice fragments, no perlitic fracture development, randomly oriented fractures filled with cryptocrystalline quartz. Phenocrysts: Plagioclase, subhedral, polysynthetic twinning, .4-2.1mm; Sanidine, subhedral, .3-1.6mm; Biotite, euhedral to subhedral, brown, pleochroic, .3-.8mm; Quartz, subhedral,

APPENDIX B (continued)

fractured, .2-.8mm; Oxides: Magentite, anhedral, opaque specks randomly distributed in the groundmass. Lithics: Volcanic lithics contain altered sanidine, biotite, and quartz phenocrysts, .6-3.0mm.

S-39: Vitric Tuff: 97% glass, 3% phenocrysts and lithics. Groundmass: Glass and Fiamme pumice fragments, no perlitic fracture development. Phenocrysts: Plagioclase, subhedral, polysynthetic twinning, fractured, .2-.8mm; Sanidine, subhedral, fractured, .4-1.0mm; Biotite, euhedral to subhedral, brown, pleochroic, .4-1.0mm; Quartz, anhedral, fractured, .2-.6mm; Oxides: Magnetite, anhedral, opaque specks randomly distributed in the groundmass; Glomerocrysts of sanidine, plagioclase and biotite, .7-2.1mm; Lithics: Volcanic lithics comprised of altered plagioclase lathes, cryptocrystalline quartz, and opaque specks of magnetite, .7-2.1mm; Fiamme pumice fragments, 1-5.0mm.

S-40: Vitric, Lithic, Tuff: 60% glass, 30% lithics, and 10% phenocrysts. Groundmass: glass and fiamme pumice fragments. Phenocrysts: Plagioclase, euhedral to subhedral, polysynthetic twinning, .3-1.3mm; Biotite, euhedral to subhedral, brown, pleochroic, .2-.9mm; Sanidine, euhedral, .4-1.7mm; Quartz, subhedral, fractured, .1-.8mm; Lithics: Altered Flow-Banded Rhyolites; Andesites, rich in plagioclase lathes and iron oxides, dark brown alteration product, .7-3.2mm; Fiamme pumice fragments, devitrified to quartz, 3-5.0mm.

S-42: Dacite: 90% matrix, 10% phenocrysts. Groundmass: microcrystalline matrix. Phenocrysts: Plagioclase lathes, abundant, euhedral to subhedral, .3-1.3mm; Sanidine, subhedral, .3-1.3mm; Biotite, anhedral,

APPENDIX B (continued)

brown, pleochroic, .2-.7mm; Sphene, subhedral, .04-.07mm; Zircon, subhedral, .2-.7mm.

W-1: Spherulite: Siliceous, devitrification structure. Asymmetric, radiating, fibrous, bundles of microcrystalline quartz; Phenocrysts: Plagioclase, anhedral, fractured, .2-.6mm; Clinopyroxene, anhedral, .2-.4mm; and Biotite, subhedral, brown, pleochroic, .1-.4mm; Oxides: Hematite, anhedral, stains.

W-5: Granular Perlite: 99% glass, 1% phenocrysts. Groundmass: glass, abundant non-aligned, random, fractures; no perlitic fracture development. Phenocrysts: Quartz, anhedral, .01-.1mm; Plagioclase, anhedral, fractured, .01-.25; Apatite, anhedral, .03-.2mm; Hornblende, anhedral, brown, .15-.4mm; Oxides: Magnetite, anhedral, opaque specks randomly distributed in the groundmass.

W-8: Vitric, Lithic, Tuff: 70% Lithics, 20% Matrix, 10% Phenocrysts. Groundmass: microcrystalline quartz. Phenocrysts: Quartz, subhedral, fractured, .5-2.0mm; Plagioclase, subhedral, fractured, polysynthetic twinning, .1-.25mm; Sanidine, subhedral, fractured, .3-.7mm; some phenocrysts altered to clay or zeolite. Lithics: Andesite, plagioclase-rich(lathes), .5-2.0mm, Basalt, hematite-rich, .3-1.4mm; Fiamme pumice fragments, .4-1.8mm; some lithics have alteration rims of clay or zeolite; Vugs lined with cryptocrystalline quartz.

W-9: Perlite: 99% glass, 1% phenocrysts. Groundmass: glass, pervasive perlitic fractures filled with cryptocrystalline quartz and/or an alteration product. Phenocrysts: Plagioclase, subhedral, fractured,

APPENDIX B (continued)

.05-.3mm; Biotite, subhedral, brown, pleochroic, .2-.9mm; Oxides: Magnetite, anhedral, opaque specks randomly distributed in the groundmass.

W-10: Perlite: 70% glass, 25% asymmetrical devitrification structures, 5% phenocrysts. Groundmass: glass, pervasive perlitic fractures; Siliceous, radial, asymmetrical devitrification structures, aligned in a subparallel manner, .4-3.0mm; Phenocrysts: Sanidine, euhedral to anhedral, .2-.9mm; Plagioclase, euhedral to anhedral, polysynthetic twinning, .3-.85mm; Biotite, euhedral, brown, pleochroic, .3-1.2mm; Hornblende, subhedral, fractured, brown, .1-.25mm; Oxides: Magnetite, anhedral, opaque specks randomly distributed in the groundmass; Glomerocrysts: euhedral plagioclase and biotite, .5-1.8mm; Glomerocrysts and Phenocrysts are aligned in a subparallel manner.

W-17: Perlite: 99% glass, 1% phenocrysts. Groundmass: glass, swirled flow-texture, no perlitic fracture development. Phenocrysts: Plagioclase, euhedral lathes, .05-.1mm; Biotite, euhedral, brown, pleochroic, .05-.1mm; Hornblende, subhedral, fractured, brown, .1-.5mm; Oxides: Magnetite, anhedral, swirls of opaque specks in the groundmass.

W-19: Rhyolite: 99% groundmass, -1% opaque mineral specks. Groundmass: microcrystalline rhyolite and glassy matrix. Oxides: magnetite, andhedral, opaque specks randomly distributed in the groundmass; Vugs filled with crystalline quartz.

APPENDIX B (continued)

G-1: Pumiceous Perlite: 97% glass, 3% phenocrysts. Groundmass: glass, highly fractured, zones of flattened vesicles, fractures filled with an alteration product, no perlitic fracture development. Phenocrysts: Sanidine, euhedral to subhedral, .4-1.3mm; Plagioclase, euhedral to subhedral, polysynthetic twinning, .5-1.2mm; Quartz, subhedral, fractured, .3-.7mm; Oxides: Magnetite, anhedral, opaque specks randomly distributed in the groundmass.

APPENDIX C

Physical Testing Data

This appendix contains physical testing data for all perlite collected for this study. Standards are included.

MR = McDonald Ranch samples

S = Swartz samples

W = Wallace Ranch samples

STD = Standard

APPENDIX C (continued)

Sample	Percent Recovered	Expanded Density	Average Brightness	Percent non-expansibles	Compacted Density	Mesh 20	Mesh 30	Mesh 50	Mesh 70	Mesh 100	Mesh 140	Pan
SID	96.5	2.87	70.7	5.9	2.75	2.5	33.9	53.7	6.8	1.6	0.8	0.6
MR-1	94.2	2.82	56.9	8.1	3.09	2.6	22.4	56.6	12.3	3.8	1.5	1.5
MR-2	95.3	4.22	60.8	13.1	4.69	1.0	18.0	59.0	12.8	4.3	1.9	2.8
MR-3	95.7	3.30	59.9	7.9	3.94	1.8	25.2	59.5	9.4	2.5	1.0	1.1
MR-4	93.9	6.13	58.5	18.7	——	0.4	8.6	67.9	17.4	3.8	0.8	0.7
MR-5	92.1	2.78	63.1	3.0	3.52	1.7	29.2	54.7	7.4	3.0	1.7	3.0
MR-6	—	—	—	—	—	—	—	—	—	—	—	—
MR-7	93.3	3.04	56.5	5.3	3.75	1.2	24.9	59.2	9.3	3.1	1.2	1.8
MR-8	91.4	4.08	55.1	9.5	4.86	0.6	19.7	59.7	10.7	4.1	1.9	3.1
MR-9	94.1	7.14	61.4	9.5	9.20	0.1	1.2	69.2	21.0	5.5	1.8	2.1
MR-10	94.2	23.40	62.2	83.5	——	0.1	0.2	36.2	42.0	19.6	1.8	0.6
MR-11	92.1	3.69	58.2	19.4	4.87	1.8	18.5	46.1	19.2	8.6	3.2	2.7
SID	97.7	2.73	70.2	5.2	2.60	4.1	33.0	52.5	7.8	2.2	0.7	0.4
SID	97.1	3.27	71.2	1.9	3.94	3.3	32.8	57.0	5.3	0.6	0.3	0.2
MR-13	96.1	5.32	52.1	24.5	7.29	1.1	29.7	60.6	5.2	1.2	0.9	1.1
MR-14	94.8	3.11	56.9	7.9	4.34	2.6	37.1	53.9	3.4	0.7	1.2	0.7
MR-15	93.8	3.37	58.1	8.9	4.54	1.0	30.6	60.5	4.3	1.3	1.1	1.0
MR-16	94.7	3.26	57.6	17.2	4.53	1.6	31.9	57.2	5.7	1.5	1.2	0.8
MR-17	94.8	2.66	63.1	6.9	3.77	2.4	34.6	55.6	4.0	1.2	1.0	1.0
MR-18	95.1	3.12	56.4	8.1	3.99	2.1	35.8	53.2	5.9	1.7	1.0	1.3
MR-19	95.1	4.56	46.2	18.1	5.26	2.5	31.8	57.8	5.3	1.0	0.7	0.9
MR-20	93.7	9.29	63.6	15.1	11.51	—	—	—	—	—	—	—
MR-21	94.4	12.25	60.7	29.7	—	—	—	—	—	—	—	—
MR-22	94.3	9.49	61.6	11.8	12.20	—	—	—	—	—	—	—
MR-23	94.5	9.82	53.2	32.3	—	—	—	—	—	—	—	—
MR-24	92.3	25.5	51.3	74.6	—	—	—	—	—	—	—	—
SID	97.3	2.58	64.6	3.3	3.81	4.5	31.6	48.6	10.1	3.3	0.9	0.9
SID	96.5	3.10	67.4	4.3	3.82	4.1	40.3	51.3	3.6	0.4	0.2	0.2
SID	96.8	3.42	70.1	4.2	3.69	2.6	25.0	52.3	14.2	5.7	1.5	0.6

APPENDIX C (continued)

Sample	Percent Recovered	Expanded Density	Average Brightness	Percent Non-expansibles	Compacted Density	Mesh 20	Mesh 30	Mesh 50	Mesh 70	Mesh 100	Mesh 140	Pan
S-2	97.4	6.70	46.0	6.9	7.52	0.1	8.4	78.5	10.9	2.0	0.4	0.4
S-3	97.2	7.14	46.4	6.3	8.48	0.02	10.4	82.5	6.4	0.7	0.2	0.0
S-4	97.1	5.95	45.8	2.9	6.91	0.0	12.8	69.9	12.9	3.5	0.6	0.5
S-5	96.6	7.36	45.8	9.7	8.67	0.1	9.3	81.7	8.7	0.7	0.1	0.0
S-6	97.3	8.20	42.1	8.3	—	0.1	7.2	79.3	12.3	1.1	0.2	0.3
S-7	97.5	7.70	48.1	4.4	—	0.1	6.2	74.5	15.4	3.4	0.2	0.3
S-8	97.1	9.46	42.2	9.1	—	0.3	0.6	86.8	11.3	0.8	0.1	0.1
S-9	95.1	28.10	32.9	81.1	—	0.1	0.6	30.2	48.2	20.2	1.4	0.4
S-10	96.9	24.27	33.1	84.3	—	0.3	0.3	46.5	44.6	8.0	0.6	0.2
S-11	96.2	20.60	36.1	61.3	—	0.0	0.1	39.4	43.2	15.6	1.4	0.5
S-12	—	—	—	—	—	—	—	—	—	—	—	—
S-13	96.2	22.70	35.3	68.3	—	0.2	0.0	36.3	44.9	16.8	1.7	0.7
S-14	96.2	21.80	35.7	67.3	—	0.0	0.0	37.5	41.1	16.7	2.3	0.6
S-15	96.8	20.60	35.8	58.2	—	0.2	0.1	43.6	42.3	12.6	1.0	0.3
S-16	96.6	23.10	34.0	81.2	—	0.3	0.1	50.0	41.6	8.4	0.5	0.3
S-17	95.4	22.80	34.8	90.4	—	0.0	0.1	52.3	40.6	7.0	0.3	0.2
S-25	96.4	21.80	37.3	74.3	—	0.3	0.3	50.0	41.7	7.9	0.6	0.4
STD	97.9	3.11	69.9	5.3	3.76	2.4	25.7	53.6	12.9	4.2	1.0	0.3
STD	96.9	2.82	69.2	4.6	3.32	3.5	32.8	50.3	9.3	3.3	0.9	0.3
S-26	96.4	6.81	43.5	7.1	7.77	0.0	3.0	78.0	14.6	3.5	0.7	0.2
S-27	97.2	7.77	42.7	5.5	8.99	0.2	2.0	87.8	9.5	1.2	0.2	0.2
S-28	97.1	9.33	39.5	8.4	—	0.0	1.0	86.5	11.8	1.0	0.1	0.1
S-29	97.2	7.80	40.2	6.1	9.56	0.1	5.3	89.2	5.2	0.2	0.1	0.1
S-30	97.5	8.60	40.1	9.2	—	0.0	2.3	82.9	12.5	1.7	0.2	0.1
S-31	97.7	11.03	40.7	29.9	—	0.1	0.9	74.6	18.8	4.4	0.7	0.1
STD	97.1	3.46	68.3	3.8	3.67	1.7	21.7	55.3	15.3	5.2	1.2	0.8
W-9	93.8	3.34	61.4	2.2	3.95	1.3	16.7	58.5	13.6	5.6	2.9	2.0
W-10	93.3	4.64	54.7	43.0	6.48	0.7	6.8	25.7	34.3	22.3	7.6	3.9
W-11	85.0	2.97	57.9	5.4	5.09	0.3	5.9	47.2	17.7	11.5	10.4	8.3

APPENDIX C (continued)

Sample	Percent Recovered	Expanded Density	Average Brightness	Percent Non-expansibles	Compacted Density	Mesh 20	Mesh 30	Mesh 50	Mesh 70	Mesh 100	Mesh 140	Pan
W-12	93.8	3.37	61.6	5.2	4.12	1.2	22.8	55.5	12.3	4.7	2.4	1.8
W-13A	95.7	5.48	43.5	6.1	6.32	0.5	15.9	67.5	13.1	2.6	0.4	0.4
W-13B	95.8	4.74	51.5	8.5	5.22	0.4	15.6	63.9	15.3	4.5	1.1	0.6
W-17	95.8	7.44	43.3	11.9	8.66	0.4	3.2	69.3	20.1	6.5	1.2	0.5
W-18A	94.5	44.79	24.9	96.8	—	0.1	0.5	1.5	49.7	39.6	8.6	0.6
W-18B	92.9	11.93	40.5	67.3	—	0.7	5.3	27.8	39.1	21.8	4.7	0.8
SID	97.5	3.48	67.1	3.3	3.83	1.8	23.1	53.3	15.7	5.5	1.0	0.3

APPENDIX C (continued)

Physical Testing Data for Drill Hole Samples
Submitted by Hahman, 1989.

APPENDIX C (continued)

Table 1. Test results on perlite samples submitted by DBO Four, Inc. (-50+100 mesh; 1300°F expansion temperature)

Sample Number	Percent Yield	Expanded Density**	Percent Brightness	Percent Sinkers	Compacted Density**
STD*	92.90	2.79	65.07	3.07	2.77
DH 4R					
30/40	90.40	21.73	39.80	52.80	24.44
60/70	91.70	12.11	49.53	14.88	12.39
90/100	95.40	10.39	53.03	9.87	11.80
130/140	91.80	6.14	60.43	19.27	9.70
DH 6					
28/30	88.60	62.40	30.57	90.47	62.4
DH 7R					
10/20	84.20	3.93	54.13	10.73	4.36
DH 7					
60/70	76.40	3.62	43.77	7.07	4.62
End STD	93.70	3.32	64.57	7.47	3.03

* STD = Grefco standard perlite (No Aqua)
** pounds per cubic foot

Table 2. Sieve analysis of expanded perlite samples submitted by DBO Four, Inc.

WEIGHT PERCENT RETAINED ON MESH

Sample Number	Mesh Size						
	20	30	50	70	100	140	pan
STD*	3.63	26.43	55.63	9.63	3.23	0.83	0.63
DH 4R							
30/40	0.00	0.00	23.40	45.60	28.40	1.60	1.00
60/70	0.00	0.20	49.20	39.60	9.00	1.00	1.00
90/100	0.00	1.17	54.37	32.77	9.77	1.17	0.97
130/140	1.20	6.60	54.40	23.00	11.80	1.40	1.60
DH 6							
28/30	0.14	0.14	1.14	42.14	51.54	3.94	0.94
DH 7R							
10/20	0.83	12.03	57.43	19.03	8.03	1.43	1.23
DH 7							
60/70	0.14	5.94	46.94	20.74	10.94	6.34	8.94
End STD*	8.40	34.40	42.60	9.80	3.40	0.60	0.80

*STD = Grefco standard perlite (No Agua)

APPENDIX C (continued)

Table 3. Test results on perlite samples submitted by DBO Four, Inc. (-50+100 mesh; 1300°F expansion temperature)

Sample Number	Percent Yield	Expanded Density**	Percent Brightness	Percent Sinkers	Compacted Density**
STD*	95.80	3.22	61.73	5.47	3.02
DH 5					
0/10a	93.50	6.96	49.73	15.80	11.47
0/10b	94.20	8.95	44.53	14.47	ERROR
10/20	94.30	7.93	49.30	5.67	12.89
20/30	94.70	14.24	48.60	12.13	12.90
30/40	94.40	11.68	50.13	9.00	13.63
40/50	94.00	7.61	54.20	4.53	11.56
50/60	91.20	4.94	47.00	18.67	11.64
60/70	90.70	6.11	48.33	23.40	12.28
70/80	89.90	4.98	54.57	34.00	9.87
80/90	89.50	5.51	50.73	46.93	10.27
90/100	86.30	43.03	26.57	92.53	ERROR
End STD*	92.60	3.09	65.17	5.33	3.16

* STD = Grefco standard perlite (No Agua)
** pounds per cubic foot

Table 4. Sieve analysis of expanded perlite samples submitted by DBO Four, Inc.

WEIGHT PERCENT RETAINED ON MESH

Sample Number	Mesh Size						
	20	30	50	70	100	140	pan
STD*	4.40	24.80	50.60	13.60	5.40	1.00	0.20
DH5							
0/10a	1.40	11.20	61.60	16.20	7.60	0.80	1.20
0/10b	0.00	1.94	52.34	35.94	8.74	0.54	0.54
10/20	0.09	1.89	52.69	33.09	9.89	1.09	1.29
20/30	0.00	0.69	63.69	29.89	4.69	0.49	0.69
30/40	0.00	0.29	54.49	38.09	5.69	1.09	0.49
40/50	0.20	4.60	67.00	22.60	4.00	1.00	0.60
50/60	0.00	1.34	34.54	36.74	23.54	2.94	0.94
60/70	0.00	3.57	48.97	31.37	14.37	1.17	0.57
70/80	0.11	5.11	61.51	21.51	7.71	1.91	2.11
80/90	0.49	1.49	34.29	30.09	25.89	4.49	3.29
90/100	0.00	0.00	1.51	34.71	57.31	5.91	0.71
End STD*	5.20	30.00	51.60	8.80	3.00	0.80	0.60

*STD = Grefco standard standard (No Agua)

APPENDIX C (continued)

Table 5. Test results on perlite samples submitted by DBO Four, Inc. (-50+100 mesh; 1300°F expansion temperature)

Sample Number	Percent Yield	Expanded Density**	Percent Brightness	Percent Sinkers	Compacted Density**
STD*	95.20	2.74	61.73	4.47	3.13
DH7					
110/120	76.10	3.77	48.30	11.53	5.02
140/150	82.90	5.70	51.77	18.93	8.44
DH8					
68/78	81.90	7.20	31.27	96.87	ERROR
100/110	84.20	5.01	52.27	25.20	6.00
DH9					
20/30	88.70	6.44	50.50	62.00	7.33
54/64	59.60	36.33	41.40	91.20	ERROR
72/82	85.80	13.69	39.63	71.73	ERROR
DH11					
32/42	86.50	53.88	29.70	97.60	ERROR
End STD*	91.40	2.69	59.77	2.53	3.75

* STD = Grefco standard perlite (No Aqua)
** pounds per cubic foot

Table 6. Sieve analysis of expanded perlite samples submitted by DBO Four, Inc.

WEIGHT PERCENT RETAINED ON MESH

Sample Number	Mesh Size						
	20	30	50	70	100	140	pan
STD*	5.43	33.03	50.23	7.43	2.23	0.63	1.03
DH7							
110/120	0.00	4.37	44.97	19.57	11.57	7.97	11.77
140/150	0.00	2.14	44.34	25.54	13.94	5.54	8.54
DH8							
68/78	0.06	0.06	1.46	47.86	45. 26	3.86	1.46
100/110	0.31	10.71	47.51	24.31	13.11	1.51	2.51
DH9							
20/30	0.94	8.34	20.94	35.74	31.14	1.74	1.14
54/64	0.00	0.51	2.11	41.31	52.51	3.51	0.11
72/83	0.06	3.46	10.06	43.26	41.26	2.06	0.00
DH11							
32/42	0.17	0.17	0.37	44.97	50.97	2.77	0.57
End STD	9.51	40.31	43.11	4.31	1.91	0.31	0.51

*STD = Grefco standard perlite (No Aqua)

APPENDIX C (continued)

Table 7. Test results on perlite samples submitted by DBO Four, Inc. (-50+100 mesh; 1300°F expansion temperature)

Sample Number	Percent Yield	Expanded Density**	Percent Brightness	Percent Sinkers	Compacted Density**
STD*	96.90	3.14	60.53	6.67	2.85
DH11					
50/60	94.00	72.50	23.50	75.73	0.00
DH12					
40/50	91.20	6.91	49.50	50.40	17.10
102/112	91.10	5.86	55.17	11.53	6.19
154/164	88.30	5.09	53.87	10.13	6.54
190/200	86.50	4.94	53.20	13.60	5.63
DH13					
18/28	90.90	5.53	53.03	16.20	6.38
100/110	90.00	6.86	53.17	41.00	7.75
DH13					
150/160	87.70	5.04	54.73	9.73	5.78
End STD*	93.80	3.80	64.03	11.47	3.50

* STD = Grefco standard perlite (No Agua)
** pounds per cubic foot

Table 8. Sieve analysis of expanded perlite samples submitted by DBO Four, Inc.

WEIGHT PERCENT RETAINED ON MESH

Sample Number	Mesh Size						
	20	30	50	70	100	140	pan
STD*	1.86	23.06	51.66	13.06	8.26	1.86	0.26
DH11							
50/60	0.00	0.00	0.77	40.37	50.57	8.17	0.57
DH12							
40/50	0.00	7.97	51.17	22.77	16.17	1.37	0.97
102/112	0.11	4.31	61.91	23.51	8.51	0.51	1.11
154/164	0.11	8.51	59.31	17.91	7.51	2.51	4.11
190/200	0.03	5.03	57.23	20.63	9.43	3.23	4.43
DH13							
18/28	0.91	9.11	61.11	16.91	7.91	1.11	2.91
100/110	0.40	6.60	46.20	28.40	15.40	1.80	1.20
150/160	0.17	5.57	59.97	18.77	8.77	2.77	3.97
End STD*	1.74	21.94	57.14	12.94	4.14	0.54	1.54

*STD = Grefco standard perlite (No Agua)

APPENDIX D

Major and Trace Element XRF Data

This appendix contains major and trace element data from XRF sample analyses.

MR = McDonald Ranch samples

S = Swartz samples

W = Wallace Ranch samples

STD = Standard

APPENDIX D (continued)

Sample	MR-1	MR-2	MR-3	MR-4	MR-5	MR-7	MR-8
Oxide (wt %)							
SiO_2	76.60	76.90	77.10	76.60	76.70	76.90	77.50
TiO_2	0.14	0.13	0.12	0.11	0.11	0.13	0.15
Al_2O_3	12.92	12.98	12.84	13.18	13.14	13.08	12.96
Fe_2O_3	1.18	1.19	1.15	1.02	1.18	1.18	1.18
MgO	0.22	0.14	0.15	0.18	0.13	0.13	0.16
CaO	0.89	0.82	0.80	1.13	0.91	0.85	0.78
MnO	0.09	0.10	0.09	0.06	0.09	0.10	0.10
Na_2O_3	2.79	3.15	3.05	2.09	2.99	2.93	2.93
K_2O	5.13	4.54	4.67	4.86	4.68	4.58	4.18
P_2O_5	0.04	0.03	0.02	0.02	0.02	0.04	0.03
S	0.02	0.01	0.01	0.01	0.01	0.01	0.01
TOTAL	100.03	99.98	99.91	99.31	99.96	99.92	99.97
Trace Element (ppm)							
Pb	90.63	42.67	61.01	44.51	46.53	55.04	45.05
Th	14.96	11.41	13.69	13.46	10.28	13.67	12.48
Rb	163.90	163.80	166.30	164.90	158.10	158.70	186.20
U	3.12	4.07	1.95	4.56	3.82	4.15	5.91
Sr	93.93	95.12	87.96	145.98	126.61	96.91	107.53
Y	27.59	25.12	24.97	23.48	24.06	25.19	25.93
Zr	117.30	95.30	92.30	86.70	86.50	94.60	117.40
Nb	18.69	18.46	17.62	17.47	17.89	18.74	18.49
Mo	6.26	7.15	6.39	5.73	7.31	7.5	7.23
Ba	952.30	896.60	3.38	897.10	861.00	925.40	961.40
Ti	2.65	2.29	2.31	2.27	2.22	2.48	2.75
V	27.43	24.73	0.81	19.01	17.2	19.85	20.64
Cr	---	53.64	---	28.18	44.55	41.56	33.98

APPENDIX D (continued)

Sample	MR-9	MR-10	MR-11	MR-25	MR-26	MR-27	MR-28
Oxide (wt %)							
SiO_2	77.20	77.40	77.50	77.60	78.50	79.30	77.00
TiO_2	0.12	0.12	0.14	0.10	0.10	0.10	0.12
Al_2O_3	13.02	12.9	12.68	12.95	12.69	11.76	12.64
Fe_2O_3	1.08	1.26	1.29	1.04	1.08	1.05	1.13
MgO	0.13	0.14	0.21	0.06	0.09	0.04	0.06
CaO	0.83	0.93	0.77	1.04	0.60	0.40	0.49
MnO	0.09	0.11	0.09	0.10	0.09	0.09	0.07
Na_2O_3	3.08	2.65	2.71	2.75	2.50	2.59	1.86
K_2O	4.39	4.44	4.58	4.38	4.29	4.57	6.59
P_2O_5	0.03	0.03	0.03	0.04	0.04	0.03	0.03
S	0.00	0.01	0.01	0.03	0.02	0.02	0.02
TOTAL	99.97	99.99	100.00	100.07	100.00	100.00	99.99
Trace Element (ppm)							
Pb	64.62	96.7	44.01	26.21	25.39	24.22	30.35
Th	14.97	13.81	11.52	14.57	14.04	12.86	12.37
Rb	197.83	242.56	158.61	152.27	151.41	161.54	179.03
U	4.34	3.13	4.36	5.90	4.69	3.34	5.53
Sr	105.10	120.39	138.74	123.29	113.20	71.54	62.43
Y	26.27	26.65	26.28	29.28	28.48	28.46	39.90
Zr	92.65	91.91	112.03	80.53	79.21	78.43	101.55
Nb	18.43	17.36	18.32	14.84	15.05	14.29	15.52
Mo	6.83	6.87	6.64	---	---	---	---
Ba	930.16	885.8	1135.02	996.3	1253.6	1013.7	1006.40
Ti	2.44	2.39	2.62	0.13	0.13	0.14	0.17
V	21.73	25.37	25.33	1.39	3.11	4.22	3.71
Cr	51.64	18.46	43.22	49.38	55.21	101.91	59.49

APPENDIX D (continued)

Sample	MR-29	MR-30	MR-31	MR-32	MR-33	STD	S-2
Oxide (wt %)							
SiO_2	82.29	79.60	77.60	81.90	82.90	77.00	77.20
TiO_2	0.13	0.12	0.13	0.12	0.12	0.06	0.13
Al_2O_3	11.39	11.76	12.47	11.02	11.12	13.09	12.78
Fe_2O_3	0.83	1.06	1.07	0.76	0.72	0.87	0.99
MgO	0.14	0.04	0.04	0.14	0.16	0.09	0.13
CaO	1.35	0.39	0.40	1.74	1.85	0.43	0.49
MnO	0.06	0.10	0.08	0.07	0.04	0.12	0.07
Na_2O_3	0.26	2.84	2.67	0.40	0.25	4.56	3.37
K_2O	3.65	4.13	4.82	2.99	2.74	3.76	4.78
P_2O_5	0.02	0.02	0.04	0.02	0.02	0.02	0.03
S	0.00	0.01	0.02	0.00	0.00	0.01	0.01
TOTAL	99.51	100.06	99.32	99.10	99.90	100.00	99.98
Trace Element (ppm)							
Pb	25.10	23.56	26.54	17.19	11.76	44.04	37.61
Th	14.14	12.82	13.43	10.05	13.45	24.49	23.98
Rb	111.82	159.11	173.42	107.27	147.26	270.16	213.55
U	3.10	3.25	0.45	0.44	3.78	8.34	5.86
Sr	468.12	63.03	58.71	490.72	151.20	2.39	30.43
Y	31.11	24.70	24.04	16.10	19.80	53.22	24.46
Zr	93.78	104.90	108.34	75.60	77.87	82.44	127.47
Nb	14.74	15.85	16.51	13.06	13.69	103.68	25.40
Mo	---	---	---	---	---	11.01	6.77
Ba	871.4	1035.8	1025.80	932.10	822.40	24.10	94.70
Ti	0.16	0.16	0.17	0.13	0.14	1.69	2.59
V	3.84	0.14	3.84	---	1.00	3.51	7.72
Cr	4.03	62.18	53.59	14.10	5.26	647.1	63.58

APPENDIX D (continued)

Sample	S-2B	S-3	S-4	S-5	S-6	S-7	S-8
Oxide (wt %)							
SiO_2	78.10	77.20	77.60	78.10	77.10	77.40	77.20
TiO_2	0.12	0.13	0.13	0.13	0.14	0.13	0.13
Al_2O_3	12.27	12.66	12.36	11.85	12.54	12.54	12.53
Fe_2O_3	0.86	1.12	1.08	1.13	1.14	1.05	1.07
MgO	0.10	0.14	0.11	0.09	0.13	0.11	0.14
CaO	0.51	0.46	0.55	0.58	0.71	0.45	0.62
MnO	0.05	0.08	0.09	0.09	0.09	0.07	0.08
Na_2O_3	4.49	3.49	3.84	2.99	3.25	3.75	3.73
K_2O	3.49	4.64	4.26	4.72	4.84	4.46	4.48
P_2O_5	0.03	0.03	0.03	0.01	0.03	0.03	0.02
S	0.01	0.01	0.01	0.02	0.02	0.01	0.02
TOTAL	100.00	99.94	100.10	99.74	99.98	99.98	100.02
Trace Element (ppm)							
Pb	34.44	47.94	39.09	35.71	36.13	---	36.15
Th	25.79	21.99	24.13	22.35	23.34	---	23.22
Rb	109.01	199.88	200.31	211.25	222.51	---	188.42
U	7.06	5.95	5.83	5.11	4.93	---	4.61
Sr	46.77	28.63	42.37	30.51	32.64	---	29.42
Y	21.85	23.75	22.54	24.01	24.48	---	23.04
Zr	11.85	119.03	118.78	120.91	121.13	---	120.36
Nb	24.80	31.98	24.86	28.10	27.53	---	27.08
Mo	5.73	10.28	7.08	7.98	7.79	---	7.99
Ba	99.18	90.07	95.77	90.91	90.33	---	85.62
Ti	2.48	2.49	2.52	2.52	2.55	---	2.52
V	3.11	6.34	2.42	0.86	8.62	---	2.75
Cr	142.59	240.56	88.73	156.66	170.24	---	48.76

APPENDIX D (continued)

Sample	S-9	S-10	S-11	S-13	S-14	S-15	S-16
Oxide (wt %)							
SiO_2	77.30	76.30	76.90	76.40	77.30	76.70	76.60
TiO_2	0.16	0.16	0.14	0.16	0.14	0.16	0.16
Al_2O_3	12.67	12.67	12.36	12.97	12.44	12.79	12.60
Fe_2O_3	1.38	1.33	1.25	1.35	1.19	1.25	1.42
MgO	0.42	0.40	0.47	0.27	0.18	0.27	0.43
CaO	1.36	0.99	0.92	1.13	0.74	0.83	1.08
MnO	0.08	0.08	0.09	0.09	0.08	0.08	0.09
Na_2O_3	2.51	3.37	3.41	3.11	3.68	3.35	2.96
K_2O	4.08	4.64	4.42	4.48	4.21	4.46	4.61
P_2O_5	0.03	0.04	0.04	0.04	0.03	0.04	0.04
S	0.01	0.01	0.01	0.01	0.00	0.01	0.00
TOTAL	99.99	99.99	100.02	100.01	99.99	99.93	100.02
Trace Element (ppm)							
Pb	35.48	30.45	550.81	53.08	46.72	42.07	38.83
Th	21.71	20.43	26.15	21.31	21.73	24.04	22.93
Rb	258.30	220.80	194.53	223.51	240.40	201.80	210.10
U	6.29	5.81	2.56	5.33	3.29	5.67	5.39
Sr	148.97	77.25	51.55	189.43	100.39	59.61	67.03
Y	23.57	23.04	26.28	25.15	23.52	24.66	24.31
Zr	116.46	121.17	113.91	125.64	119.94	123.65	121.71
Nb	25.93	27.59	22.92	23.82	22.22	25.45	24.94
Mo	7.55	8.78	6.29	7.31	6.46	7.37	7.12
Ba	140.51	131.63	120.99	170.76	125.05	122.28	122.93
Ti	2.91	2.84	2.63	2.95	2.63	2.84	2.87
V	11.08	13.19	5.10	11.66	8.13	15.13	12.03
Cr	181.82	189.04	55.18	71.71	64.48	55.01	55.59

APPENDIX D (continued)

Sample	S-17	S-25	S-32	S-33	S-34	S-35	S-36
Oxide (wt %)							
SiO_2	76.60	76.50	77.40	79.60	78.50	79.20	79.00
TiO_2	0.16	0.15	0.12	0.13	0.12	0.12	0.11
Al_2O_3	12.79	12.22	12.34	12.15	12.05	11.72	12.03
Fe_2O_3	1.37	1.38	1.18	0.84	0.98	0.86	0.92
MgO	0.44	0.57	0.08	0.06	0.05	0.04	0.04
CaO	0.91	1.79	0.43	0.27	0.41	0.26	0.34
MnO	0.09	0.09	0.06	0.07	0.07	0.05	0.07
Na_2O_3	3.84	3.34	2.46	2.68	3.13	2.86	2.95
K_2O	3.68	3.87	5.85	4.19	4.24	4.14	4.53
P_2O_5	0.06	0.04	0.02	0.02	0.02	0.02	0.01
S	0.01	0.01	0.01	0.00	0.01	0.00	0.01
TOTAL	99.95	99.96	99.97	100.00	99.60	99.30	100.01
Trace Element (ppm)							
Pb	38.57	77.22	28.63	25.73	33.15	32.43	27.31
Th	20.66	22.17	24.31	26.31	24.92	26.74	25.24
Rb	195.69	229.54	193.18	189.79	183.44	188.18	194.76
U	4.11	6.84	3.51	6.74	7.46	7.44	4.30
Sr	73.15	154.08	54.83	28.82	34.21	26.97	28.26
Y	23.44	23.34	19.88	19.68	20.97	22.94	19.64
Zr	118.61	114.45	106.49	111.24	113.54	112.67	109.60
Nb	24.51	24.11	21.87	22.01	22.74	22.64	22.44
Mo	7.34	6.82	---	---	---	---	---
Ba	142.71	130.01	140.75	90.58	102.34	87.74	92.06
Ti	2.95	2.71	0.17	0.15	0.15	0.16	0.15
V	14.23	16.16	8.25	1.39	---	1.63	1.30
Cr	50.58	29.65	90.40	67.06	78.50	99.31	84.71

APPENDIX D (continued)

Sample	S-37	S-38	S-39	S-40	S-41	S-42	S-43
Oxide (wt %)							
SiO_2	76.60	79.70	78.90	77.60	82.70	79.60	79.00
TiO_2	0.18	0.10	0.14	0.14	0.11	0.11	0.11
Al_2O_3	13.61	12.38	13.13	12.41	10.12	11.85	11.76
Fe_2O_3	1.45	1.23	1.05	1.25	0.76	0.87	1.05
MgO	0.16	0.22	0.25	0.08	0.12	0.05	0.03
CaO	0.63	1.78	1.49	0.53	1.06	0.36	0.28
MnO	0.07	0.07	0.04	0.05	0.06	0.07	0.07
Na_2O_3	2.33	0.95	0.52	3.01	0.80	2.83	3.31
K_2O	4.99	3.58	4.50	4.88	3.27	4.24	4.41
P_2O_5	0.02	0.02	0.01	0.03	0.01	0.02	0.01
S	0.00	0.01	0.00	0.02	0.00	0.01	0.01
TOTAL	100.05	100.09	100.04	99.99	99.80	100.01	100.04
Trace Element (ppm)							
Pb	25.93	28.78	19.67	26.70	21.01	24.35	29.28
Th	24.64	22.10	21.20	24.18	24.07	25.33	26.29
Rb	194.74	103.16	132.18	193.01	108.26	191.06	186.93
U	3.32	1.37	---	6.66	3.56	3.72	5.86
Sr	136.51	690.42	604.31	83.08	837.20	35.20	25.72
Y	21.54	15.89	20.21	19.78	15.09	19.31	20.91
Zr	123.64	102.84	104.32	113.35	92.91	104.11	113.36
Nb	20.70	20.08	19.40	21.03	18.72	21.74	23.15
Mo	---	---	---	---	---	---	---
Ba	310.68	277.14	478.19	175.14	186.05	111.42	60.47
Ti	0.25	0.21	0.18	0.20	0.14	0.15	0.15
V	11.38	11.97	3.78	5.61	---	---	---
Cr	70.55	24.14	16.70	94.67	24.41	46.27	168.94

APPENDIX D (continued)

Sample	S-44	S-45	W-1	W-2	W-3	W-9	W-11
Oxide (wt %)							
SiO_2	81.30	79.60	77.70	76.50	76.90	77.20	75.20
TiO_2	0.12	0.14	0.18	0.18	0.15	0.16	0.16
Al_2O_3	11.07	11.93	13.10	12.90	13.30	12.48	15.81
Fe_2O_3	0.82	1.02	1.08	1.07	0.96	1.31	1.38
MgO	0.08	0.18	0.09	0.07	0.06	0.14	0.32
CaO	0.73	1.31	0.56	0.56	0.60	0.65	0.61
MnO	0.07	0.06	0.04	0.04	0.04	0.06	0.06
Na_2O_3	1.42	1.61	2.42	2.53	2.88	3.18	1.97
K_2O	4.43	4.17	5.56	5.63	5.19	4.75	4.54
P_2O_5	0.02	0.01	0.03	0.03	0.02	0.03	0.01
S	0.00	0.00	0.00	0.00	0.06	0.06	0.01
TOTAL	100.00	100.03	100.70	99.60	100.20	100.01	100.05
Trace Element (ppm)							
Pb	26.36	22.70	29.61	29.19	28.75	69.56	39.96
Th	22.61	22.10	13.57	14.18	33.02	27.41	33.71
Rb	214.94	303.08	161.21	167.17	213.05	197.89	201.11
U	3.71	3.77	4.21	5.54	5.96	6.49	6.24
Sr	37.07	65.81	119.63	119.48	33.17	51.28	36.57
Y	18.94	16.61	25.04	23.33	36.21	38.65	37.83
Zr	107.62	102.61	88.53	87.44	114.28	135.39	130.91
Nb	21.79	20.12	18.68	17.94	32.92	34.78	39.19
Mo	---	---	5.77	5.25	7.28	10.77	9.19
Ba	67.04	83.63	862.65	846.29	148.54	258.89	155.82
Ti	0.14	0.17	2.26	2.23	2.55	2.86	2.77
V	---	2.70	15.45	16.70	4.31	15.37	7.93
Cr	46.18	40.34	43.73	48.11	55.09	283.75	195.66

APPENDIX D (continued)

Sample	W-13A	W-13B	W-17	W-19	W-20	W-21	W-22
Oxide (wt %)							
SiO_2	77.80	79.60	76.80	79.00	78.60	77.60	78.00
TiO_2	0.14	0.13	0.16	0.13	0.13	0.13	0.13
Al_2O_3	13.12	13.39	13.50	12.10	12.38	12.11	12.43
Fe_2O_3	0.00	1.33	1.28	1.02	0.89	1.18	1.03
MgO	0.35	0.32	0.57	0.07	0.16	0.04	0.04
CaO	0.79	0.79	0.83	0.46	0.58	0.42	0.35
MnO	0.08	0.07	0.07	0.04	0.05	0.06	0.04
Na_2O_3	2.96	2.55	2.32	2.69	1.56	3.11	2.87
K_2O	4.73	1.83	4.48	4.43	4.57	4.57	5.07
P_2O_5	0.03	0.01	0.02	0.02	0.01	0.01	0.01
S	0.01	0.01	0.01	0.01	0.00	0.01	0.01
TOTAL	100.01	100.04	100.10	99.97	98.90	99.90	99.99
Trace Element (ppm)							
Pb	53.01	53.56	34.41	24.90	27.04	24.99	25.46
Th	31.97	32.13	28.51	30.36	33.21	30.28	30.11
Rb	219.28	219.18	207.05	206.45	222.10	211.35	222.83
U	4.53	5.73	3.89	8.67	5.40	4.96	5.62
Sr	43.04	40.40	58.69	59.57	43.65	56.62	52.82
Y	40.31	40.34	42.55	35.17	37.93	34.79	35.38
Zr	120.51	122.39	137.72	127.61	112.30	128.17	126.36
Nb	35.33	39.31	33.21	27.03	29.44	27.12	26.87
Mo	8.97	11.48	8.21	---	---	---	---
Ba	151.45	166.71	267.31	334.31	122.76	306.59	302.23
Ti	2.47	2.53	2.88	0.20	0.15	0.19	0.19
V	5.06	8.39	7.17	4.88	0.65	3.01	3.10
Cr	103.44	450.69	151.62	33.11	39.97	60.81	43.04

APPENDIX E

Optical Description of Nonexpansibles

This appendix contains optical descriptions of nonexpansibles from binocular microscope observations.

MR = McDonald Ranch samples

S = Swartrz samples

W = Wallace Ranch samples

STD = Standard

APPENDIX E (continued)

STD-1 90% partially expanded clear glass, 10% clear glass shards and clear, euhedral feldspar phenocrysts.

MR-1 50% unexpanded, dull white, granular glass; 35% partially expanded, clear glass; lesser clear, broken glass vesicle walls; clear glass shards; black biotite phenocrysts; amber sphene fragments; and clear euhedral feldspar phenocrysts.

MR-2 95% partially expanded, clear glass; lesser, clear glass shards; black subhedral biotite; clear quartz fragments; iron stained, opaque, white glass; broken glass vesicle walls.

MR-3 50% partially expanded, clear glass; 45% opaque gray, glass fragments; lesser subhedral brown biotite; clear glass shards.

MR-4 85% unexpanded, milky white, granular glass; 10% opaque gray, glass fragments; clear glass fragments.

MR-5 90% broken glass vesicle walls; 9% partially expanded, opaque white glass; rare opaque gray glass fragments.

MR-7 70% partially expanded, clear glass; 20% unexpanded opaque white, granular glass; lesser, subhedral, black biotite; opaque gray, glass fragments; clear glass shards; rare, amber, sphene fragments.

MR-8 60% partially expanded, clear glass; 25% partially expanded, opaque white, granular, glass particles; lesser, opaque gray, glass fragments; black,

APPENDIX E (continued)

subhedral biotite; clear glass shards; clear, subhedral, feldspar phenocrysts.

MR-9 85% partially expanded, opaque white, granular glass; 10% opaque gray, glass fragments; lesser, subhedral, black, biotite; clear glass shards.

MR-10 90% unexpanded, opaque white, granular, vitreous, glass particles. Some with red hematite staining; lesser, opaque gray, glass fragments; rare, subhedral, black, biotite phenocrysts.

MR-13 95% unexpanded and partially expanded, clear glass; fragments; lesser, subhedral, black biotite phenocrysts; clear quartz fragments; clear feldspar phenocrysts.

MR-14 Identical to MR-13

MR-15 Identical to MR-13. Pink, hematitic glass fragments.

MR-16 Identical to MR-13. Orange stained glass fragments.

MR-18 Identical to MR-13. Opaque white glass fragments and pink, hematite stained, glass fragments.

MR-20 99% unexpanded, opaque white, glass fragment; rare, black, subhedral biotite phenocrysts; rare, amber sphene fragments.

MR-21 Identical to MR-20. Rare, clear feldspar phenocrysts and black, subhedral biotite phenocrysts.

APPENDIX E (continued)

MR-22 99% unexpanded, opaque white, glass fragments, some with red, hematitic stains; rare, black, subhedral biotite phenocrysts; rare, clear, feldspar phenocrysts.

MR-23 Same as MR-22. Pink, hematite stained, glass fragments.

MR-24 Same as MR-22. Amber sphene fragments.

STD-2 85% partially expanded, clear glass particles; clear glass shards; lesser, unexpanded, opaque white, granular glass fragments; rare, black, subhedral biotite.

STD-1 99% unexpanded and partially expanded, clear, glass particles; rare, clear quartz fragments; rare, clear feldspar phenocrysts.

S-3 90% unexpanded and partially expanded glass particles; 5% black, subhedral biotite phenocrysts; clear, quartz fragments; clear feldspar phenocrysts.

S-4 Identical to S-3.

S-5 Identical to S-3.

S-6 Identical to S-3.

S-7 Identical to S-3. Rare, amber, sphene fragments.

S-8 Identical to S-3.

APPENDIX E (continued)

S-9 Identical to S-3. Rare, black, biotite phenocrysts.

S-10 Identical to S-3. Rare, black, biotite phenocrysts.

S-11 100% unexpanded and partially expanded glass particles.

S-13 90% unexpanded and partially expanded glass particles; red clasts; rare, black, subhedral biotite phenocrysts; rare, clear feldspar phenocrysts.

S-14 99% unexpanded and partially expanded glass particles; rare, black, subhedral biotite phenocrysts; rare, red clasts.

S-15 95% unexpanded and partially expanded glass particles; lesser, quartz fragments; rare, black, subhedral biotite phenocrysts; rare, clear, subhedral feldspar phenocrysts; rare volcanic lithics.

S-16 95% unexpanded and partially expanded glass particles; lesser, quartz fragments; rare, clear. subhedral feldspar phenocrysts; rare volcanic lithics.

S-17 98% unexpanded and partially expanded glass particles; lesser quartz fragments; rare volcanic lithics.

S-25 Identical to S-17. Rare, clear, feldspar phenocrysts and rare, black, subhedral biotite phenocrysts.

APPENDIX E (continued)

S-26 80% unexpanded and partially expanded glass particles; lesser, pink, hematite stained, glass fragments; black, subhedral biotite phenocrysts; clear, feldspar phenocrysts; clear, quartz fragments.

S-27 Identical to S-26. Amber sphene fragments.

S-28 Identical to S-26. No pink, hematite stained, glass fragments.

S-29 Identical to S-27.

S-31 Identical to S-27. Pink, hematite stained, glass fragments.

STD-1 99% unexpanded and partially expanded, clear, glass particles; broken glass vesicle walls; rare, clear, quartz fragments; rare, clear glass shards.

W-1 Wallace granular perlite. 98% unexpanded and partially expanded glass particles; lesser, black, subhedral biotite; rare, green, euhedral hornblende phenocrysts; rare, clear quartz fragments.

W-9 95% unexpanded and partially expanded glass particles; lesser, black, subhedral biotite phenocrysts; clear quartz fragments; rare, clear, feldspar phenocrysts; rare, green, euhedral, hornblende phenocrysts.

APPENDIX E (continued)

W-11 95% broken, expanded glass particles; lesser, partially expanded, opaque white, granular, glass particles; clear glass shards.

W-12 90% partially expanded, glass particle; lesser, orange stained, glass fragments; clear, euhedral, feldspar phenocrysts; clear glass shards; rare, black, subhedral biotite phenocrysts.

W-13 90% unexpanded and partially expanded, opaque white, black oxide-stained, glass particles; clear glass shards; rare, black, subhedral biotite phenocrysts; rare, amber sphene fragments; rare volcanic lithics.

W-17 98% unexpanded and partially expanded glass particles; lesser, clear glass shards; clear quartz fragments; rare, green, euhedral hornblende phenocrysts.

W-18-A 80% red, black and gray volcanic lithics; lesser, clear quartz fragments; 5% partially expanded, clear glass shards; rare, black, subhedral biotite phenocrysts; rare, clear, euhedral feldspar phenocrysts.

REFERENCES CITED

Ballman, D., 1960, geology of the Knight Peak Area, Grant County, New Mexico: New Mexico Bureau of Mines and Mineral Resources: Bulletin 70, 36 p.

Barker, J., and Hingtgen, J., 1985, Perlite Testing at the New Mexico Bureau of Mines and Mineral Resources: SME-AIME paper no. 85-420, 14 p.

Breese, R., and Piper, J., 1985, Occurrence and Origin of Perlite: SME-AIME paper no. 85-359, 12 p.

Elston, W., 1957, Geology and mineral resources of Dwyer quadrangle, Grant, Luna, and Sierra Counties, New Mexico: New Mexico Bureau of Mines and Mineral Resources Bulletin 38, 86 p.

Finnell, T., 1987, Geologic map of the Cliff quadrangle, Grant County, New Mexico: U.S. Geological Survey Miscellaneous Investigation Map I-1768, scale 1:50,000.

Friedman, I., and Smith, R., 1958, The deuterium content of water in some volcanic glasses: Geochimica et Cosmochimica Acta, v. 15, p. 218-228.

Friedman, I., and Long, W., 1976, Hydration rate of obsidian: Science, v. 191, p. 347-352.

Hahman, W. R., 1989, Wallace Ranch Perlite Deposit, Grant County, New Mexico, unpublished consulting report, Las Cruces, New Mexico, 10 p.

Hedlund, D., 1978, Geologic Map of the Werney Hill Quadrangle, Grant County, New Mexico: United States Geologic Survey, Map MF-1038, 1 p.

Hildreth, W., 1981, Gradients in silicic magma chambers: Implications for lithospheric magmatism: Journal of Geophysical Research, v. 86, p. 10153-10192.

Jenkins, D., 1989, Perlite: The Story of GREFCO at Socorro, New Mexico, 8 p.

Jenkins, L. B., 1972, A Review of Classical Silicate-Rock Analysis and Recommended Modifications of Classical Methods of Analysis: United States Geological Survey, Circular 864, p. 1-30.

Lofgren, G., 1971, Experimentally produced devitrification textures in natural rhyolitic glass: Geological Society of America Bulletin, v. 82, p. 111-124.

Naert, K.A., 1974, Geology, extrusion history, analysis of perlites from No Agua Peaks, Taos County, New Mexico, unpublished Ph. D. thesis, Pennsylvania State University, State College, Pennsylvania, 223 p.

Spell, T., 1987, Geochemistry of Valle Grande Member Ring Fracture Rhyolites Valles Caldera, New Mexico, M.S. Thesis, New Mexico Institute of Mining and Technology, New Mexico, 213 p.

Taylor, H.P., 1968, The oxygen isotope geochemistry of igneous rocks: Contributions to Mineralogy and Petrology, V. 19, p. 1-71.

Trauger, M., 1972, Water Resources and General Geology of Grant County, New Mexico: New Mexico Bureau of Mines and Mineral Resources, Hydrologic Report 2, p. 20-29.

Weber, R., and Austin, G., 1972, Perlite in New Mexico: New Mexico Bureau of Mines and Mineral Resources, Circular 182, p. 97-101.

Whitson, D., 1982, Geology of the perlite deposit at No Agua Peaks, New Mexico: New Mexico Bureau of Mines and Mineral Resources, Circular 182, p. 89-95.

This thesis is accepted on behalf of the faculty of the Institute by the following committee:

William F. Claiborne, Jr.
Adviser

Peter Taylor

Andrew Campbell

James M. Barker

19 May, 1992
Date